MODELING AND CONTROL OF TRANSPORT BEHAVIOR OF MOVING WEBS THROUGH HEAT TRANSFER PROCESSES

By

YOUWEI LU

Bachelor of Science in Mechanical Engineering
Huazhong University of Science and Technology
Wuhan, China
2007

Master of Science in Mechatronic Engineering
Harbin Institute of Technology
Harbin, China
2009

Submitted to the Faculty of the
Graduate College of the
Oklahoma State University,
in partial fulfillment of
the requirements for
the Degree of
DOCTOR OF PHILOSOPHY
July, 2015

MODELING AND CONTROL OF TRANSPORT BEHAVIOR OF MOVING WEBS THROUGH HEAT TRANSFER PROCESSES

Dissertation Approved:

Dr. Prabhakar R. Pagilla

Dissertation Adviser

Dr. Karl N. Reid

Dr. Xiaoliang Jin

Dr. Martin T. Hagan

ACKNOWLEDGMENTS

I wish to express my sincerest appreciation to my advisor, Dr. Prabhakar R. Pagilla for his valuable guidance, inspiration, intelligent supervision, and friendship during my doctoral program. I am forever indebt to him for his motivation and technical insights.

I would like to extend my warmest thanks to my committee members: Dr. Karl N. Reid, Dr. Xiaoliang Jin, Dr. Martin T. Hagan, and former committee member Dr. Gary E. Young for their support and guidance in completion of this research.

I thank the engineers from the Armstrong World Industries, Tim Gottlob and Jamie Lynch, and the engineer from the Pohang Iron and Steel Company in South Korea, Changwoon Jee, for their help in the collection of measured data.

I would also like to thank my research colleagues at Oklahoma State University: Aravind Seshadri, Carlo Branca, Pramod Raul, Mauro Cimino, Kadhim Jabbar, Shyam Konduri, Orlando Cobos, Ben Pacini, Muthappa Ponjanda-Madappa, Supraj Paleti, Austin Elledge, Theo Ramseyer, Maya Wulandari, Emilio Gabino, Andrew Burnap, Matt Hollen, and Rushd Julfiker, for their friendship and technical support.

Finally and most deeply, I would like to express my appreciation to my parents, wife, parents-in-law, son, and family for their love and support throughout my life.

This work was supported by the National Science Foundation under Grant 1246854.

Acknowledgements reflect the views of the author and are not endorsed by committee members or Oklahoma State University.

Name: YOUWEI LU

Date of Degree: JULY, 2015

Title of Study: MODELING AND CONTROL OF TRANSPORT BEHAVIOR OF MOVING WEBS THROUGH HEAT TRANSFER PROCESSES

Major Field: MECHANICAL AND AEROSPACE ENGINEERING

Abstract: Heat transfer processes are widely employed in Roll-to-Roll (R2R) process machines to heat/cool moving webs. The general goal is to efficiently transport webs over heating/cooling rollers and ovens while achieving the specified web temperature at different locations of the R2R machine. One of the key controlled variables is web tension. When webs are heated or cooled during transport, the temperature distribution in the web causes changes in the mechanical and physical material properties and induces thermal strain. Because web strain and elastic modulus are functions of temperature distribution in the web, web tension resulting from mechanical strain is affected by heating/cooling of the web.

A multi-layer heat transfer model for composite webs is developed. Based on this model, temperature distribution in moving webs is obtained for webs transported on a heat transfer roller and in web spans between two adjacent rollers. Model simulations are conducted for a section of a production R2R coating and fusion process line, and temperature data from these simulations are compared with measured data obtained at key locations within the process line. In addition to determining thermal strain in moving webs, the model can be employed to design heating/cooling equipment that is required to obtain a certain desired temperature at a specific location within the process line. The governing equations for web strain and tension are then obtained by considering the temperature effects. Based on the web tension governing equation that includes both mechanical and thermal effects, a nonlinear adaptive tension control scheme is developed for control of tension in each tension zone of an R2R system. The control scheme is implemented on a modular R2R experimental platform containing two heat transfer rollers. Experimental results indicate that better tension regulation is obtained in the heated tension zone. Further, the temperature distribution model and the governing equations for web dynamics are utilized to design a tension observer for heating/cooling spans of a continuous strip annealing line where tension measurement is not available.

TABLE OF CONTENTS

Chapter Page

1 INTRODUCTION 1

1.1 Heat Transfer Process 2

1.2 Web Tension Control 5

1.3 Contributions 9

1.4 Organization of the Dissertation 11

2 MODELING OF TEMPERATURE DISTRIBUTION IN MOVING WEBS 13

2.1 Multi-layer Web Heat Transfer Model 16

2.1.1 Web in a Span Between Consecutive Rollers (Convection + Convection Condition) 20

2.1.2 Web Wrapped on a Heat Transfer Roller (Conduction + Convection Condition) 21

2.1.3 Web Between Two Nipped Rollers (Conduction + Conduction Condition) 23

2.1.4 Model with Thermal Contact Resistance 24

2.2 Special Cases of Single Layer Web Model 25

2.2.1 Temperature Distribution in a Single Layer Web Span Between Two Consecutive Rollers 26

2.2.2 Temperature Distribution in the Region of Single Layer Web Wrapped on a Heat Transfer Roller 26
2.3 Determination of Eigenvalues 29
2.4 Determination of Heat Transfer Period 30
2.5 The Coefficient of Heat Transmission of a Web Span Surrounded by Steady Air 34
2.5.1 The Coefficient of Heat Transmission of a Web Span Surrounded by Forced Air 36
2.5.2 The Coefficient of Heat Transmission of a Web Heated by Radiation 38
2.5.3 Viscosity and Thermal Conductivity of Air 39
2.6 Summary 41

3 APPLICATIONS OF TEMPERATURE DISTRIBUTION MODEL 42
3.1 Coating and Fusion Process Line 42
3.1.1 Heat Transfer Roller 43
3.1.2 Embossing Section 46
3.2 Roll-to-Roll Machine for Atomic/Molecular Layer Deposition 50
3.3 Summary 52

4 STRAIN AND TENSION GOVERNING EQUATIONS AND CONTROL 55
4.1 Governing Equations for Web Strain and Tension Considering Temperature Effects 56
4.1.1 Governing Equation for Web Strain and Tension 57
4.1.2 Governing Equation for Roller Speed 61
4.2 Adaptive Nonlinear Control Design 62

4.3 Experiments on a Modular Roll-to-Roll Machine 66
4.3.1 Pure Speed Control Experiments 69
4.3.2 Tension Control Experiments 71
4.4 Summary 74

5 TENSION OBSERVER DESIGN AND MODELING OF ROLL TO ROLL LAMINATION PROCESS 81

5.1 Tension Observer Design for Steel Strip Processing Line 81
5.1.1 Analysis of Continuous Galvanizing/Annealing Lines Furnace 83
5.1.2 Tension Observer Design for Strip in a Single Span 86
5.1.3 Tension Observer Design for Multiple Spans 91
5.1.4 Model Simulations of Continuous Annealing Line 94
5.2 Modeling and Control of Roll-to-Roll Lamination Process 98
5.2.1 Lamination Process and Governing Equations for Single Layer Webs 99
5.2.2 Mechanical and Physical Properties of Web Laminates 100
5.2.3 Governing Equations for Laminated Web 101
5.2.4 Control Algorithm of Lamination Process 104
5.2.5 Model Simulations off Lamination Process 106
5.3 Summary 107

6 SUMMARY AND FUTURE WORK 110

BIBLIOGRAPHY 113

LIST OF TABLES

Table		Page
2.1	Criterion of eigenfunction cross zeros point between β and $\beta + \Delta\beta$.	30
2.2	Coefficients of the collision integral equation (2.55)	40
2.3	Coefficients and exponents of the residual air viscosity equation (2.56)	40
2.4	Coefficients and exponents of the residual air thermal conductivity equation (2.59)	41
3.1	Properties of each layer of web and oil drum outer shell	43
3.2	Parameters of a heat transfer section of the embossing line	49
3.3	Properties of each layer in R2R ALD/MLD machine	52
4.1	Diameters and wrap angles of driven rollers	69
5.1	Simulation parameters	96
5.2	Properties and parameters of webs	106

LIST OF FIGURES

Figure Page

1.1 Web free span and web wrapped on a heat transfer roller 4

1.2 Control strategy with two PI controllers 9

2.1 Web span and web wrapped on a heat transfer roller 14

2.2 Picture of a heat transfer roller 15

2.3 Multi-layer web sketch 16

2.4 Convective heat transfer in web span 20

2.5 Web wrapped and transported on a heated/chilled roller 22

2.6 Web nipped between two heat transfer rollers 23

2.7 Web and roller surface contact: (a) Imperfect contact model, (b) Equivalent model 25

2.8 Graphs of $\tan(\lambda l)$ and $\frac{2\gamma k\lambda}{k^2\lambda^2-\gamma^2}$. The Abscissas of intersection are the solutions of λ 27

2.9 Graphs of $\tan\left(l_r\frac{\beta}{\sqrt{\kappa_r}}\right)$ and $\frac{k_r}{k_w}\sqrt{\frac{\kappa_w}{\kappa_r}}G(\beta)$. The abscissas of intersection are the solutions of β, and $G(\beta)$ is defined in (2.35) 28

2.10 Sketch of intersections of eigenfunction $f(\beta)=0$ and the β axis . . . 30

2.11 Graphs of $\tau(x,t)$, t_d is the abscissa of intersection of $\tau=t$ and $\tau=g(x,t)$ 32

2.12 Illustration of numerical method to determine τ 33

2.13 Web span surrounded in steady air 34

2.14 Configuration of jet impingement 36

2.15 Slot jet array configuration 37

3.1 Schematic of a coating and fusion process line 43
3.2 Gel and clearcoat section of the R2R machine 44
3.3 Heat transfer roller with wrapped web and temperature sensors . . . 45
3.4 Web temperature profile from model simulations and experiments with the heat transfer roller 46
3.5 Evolution of temperature at S1, S2 and S3 from experiments with the heat transfer roller 47
3.6 Simulation of temperature at different web thicknesses wrapped on the roller 48
3.7 A heating/cooling section of an embossing process line with infrared temperature sensors A and B 48
3.8 Top layer temperature of web in the heating/cooling section of the embossing line 50
3.9 ALD/MLD machine web path layout 51
3.10 Simulation of the average temperature of NMC layer with radiator of 420 °C 53
3.11 Simulation of the average temperature of graphite layer with radiator of 280 °C 53
3.12 Simulation of the average temperature of Kapton with radiator of 250 °C 54

4.1 Driven rollers and web spans 57
4.2 Tension zone with two rollers and web span 58
4.3 Effect of temperature on elastic modulus of polypropylene 60
4.4 Control strategy with dual-loop adaptive nonlinear controller 66

4.5 Line schematic of the experimental platform 67
4.6 Picture of the experimental platform 68
4.7 Web tension in the unwind zone with and without heating from pure speed control experiments 70
4.8 Web tension in the heating zone with and without heating from pure speed control experiments 71
4.9 Elastic modulus vs. temperature for HDPE [1] 72
4.10 Web temperature distribution in the heating zone 73
4.11 Tension in unwind zone with heater off under reference 5 lbf from tension control experiments 75
4.12 Tension in unwind zone with heater on under reference 5 lbf from tension control experiments 75
4.13 Tension in heating zone with heater off under reference 5 lbf from tension control experiments 76
4.14 Tension in heating zone with heater on under reference 5 lbf from tension control experiments 76
4.15 Estimate of c_1 in the heating zone under reference 5 lbf from tension control experiments 77
4.16 Estimate of c_1 in the unwind zone under reference 5 lbf from tension control experiments 77
4.17 Tension in unwind zone with heater off under reference 10 lbf from tension control experiments 78
4.18 Tension in unwind zone with heater on under reference 10 lbf from tension control experiments 78
4.19 Tension in heating zone with heater off under reference 10 lbf from tension control experiments 79

4.20 Tension in heating zone with heater on under reference 10 lbf from tension control experiments 79
4.21 Estimate of c_1 in the heating zone under reference 10 lbf from tension control experiments 80
4.22 Estimate of c_1 in the unwind zone under reference 10 lbf from tension control experiments 80

5.1 Sketch of heating/cooling sections of an annealing furnace 84
5.2 CGL/CAL Control block diagram 85
5.3 Temperature Map within Annealing Furnace 87
5.4 Simulation of tension response and estimate of multi-span with controller and observer 96
5.5 Simulation of modulus in different spans 97
5.6 Sketch of lamination process 99
5.7 Lamination of two webs 101
5.8 Separation of laminated webs 104
5.9 Control strategy for two driven rollers upstream of laminator 105
5.10 Simulation of average temperature of web in tension zone 1A 107
5.11 Simulation of tensions in the individual webs prior to lamination . . . 108
5.12 Simulation of strains in the individual webs prior to lamination . . . 108

NOMENCLATURE

A	Cross section area of web
b_f	Coefficient of friction in the roll shaft
c	Specific heat
D	Characteristic length of web
e	State error
E	Young's (elastic) modulus
F	Force
H	Distance between jet nozzle and web surface
h_i	The y-axis coordinate of the boundary of the i^{th} and $(i+1)^{\text{th}}$ layers
J	Inertia of all the rotating elements on the motor side of roller
k	Thermal conductivity
K	Control gain
l	Thickness of each layer of the web
L	Span length of web between rollers or arc length of wrapped web
m	Mass
n	Gear ratio between the motor shaft and the roll shaft
$\mathbb{N}$	The set of all natural numbers

Nu	Nusselt number
Pr	Prandtl number
r	Thermal contact resistance
R	Refer to a roller or its radius
$\mathbb{R}$	The set of all real numbers
Re	Reynolds number
S	Distance between two jet nozzles
t	Time
t_i	Web tension in i^{th} tension zone
u	Input torque on motor
U	Transient part of the solution of heat equation
v	Speed
V	Volume
w	Web width
W	Width of jet nozzle
x	Web transport direction
y	Web transverse (thickness) direction
z	Web lateral (width) direction
α	Thermal expansion coefficient
β	Eigenvalue of the multi-layer web
γ	Heat transfer coefficient
ϵ	Emissivity
ε	Strain
θ	Temperature of surrounding environment
ϑ	Temperature Distribution

κ	Thermal diffusivity($= k/(\rho c)$)
λ	Eigenvalues of each layer of the web
ν	Viscosity of air
ρ	Density
σ	Stress
ς	Stefan-Boltzmann constant, $5.670 \times 10^{-8}\mathrm{Wm}^{-2}\mathrm{K}^{-4}$
τ	Time period of heat transfer process at x
ϕ	The angle of web wrapped on roller
ψ	Steady-state part of the solution of heat equation

Superscripts

e	Tension dependent term
ϑ	Temperature dependent term

Subscripts

c	Pertaining to the heating/cooling source contacting the surface of web
C	State of the region of web wrapped on heat transfer roller
e	Equivalent value
F	State of the region of web span between two consecutive rollers
r	Pertaining to the roller outer shell
R	Reference term
s	Stretched state
u	Pertaining to ambient air
w	Pertaining to web

CHAPTER 1

INTRODUCTION

Roll-to-Roll (R2R) manufacturing involves continuous transport of flexible materials (webs) on rollers through processing machinery. In recent years there has been a significant focus on R2R manufacturing because it is an efficient and scalable method to manufacture many consumer products from flexible materials. It offers significant advantages over batch manufacturing, such as high speed automation and mass production at substantially lower costs.

Many processes require heating and cooling of the moving web. The moving web is heated/cooled by transporting it over heated/chilled rollers or through ovens. Typical processes include coating, embossing, printing, drying, lamination, etc. Although much of the current practice in heating/cooling webs is based on empirical understanding of the process which has been tuned by experience over a number of decades, development of new products such as flexible panel displays, printed electronics, etc., using R2R manufacturing methods will require a better understanding of the heat transfer process [2–4]. A typical R2R manufacturing procedure for flexible displays includes slot die coating, screen printing to print layers in the form of stripes, etching resistant material during anode patterning and encapsulating using an adhesive in a lamination process [5, 6], and each step involves heating or cooling processes. As electrical devices are very brittle to heat and stress, the study of temperature distribution and tension control with heating process are crucial in flexible electronics manufacturing.

During heat transfer processes in R2R manufacturing, the transport behavior of the web is affected by changes in physical and mechanical properties and thermal strain due to heating and cooling. Control of web tension is critical in all R2R systems. Web tension during transport is affected by the temperature distribution in the web. Tension variations may lead to web wrinkles, curl, coating thickness variations, or print registration errors [7–9].

1.1 Heat Transfer Process

There is a need to develop an accurate heat transfer model for different methods of heating and cooling of moving webs in developing the governing equation for tension in the web. The model can also be used to design the heating/cooling sources and their locations within the process line and to determine operating conditions such as web speed. For example, the model would be useful in sizing of heating/cooling sources such as heating/cooling rollers, radiators, and ovens, and the resident time required to heat/cool the moving web to the desired temperature at key locations within the process [10].

Although significant amount of work has been done in the area of heat transfer with fundamental work reported in [11–17], there has not been much reported work on thermal behavior of moving webs, except in [8, 18–20]. In [18], a simple expositional formula for temperature distribution in a web along the transport direction was used. In [19], a dryer was considered in the R2R system, but the web was assumed to be of the same temperature as the ambient air in the dryer. In [8], a lumped capacitance method was used to obtain the temperature distribution in the web. In [20], a modeling procedure to determine the temperature distribution in the web is developed.

Many web products are currently manufactured from laminated composites. The knowledge of temperature distribution in composite webs is even more important than single layer webs because natural thermal expansion needs to be taken into account, and the mismatch in thermal expansion coefficients between layers during heat transfer process may cause high levels of residual stress and film cracking [2]. Studies using numerical or finite element methods for laminated materials can be found in many articles [21–24]. But an analytical thermal model would be valuable in predicting the temperature and strain distribution in the composite web and for real-time control of tension in R2R manufacturing. Some multi-layer heat transfer studies for thin materials can be found in [25–33]. The solutions to the special case of the two layer model can be found in [25, 26]. The model for three layers in the contact region in a rolling machine can be found in [27]. A multi-layer heat transfer model with any numbers of layers is given in [28], where an analytic technique is used for solving the heat equations. Multi-layer heat transfer equations with a simple approximation for the average diffusivity in each layer is also given in [29]. Multi-layer model with special periodic boundary conditions can be found in [30], while more complex boundary conditions are discussed in [31–33], which neither consider the moving webs or the boundary conditions and solution forms associated with heating/cooling of moving webs.

While developing the heat transfer models, thermal contact resistance needs to be considered for imperfect contact. When two solid bodies come in contact, a temperature drop occurs between the two surfaces in contact. This phenomenon is said to be a result of a thermal contact resistance existing between the contacting surfaces, due to the microscopic qualities of the surfaces where the roller and web meet. All real surfaces are microscopically rough, and when two surfaces are brought into contact, imperfect bonding is expected. Thermal contact resistance is defined as the ratio

between the temperature drop and the average heat flow across the interface [34].

The heating/cooling conditions in R2R manufacturing can be classified into two parts: with or without a heat transfer roll. Thus in this dissertation, all heat transfer processes are classified into two kinds: web wrapped on a heat transfer roller and web heated/cooled in a free span, and two basic models are considered. The two kinds of heat transfer processes are shown in Fig. 1.1. Many methods are used in industry to adjust the convective heat transfer rate, like using an oven or fan. These methods change the heat convective transfer coefficients, and the coefficients are also discussed in this dissertation. For moving webs, since the web thickness is often thin, the temperature difference between the two surfaces of web along the thickness is often much larger than the difference along the web transport direction. Thus heat transfer in the transverse direction (along web thickness) is dominant.

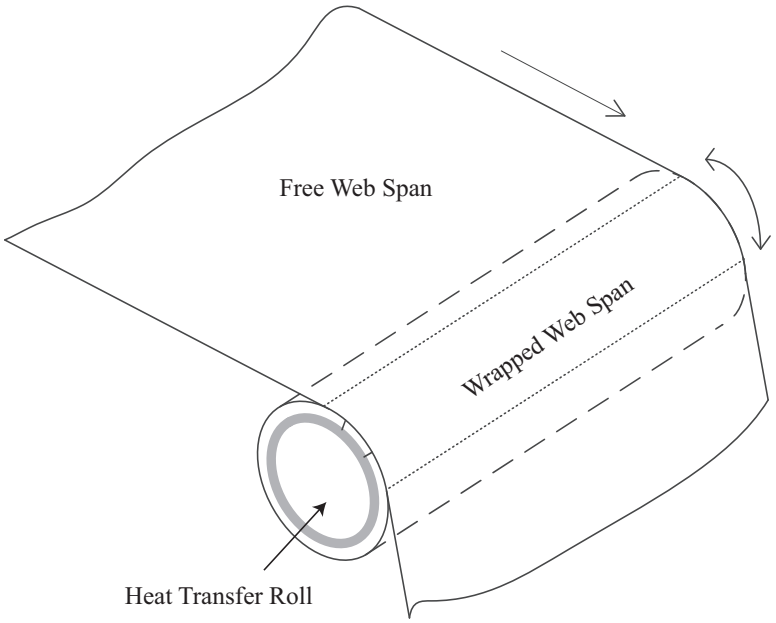

Figure 1.1: Web free span and web wrapped on a heat transfer roller

Consequently, in this dissertation a heat transfer model for composite webs considering multiple layers of dissimilar webs is presented, and solutions with relevant

boundary conditions for different types of heating/cooling methods are described. To account for the imperfect thermal contact between the moving web and the heat transfer roller, a thermal contact resistance model is considered. The heat transfer period required in solving the model is discussed and a numerical procedure for computing it for the moving web is given. Model simulations are conducted for heat transfer sections and compared with temperature measurements in an industrial coating and fusion production R2R line. Simulations are also conducted for the heater size design in an atomic/molecular layer deposition line.

1.2 Web Tension Control

During heating or cooling of moving webs, thermal strain and elastic modulus are affected. The thermal strain is generally taken as linearly dependent on the temperature change, but the effects of temperature change on elastic modulus and other temperature-relevant parameters are not well studied, especially for composite products.

The conventional tension model in a moving web without considering the effects of temperature is widely available in many articles [19, 35–39]. The model describes tension behavior in a web span when the web temperature is same as the ambient air. This model does not describe the tension behavior of the web undergoing heating/cooling because the elastic modulus and the thermal strain of the strip are not uniform within the web span. An effort to include thermal strain in an R2R system can be found in [19], where a dryer was considered, but the web was assumed to be of the same temperature as the ambient air in the dryer. Basic methods of continuum mechanics were applied to web tension models including thermal effects in [40], and a lumped capacitance method was used to describe heating of the web;

this neglects the temperature difference along transverse direction inside the moving web. In [41], temperature distribution for single layer webs was used to develop a tension governing equation. The change in Young's modulus of several materials as a function of temperature was studied in many articles [1, 42, 43]. A governing equation for web tension is developed by considering thermal strain and web elastic modulus as a function of web temperature in this dissertation.

Due to nonlinearities and parameter uncertainties (Young's modulus relevant terms) present in the tension governing equation, a nonlinear controller is preferred to control the tension in a moving web undergoing heating/cooling. Several nonlinear design tools are available [44–46]. In many cases the nonlinear systems can be formed into Nonlinear Block Controllable (NBC) forms for both SISO and MIMO systems. Such a representation enables to reduce the original control law synthesis problem into a sequence of low-order subproblems [47]. This strategy is employed for control of tension in web transport systems. A nonlinear adaptive controller was proposed to control web strain in [48].

The interconnected R2R systems are usually divided into many subsystems (tension zones). The information exchange between subsystems of a large-scale system is not needed by designing decentralized controllers which are simple and use only locally available information. A large body of literature exists in decentralized control of large-scale systems [49–51]. Decentralized control schemes that can achieve desired robust performance in the presence of uncertain interconnections can be found in [52, 53]. A stability condition is developed using small gain theory in [54]. A design of a decentralized controller for R2R systems can be found in [37], in which a fully decentralized state feedback controller was proposed for conventional R2R system without heat transfer processes.

Continuous annealing lines are productive manufacturing lines used by steel mak-

ing companies for the manufacture of thin steel sheet products. In these lines, the steel strip is continuously heated and cooled depending on the heat processing cycle required for a particular product. The heating/cooling cycle plays a critical role in programming the material properties of sheet products. The annealing furnace consists of several heat transfer sections, such as heating section, soaking section, rapid cooling section, and cooling section. To improve transport behavior through the furnace, all the rollers are independently driven by a motor which are used to control strip speed and tension. Although rotational speed is measured for each driven roller shaft, tension measurement is spatially intermittent and located between any two heat transfer sections because of the inability to reliably measure tension within each heat transfer section. Since tension measurement is not available within the heat transfer sections, control of tension is challenging in these sections. An algorithm that provides tension estimation within each transfer section based on the model and tension measurements between each section is beneficial in regulating tension within acceptable levels in each section. The strip tension control considering the temperature change in multiple spans with the assumption that the tension is same in every span in the furnace can be found in [55], while an observer is used as local tension estimate in every span in [56]. A decentralized controller and observer that can achieve global exponential stabilization under two sufficient conditions are given in [57]. A completely decentralised observer-based control scheme for interconnected dynamical systems is proposed in [58]. An observer based control strategy for a continuous R2R strip processing line based on a model is given in [59]. Two tension observers are suggested using sliding-mode approach for a multi-motor web-winding system [60]. After presenting the dynamic equations of a web-handling machine, the structure is exploited to design a reduced order, nonlinear observer with linear time-varying error dynamics [61].

Lamination in R2R manufacturing is a process that involves joining two or more layers of webs to form a composite web [62–65]. Typical lamination processes use nip rollers to provide contact pressure to combine several layers into one composite web. There are two types of lamination: cold lamination and hot lamination. In cold lamination, neither of the laminator rolls are heated and contact bonding between webs is obtained by contact pressure or an adhesive material on one of the webs. In hot lamination, one of the laminator rolls is heated to heat the contacting web. In addition, one or more layers may be heated prior to lamination. Curl elimination is a major goal in many lamination processes.

In typical R2R processes, tension control is accomplished by regulating either speed or torque on driven rollers. In most industrial web process lines, the decentralized control scheme for each section has two cascaded PI control loops, as shown in Fig. 1.2 [37]. The output of the tension loop becomes reference speed error correction for the speed loop. A good temperature distribution model would be facilitated in the development of an accurate governing equation for web strain and subsequently for web tension using a constitutive relation between web strain and tension that is applicable to the heated/cooled web; the constitutive relations that are typically used are either elastic or viscoelastic based on the material properties which can change due to heating/coolign of the moving web. Since model based tension controllers are currently being used for precise control of web tension, it is beneficial to obtain an accurate tension governing equation that reflects the actual process conditions including the heating/cooling of the web.

In this dissertation, a governing equation for mechanical strain by considering thermal strain as part of the total strain is developed. An elastic constitutive relation between strain and tension is considered to develop a governing equation for tension in a web span. Using the governing equation for tension in a span and web velocity, one

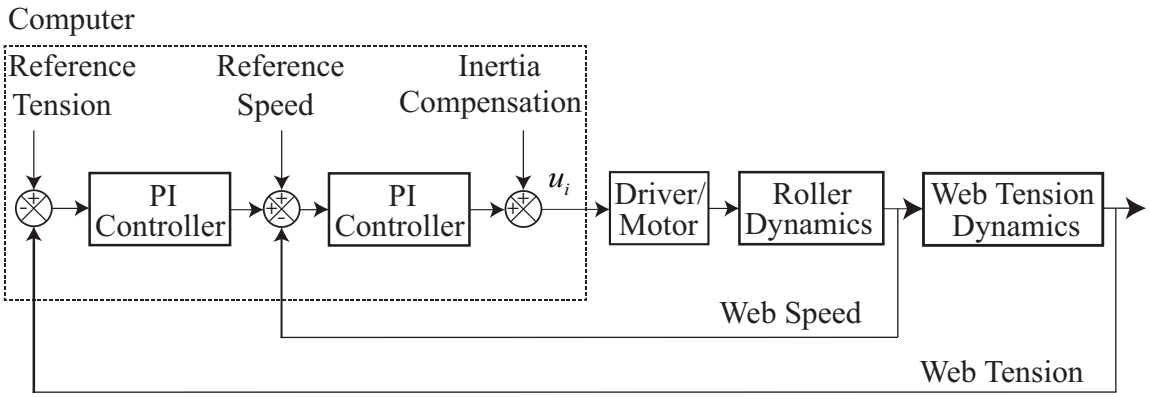

Figure 1.2: Control strategy with two PI controllers

can form the governing equations for the entire R2R process line. For development of a tension controller, one tension zone is considered; a tension zone is the web between any two driven rollers. The proposed nonlinear scheme in this dissertation mimics an existing industrial linear speed-based tension control strategy as shown in Fig. 1.2 where an inner speed loop is employed to control speed and an outer loop based on tension error provides a trim to the speed reference of the inner loop to regulate tension. Therefore, a similar real-time strategy as the one currently used in industry can be employed in the implementation of the proposed nonlinear scheme, as shown in Fig. 4.4. Since the elastic modulus is not well known, one can use an adaptive nonlinear controller and estimate the unknown parameters. Experiments conducted on a modular R2R machine that contains heat transfer rollers show that the typically used pure speed control scheme does not provide regulation of web tension in heating zone. The proposed scheme provides regulation of tension at its desired value. A number of experiments were conducted to evaluate the proposed scheme.

1.3 Contributions

The contributions of this work are summarized as follows.

A general heat transfer model for composite webs with any numbers of layers is developed and solutions are obtained for different heating/cooling boundary conditions. The developed model can handle web heating by any type of heat transfer method, including heating/cooling rollers, fans, radiators or ovens. The boundary conditions of heat transfer model for a composite web for different types of heating/cooling may be classified into three main conditions and explicit solutions using these heat transfer boundary conditions are obtained from the general solutions.

The elastic modulus and thermal strain of web are dependent on web temperature and these dependencies are included in the tension governing equation. A nonlinear governing equation for web tension considering heat transfer in the moving web is developed. In the governing equation, thermal strain is assumed to be proportional to the temperature difference between original and heated/cooled web, and the equivalent Young's modulus is used to deal with the Young's modulus change after heating/cooling.

A nonlinear adaptive controller including parameter estimator is designed to account for variations in the elastic modulus with temperature changes. The NBC forms of the established nonlinear tension and velocity governing equations are presented and a dual-loop speed-based tension controller is developed.

Two important problems involving the dynamic models and control strategies considering heat transfer in the moving webs are studied: tension observer and lamination process. A tension observer is designed for estimation of tension in spans within an annealing furnace of a steel strip process line where the tension measurements are not available. Lamination process is modeled based on the individual web tension dynamics, where the tension and velocity governing equations are developed for both the single layer webs before lamination and the laminated web. The reference tension formulas are developed so that the strains of the individual webs are the same prior

to lamination at the nip rollers and curl can be eliminated.

1.4 Organization of the Dissertation

The rest of the report is organized as follows. A multi-layer model for temperature distribution in moving webs for different heating/cooling sources is first developed, and the coefficients of heat transmission are then discussed for different heating/cooling situations in Chapter 2. In Chapter 3, a coating and fusion process line and an atomic/molecular layer deposition machine involving temperature distribution computation are presented to demonstrate the temperature distribution model. Based on the temperature distribution model, governing equations for web strain and tension are obtained in Chapter 4. Design of a controller for web tension in heat transfer processes is also discussed in Chapter 4 with experiments on a modular R2R machine that contains heat transfer rollers to verify the controller efficiency. In Chapter 5, tension observer is designed and implemented in a continuous annealing furnace; lamination process is modeled, and reference tension for individual webs and control strategy are developed for curl elimination. The summary of this dissertation and future work are presented in Chapter 6.

The following assumptions are made to facilitate the development of the heat transfer model and governing equations of tension dynamics in this dissertation:

1. The thermal expansion coefficient is independent of temperature.
2. The web does not expand along the thickness direction.
3. The temperature along the lateral direction is uniform.
4. The thicknesses of the web and the outer shell are small compared to the diameter of the heat transfer roller.

5. The web is elastic in certain temperature range.

6. The slip between the web and roller surfaces is not significant.

7. The web strain is very small.

8. The web tension and mechanical strain are uniform in a tension zone.

CHAPTER 2

MODELING OF TEMPERATURE DISTRIBUTION IN MOVING WEBS

To heat or cool a moving web through roll-to-roll processing machinery, thermal energy is usually introduced by three mechanisms [7]: Convection, in which the heat is transferred to the web by directing hot air, such as in an oven; Conduction, in which the heat is transferred to the web by direct contact with a heated/cooled surface, such as a heat transfer roller; Radiation, in which the heat is transferred by electromagnetic radiation to the web from electric heaters or gas burners. Heat transfer between the web and the heating source takes place in two regions of web transport: web wrapped on a heat transfer roller and the web span between two consecutive rollers. Heat transfer via conduction along the thickness is assumed inside the web material, but the mechanism of heat transfer varies with the surface conditions. For the surface heat transfer where the web and roller are in contact with each other, conduction is assumed together with a contact resistance model. For the web surface exposed to ambient air, the web on both sides is heated/cooled mainly by convection through the surrounding air. The radiation boundary condition (resulting from the use of radiative hot filaments in the vicinity of the web surface) may be approximated by a convection boundary condition [66].

Figure 2.1 shows a web transported on a heat transfer roller and a free web span. A heat transfer roller typically consists of an outer shell, an inner shell, and a liquid chamber between the two with channel separators for spiral flow of liquid between

the two shells from one end of the roller to the other end. Hot oil is pumped through the chamber for heating and chilled water for cooling. A picture of a typical double-walled, spiral baffled heat transfer roller is shown in Fig. 2.2.

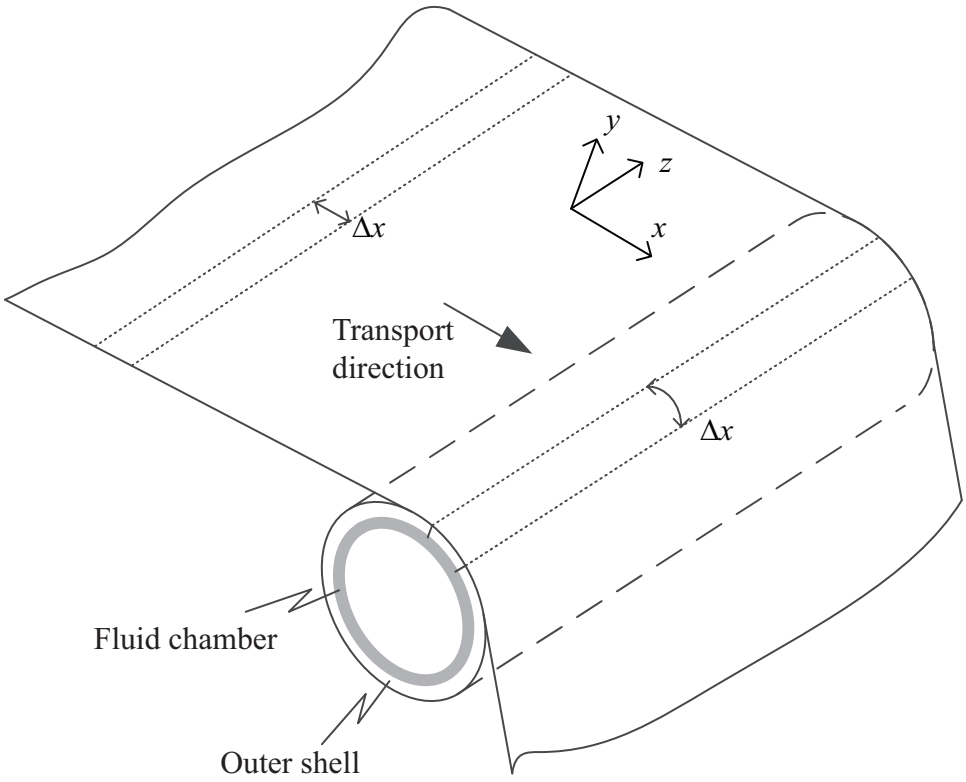

Figure 2.1: Web span and web wrapped on a heat transfer roller

A general heat transfer model for composite webs with any numbers of layers is developed and solutions are obtained for different heating/cooling boundary conditions in this chapter. The following assumptions are made to facilitate the development of the heat transfer model: (i) the thermal properties of web are independent of temperature, (ii) the web does not expand along the thickness direction (y-direction), (iii) the temperature along the lateral direction (z-direction) is uniform and (iv) the thicknesses of the web and the outer shell are small compared to the diameter of the heat transfer roller. Assumptions (i) and (ii) are applicable for those R2R processes

Figure 2.2: Picture of a heat transfer roller

where the physio-chemical (chemical reactions at heating) and thermo-mechanical (specific heat, thermal expansion coefficient, thermal conductivity, etc.) effects are not significant. The third assumption is reasonable if the liquid in the chamber is at a uniform temperature throughout, that is, the heating/cooling liquid is an ideal continuous steady heating/cooling source. The fourth assumption allows for the use of Cartesian coordinates in the region of wrap as well as the free span. Since the thickness of the web and the outer shell are assumed to be small compared to the web width, the heat flux gradient is the largest along the thickness direction. As a result heat transfer along the thickness direction is considered which may be modeled by a one-dimensional heat equation. Ignoring conduction along the length of the web is reasonable given the relatively low longitudinal thermal gradient as the ratio of thickness/length is small [66, 67]. Therefore, the heat transfer problem in the transport and thickness directions (x- and y-directions) are studied; the heat distribution in the web is assumed to be uniform across the width or lateral direction (z-direction).

2.1 Multi-layer Web Heat Transfer Model

For development of the model, consider a composite web with N layers as shown in Fig. 2.3. The thickness of the i^{th} layer is denoted by l_i and the y-axis coordinate of the boundary of the i^{th} and $(i+1)^{\text{th}}$ layers is denoted by h_i which means that $h_i = h_0 + \sum_{j=1}^{i} l_j$, and let $h_0 = 0$.

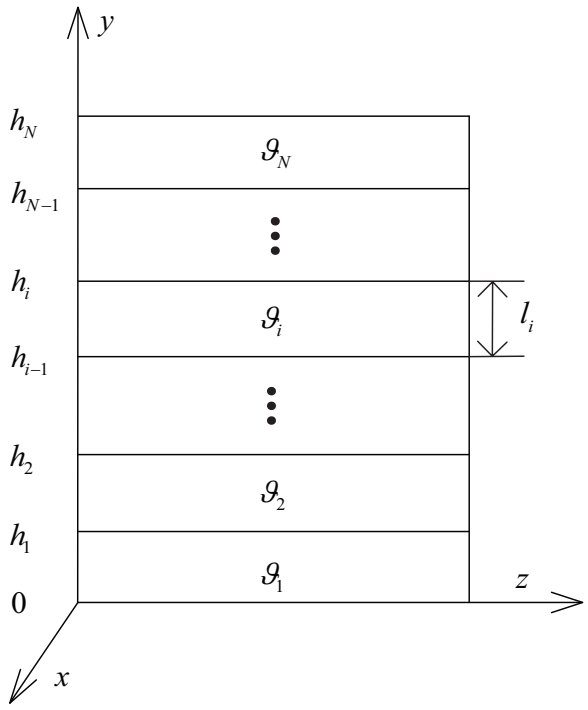

Figure 2.3: Multi-layer web sketch

The governing equations are given by

$$\frac{\partial \vartheta_i(y,\tau)}{\partial \tau} = \kappa_i \frac{\partial^2 \vartheta_i(y,\tau)}{\partial y^2}, \ h_{i-1} \le y \le h_i, \ \tau > 0, \tag{2.1}$$

where $i = 1, 2, \ldots, \ N$, κ is the web thermal diffusivity, and τ is the time period of heat transfer process at location x. In the following i takes values in the range of 1 through N unless explicitly specified. Regardless of the outer boundary conditions at $y = h_0$ and $y = h_N$, the boundary conditions at the inner layers, assuming ideal

contact between adjacent layers, are given by [15]

$$\vartheta_i(h_i,\tau) = \vartheta_{i+1}(h_i,\tau), \tag{2.2a}$$

$$k_i\frac{\partial\vartheta_i(h_i,\tau)}{\partial y} = k_{i+1}\frac{\partial\vartheta_{i+1}(h_i,\tau)}{\partial y}, \tag{2.2b}$$

where $i = 1, 2, \ldots, N-1$. In the following a procedure for computing the solution of the above governing equations is given as a function of the outer boundary conditions which will be specified later based on the different mechanisms that are employed to heat and cool the web.

The following standard form for the solution of the above governing equations is considered to facilitate the use of the separation of variables approach:

$$\vartheta_i(y,\tau) = U_i(y,\tau) + \psi_i(y). \tag{2.3}$$

This will allow for expressing the outer boundary conditions at $y = h_0$ and $y = h_N$ in homogeneous form. The transient solution, $U_i(y,\tau)$, and the associated inner boundary conditions are given by

$$\frac{\partial U_i(y,\tau)}{\partial\tau} = \kappa_i\frac{\partial^2 U_i(y,\tau)}{\partial y^2}, \tag{2.4}$$

and

$$U_i(h_i,\tau) = U_{i+1}(h_i,\tau), \tag{2.5a}$$

$$k_i\frac{\partial U_i(h_i,\tau)}{\partial y} = k_{i+1}\frac{\partial U_{i+1}(h_i,\tau)}{\partial y}. \tag{2.5b}$$

The steady-state solution, $\psi_i(y)$, is chosen as

$$\psi_i(y) = C_i y + D_i. \tag{2.6}$$

Substitution of Eqns. (2.3) and (2.6) in (2.1) and using Eqns. (2.4) and (2.5) results

in the following recursive constraints for C_i and D_i:

$$C_i = \frac{k_1}{k_i} C_1, \ i = 2, 3, \ldots, N, \tag{2.7a}$$

$$D_i = D_{i-1} + h_{i-1}(C_{i-1} - C_i), \ i = 2, 3, \cdots, N. \tag{2.7b}$$

As stated before, C_1 and D_1 in the above equations will be obtained later by using the outer boundary conditions at $y = h_0$ and $y = h_N$ based on type of mechanism used for web heating/cooling.

With the separation of variables,

$$U_i(y, \tau) = Y_i(y) T_i(\tau), \tag{2.8}$$

one can write the solution for $T_i(\tau)$ and $Y_i(y)$ as

$$T_i(\tau) = e^{-\lambda_i^2 \kappa_i \tau}, \tag{2.9a}$$

$$Y_i(y) = A_i \cos[\lambda_i (y - h_{i-1})] + B_i \sin[\lambda_i (y - h_{i-1})], \tag{2.9b}$$

where λ is the eigenvalues of each layer, and the recursive expressions for A_i and B_i may be obtained by substituting Eqns. (2.9) into (2.5). Denoting $A_i = dK_{Ai}$ and $B_i = dK_{Bi}$, where d is a constant, one can get the following recursive equations for K_{Ai} and K_{Bi}:

$$K_{A,i+1} = K_{A_i} \cos(\lambda_i l_i) + K_{B_i} \sin(\lambda_i l_i), \tag{2.10a}$$

$$K_{B,i+1} = \frac{-k_i K_{Ai} \lambda_i \sin(\lambda_i l_i) + k_i K_{Bi} \lambda_i \cos(\lambda_i l_i)}{k_{i+1} \lambda_{i+1}}, \tag{2.10b}$$

where $i = 1, 2, \cdots, N-1$. Again, the unknowns K_{A1} and K_{B1} are obtained using the outer boundary condition at $y = h_0$ and the eigenvalues $\beta^2 = \lambda_i^2 \kappa_i$ are obtained from the outer boundary condition at $y = h_N$.

The constant d is obtained as follows. From W_i defined by

$$W_i(y, \beta) = K_{Ai} \cos[\lambda_i (y - h_{i-1})] + K_{Bi} \sin[\lambda_i (y - h_{i-1})], \tag{2.11}$$

the existence of the following orthogonality condition can be shown [68]:

$$\sum_{i=1}^{N} \int_{h_{i-1}}^{h_i} \rho_i c_i W_i(y,\beta_m) W_i(y,\beta_n) dy = \begin{cases} 0, m \neq n, \\ M, m = n, \end{cases} \tag{2.12}$$

where M is a constant. For each β_n, there is a corresponding d_n given by

$$d_n = \frac{\sum_{i=1}^{N} \int_{h_{i-1}}^{h_i} \rho_i c_i U_i(y,0) W_i(y,\beta_n) dy}{\sum_{i=1}^{N} \int_{h_{i-1}}^{h_i} \rho_i c_i W_i^2(y,\beta_n) dy}, \ n \in \mathbb{N}. \tag{2.13}$$

Therefore, the temperature distribution in each web layer is given by

$$\vartheta_i(y,\tau) = \sum_{n=1}^{\infty} d_n W_i(y,\beta_n) e^{-\beta_n^2 \tau} + \psi_i(y), \tag{2.14}$$

where $h_{i-1} \leq y \leq h_i$ and $\tau > 0$ is the heat transfer period. Note that this solution doesn't specify the heating/cooling processes, i.e. the solution expressions are the same for both conditions.

The solution requires computation of K_{A1}, K_{B1}, C_1, D_1 and the eigenvalues, which will be obtained next for each set outer boundary conditions for different web heating/cooling mechanisms. The homogeneous forms of boundary conditions at either $y = h_0$ or $y = h_N$ are of: (i) the first kind, $U = 0$, (ii) the second kind, $\partial U/\partial y = 0$, and (iii) the third kind, $\pm k\frac{\partial U}{\partial y} = \gamma U$ where the sign is determined by direction of heat flow (positive for inlet and negative for outlet). The second kind (ii) is realized by bonding a thin film or patch electric heater to the surface, which is seldom used in R2R processing. Hence only the two homogeneous forms of the boundary conditions, (i) and (iii), and their combination are considered in the following subsections sections 2.1.1 to 2.1.3.

2.1.1 Web in a Span Between Consecutive Rollers (Convection + Convection Condition)

In the free web span between two consecutive rollers, a significant portion of the heat transfer takes place by convection between the web surface and the ambient air. The heat transfer coefficient γ is determined by the ambient flow around the web surface, and air jets are usually used to change the flow. Due to the thin thermal and hydrodynamic boundary layers formed on the web surface, the heat transfer coefficient associated with jet impingement is larger than for the web surrounded by steady air; air jets are often used to reduce the heating/cooling time (see Fig. 2.4, in which θ_u denotes the ambient air temperature).

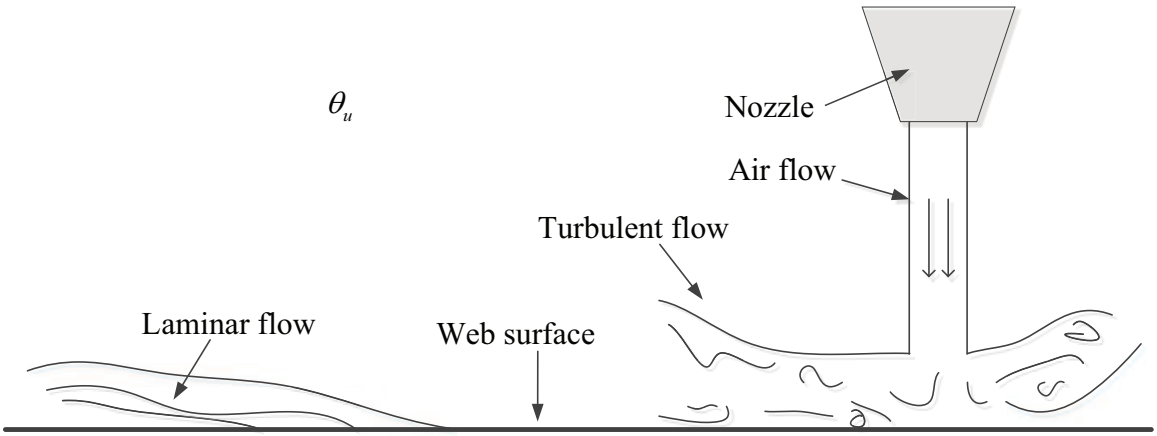

Figure 2.4: Convective heat transfer in web span

The outer boundary conditions for the web in the free span between consecutive rollers are

$$k_1 \frac{\partial \vartheta_1(h_0,\tau)}{\partial y} = \gamma_1[\vartheta_1(h_0,\tau) - \theta_{u1}], \tag{2.15a}$$

$$-k_N \frac{\partial \vartheta_N(h_N,\tau)}{\partial y} = \gamma_N[\vartheta_N(h_N,\tau) - \theta_{uN}]. \tag{2.15b}$$

To obtain homogeneous conditions at $y = h_0$ and $y = h_N$,

$$k_1 \frac{\partial U_1(h_0, \tau)}{\partial y} = \gamma_1 U_1(h_0, \tau), \tag{2.16a}$$

$$- k_N \frac{\partial U_N(h_N, \tau)}{\partial y} = \gamma_N U_N(h_N, \tau), \tag{2.16b}$$

one can solve for C_1 and D_1 required by (2.7), resulting in

$$C_1 = \frac{\gamma_1 \gamma_N \left(\theta_{uN} - \theta_{u1}\right)}{k_1\gamma_N + k_1\gamma_1 + \gamma_1\gamma_N h_N \frac{k_1}{k_N} + \gamma_1\gamma_N k_1 \sum_{i=1}^{N-1} h_i \left(\frac{1}{k_1} - \frac{1}{k_{i+1}}\right)}, \tag{2.17a}$$

$$D_1 = \frac{k_1 C_1 + \gamma_1 \theta_{u1}}{\gamma_1}. \tag{2.17b}$$

Then, substituting (2.8) and (2.9) into the homogeneous outer boundary condition at $y = h_0$ yields

$$K_{A1} = 1, \tag{2.18a}$$

$$K_{B1} = \gamma_1/(k_1\lambda_1). \tag{2.18b}$$

Now, K_{AN} and K_{BN} may be obtained using (2.10). Using these and the outer boundary condition at $y = h_N$, the following eigenfunction is obtained, which is used to calculate the eigenvalues:

$$\begin{aligned} &k_N K_{AN} \lambda_N \sin(\lambda_N l_N) - k_N K_{BN} \lambda_N \cos(\lambda_N l_N) \\ &= \gamma_N K_{AN} \cos(\lambda_N l_N) + \gamma_N K_{BN} \sin(\lambda_N l_N). \end{aligned} \tag{2.19}$$

2.1.2 Web Wrapped on a Heat Transfer Roller (Conduction + Convection Condition)

For the web wrapped and transported on a heat transfer roller, the temperature at the internal surface of the outer roller shell is assumed to be constant because of contact with the internal fluid which is at a steady temperature. Convective heat transfer between the outer web surface and ambient air is assumed (see Fig. 2.5). The two

outer boundary conditions for this case assuming the first layer to be the outer shell of the roller are

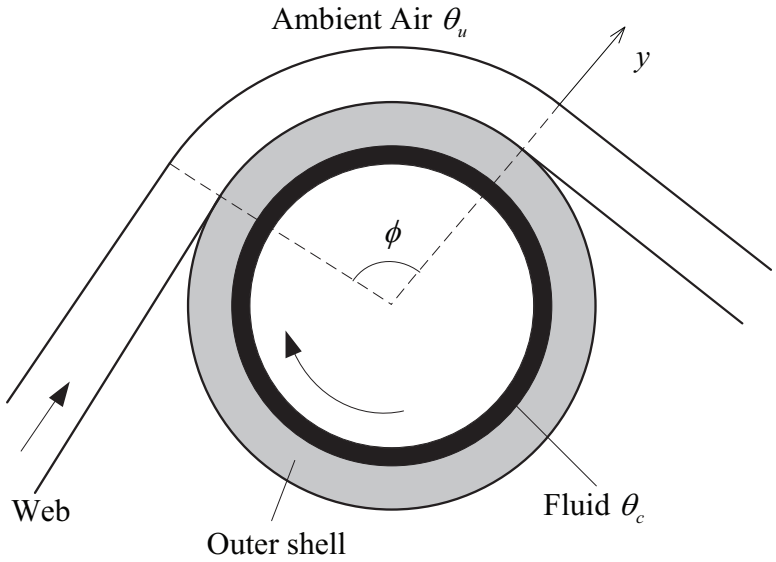

Figure 2.5: Web wrapped and transported on a heated/chilled roller

$$\vartheta_1(0,\tau) = \theta_c, \tag{2.20a}$$

$$-k_N \frac{\partial \vartheta_N(h_N,\tau)}{\partial y} = \gamma[\vartheta_N(h_N,\tau) - \theta_u]. \tag{2.20b}$$

The expressions for C_1 and D_1 to obtain the homogeneous conditions at $y = h_0$ and $y = h_N$ are

$$C_1 = \frac{\gamma(\theta_u - \theta_c)}{k_1 + \gamma h_N \frac{k_1}{k_N} + \gamma k_1 \sum_{i=1}^{N-1} h_i \left(\frac{1}{k_i} - \frac{1}{k_{i+1}}\right)}, \tag{2.21a}$$

$$D_1 = \theta_c. \tag{2.21b}$$

Then, substituting (2.8) and (2.9) into the homogeneous outer boundary condition at $y = h_0$ yields

$$K_{A1} = 0, \tag{2.22a}$$

$$K_{B1} = 1. \tag{2.22b}$$

Since the outer boundary condition at $y = h_N$ is the same as in the previous case, the form of the eigenfunction given by (2.19) is used to obtain the eigenvalues.

2.1.3 Web Between Two Nipped Rollers (Conduction + Conduction Condition)

This applies when both the web surfaces are in physical contact with constant temperature sources; an example is when the web is nipped between two heat transfer rollers (see Fig. 2.6). The two outer boundary conditions when the heat transfer on both web surfaces is due to conduction are

$$\vartheta_1(0, \tau) = \theta_{c1}, \tag{2.23a}$$

$$\vartheta_N(h_N, \tau) = \theta_{cN}. \tag{2.23b}$$

The expressions for C_1 and D_1 to obtain the homogeneous conditions at $y = h_0$ and

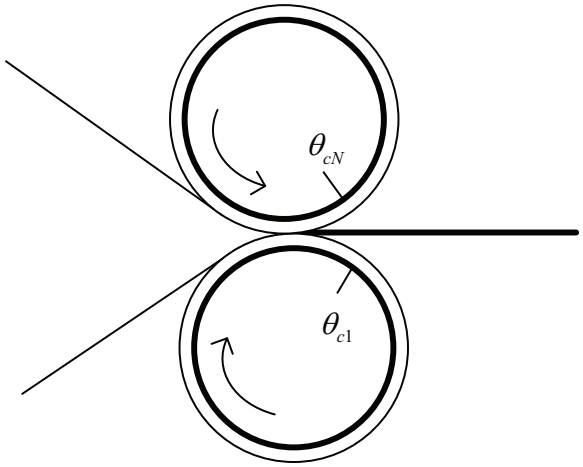

Figure 2.6: Web nipped between two heat transfer rollers

$y = h_N$ are

$$C_1 = \frac{\theta_{cN} - \theta_{c1}}{h_N \frac{k_1}{k_N} + k_1 \sum_{i=1}^{N-1} h_i \left(\frac{1}{k_i} - \frac{1}{k_{i+1}} \right)}, \tag{2.24a}$$

$$D_1 = \theta_{c1}. \tag{2.24b}$$

Then, substituting (2.8) and (2.9) into the homogeneous outer boundary condition at $y = h_0$ yields

$$K_{A1} = 0, \tag{2.25a}$$

$$K_{B1} = 1. \tag{2.25b}$$

The corresponding eigenfunction is

$$\tan(\lambda_N l_N) = -\frac{K_{AN}}{K_{BN}}, \tag{2.26}$$

which can be solved to obtain the following eigenvalues:

$$\lambda_N = \frac{\arctan\left(-\dfrac{K_{AN}}{K_{BN}}\right)}{l_N} + n\pi, n \in \mathbb{N}. \tag{2.27}$$

2.1.4 Model with Thermal Contact Resistance

In the above developments, perfect contact was assumed between layers. This assumption is reasonable for different web layers within the composite web as the layers are laminated together firmly, but may not be acceptable for the contact between the web and the roller shell. The contact resistance is introduced to account for the improper contact between surfaces; imperfect contact is illustrated in Fig. 2.7(a). Contact resistance can have a major effect on the effectiveness of heated rollers. The surface characteristics of the roughest surface generally determine the actual area of contact. Increasing pressure (web tension), smoother surfaces, and higher thermal diffusivity interstitial fluids increase the heat flow and decrease the contact resistance [34]. The value of the contact resistance is also a function of the amount of air entrained between the moving web and roller surfaces during transport. It will depend on the web material, roller surface finish, web tension, and web speed.

Between the roller shell and web surfaces, conduction through the contact spots is still the most significant heat transfer mechanism, but there is also radiation exchange as well as convection currents through the air gaps in the contacting surfaces. An actual contact is shown in Fig. 2.7(a) and all the mixed heat transfer effect is considered by using the contact resistance r.

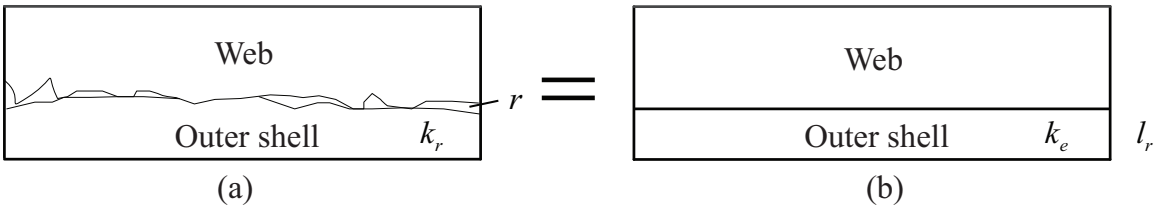

Figure 2.7: Web and roller surface contact: (a) Imperfect contact model, (b) Equivalent model

Since only the temperature distribution in the web is of concern, one can use an equivalent model, which assumes a perfect contact with modified shell thermal conductivity, as shown in Fig. 2.7(b). An equivalent thermal conductivity of shell is introduced which is obtained by equating thermal resistance of the two models, that is, $l_r/k_r + r = l_r/k_e$, which yields

$$k_e = \frac{l_r}{l_r/k_r + r}. \tag{2.28}$$

2.2 Special Cases of Single Layer Web Model

As examples of the general heat transfer model, two most common cases in industry with single layer web are presented in this section: the single layer web in a span between consecutive rollers and the single layer web wrapped on a heat transfer roller.

2.2.1 Temperature Distribution in a Single Layer Web Span Between Two Consecutive Rollers

The single layer web span between two consecutive rollers is simply a one layer case of Section 2.1.1 and usually has the same ambient temperature at both sides of the surfaces. Heat convection takes places at both surfaces. Using the solution (2.14) we obtain the temperature distribution in the web, eigenfunction equation, and coefficients as given by

$$\vartheta(y,\tau) = \sum_{n=1}^{\infty} d_n \left[\frac{k\lambda_n}{\gamma}\cos(\lambda_n y) + \sin(\lambda_n y)\right] e^{-\kappa\lambda_n^2\tau} + \theta_u, \tag{2.29}$$

$$\tan(\lambda l) = \frac{2\gamma k\lambda}{k^2\lambda^2 - \gamma^2}, \tag{2.30}$$

$$d_n = \frac{\int_0^l \left[\vartheta(y,0) - \theta_u\right]\left[\frac{k\lambda_n}{\gamma}\cos(\lambda_n y) + \sin(\lambda_n y)\right] dy}{\int_0^l \left[\frac{k\lambda_n}{\gamma}\cos(\lambda_n y) + \sin(\lambda_n y)\right]^2 dy}. \tag{2.31}$$

The plots of the right and left side of the eigenfunction equation with respect to λ are shown in Fig. 2.8.

2.2.2 Temperature Distribution in the Region of Single Layer Web Wrapped on a Heat Transfer Roller

The single layer web wrapped on a heat transfer roller is a two-layer case of Section 2.1.2. The bottom layer is the outer roller shell and the top layer is the web, and the bottom surface has the same temperature with the heating/cooling liquid, while heat convection takes place at the top surface. Using the solution (2.14) we obtain the temperature distributions in both the roller shell and the web, eigenfunction

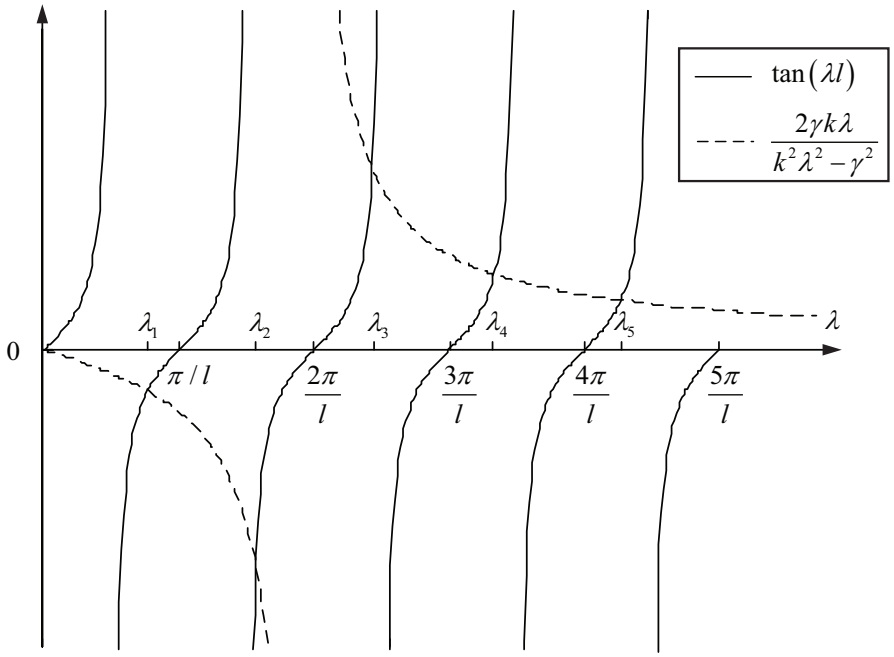

Figure 2.8: Graphs of $\tan(\lambda l)$ and $\dfrac{2\gamma k\lambda}{k^2\lambda^2-\gamma^2}$. The Abscissas of intersection are the solutions of λ

equation, and coefficients as given by

$$\vartheta_r(y,\tau) = \sum_{n=1}^{\infty} d_n[\tan(l_r\lambda_{rn})\cos(\lambda_{rn}y) + \sin(\lambda_{rn}y)]e^{-\beta_n^2\tau} + \frac{\gamma\theta_u - \gamma\theta_c}{k_r + \gamma l_w\dfrac{k_r}{k_w} + l_r\gamma}y + \theta_c + l_r\frac{\gamma\theta_u - \gamma\theta_c}{k_r + \gamma l_w\dfrac{k_r}{k_w} + l_r\gamma}, -l_r \le y \le 0, \tau \ge 0, \tag{2.32a}$$

$$\vartheta_w(y,\tau) = \sum_{n=1}^{\infty} d_n\frac{k_r}{k_w}\sqrt{\frac{\kappa_w}{\kappa_r}}\left[G(\beta_n)\cos\left(\lambda_{wn}y\right) + \sin\left(\lambda_{wn}y\right)\right]e^{-\beta_n^2\tau} + \frac{k_r}{k_w}\frac{\gamma\theta_u - \gamma\theta_c}{k_r + \gamma l_w\dfrac{k_r}{k_w} + l_r\gamma}y + \theta_c + l_r\frac{\gamma\theta_u - \gamma\theta_c}{k_r + \gamma l_w\dfrac{k_r}{k_w} + l_r\gamma}, 0 \le y \le l_w, \tau \ge 0, \tag{2.32b}$$

$$\tan\left(l_r\frac{\beta}{\sqrt{\kappa_r}}\right) = \frac{k_r}{k_w}\sqrt{\frac{\kappa_w}{\kappa_r}}G(\beta), \tag{2.33}$$

$$d_n = \frac{\rho_r c_r \int_{-l_r}^{0} U_r(y,0) E_{rn}(y) dy + \rho_w c_w \int_0^{l_w} U_w(y,0) E_{wn}(y) dy}{\rho_r c_r \int_{-l_r}^{0} E_{rn}^2 dy + \rho_w c_w \int_0^{l_w} E_{wn}^2 dy}, \tag{2.34}$$

where

$$G(\beta) = \frac{k_w \dfrac{\beta}{\sqrt{\kappa_w}} + \gamma \tan\left(l_w \dfrac{\beta}{\sqrt{\kappa_w}}\right)}{k_w \dfrac{\beta}{\sqrt{\kappa_w}} \tan\left(l_w \dfrac{\beta}{\sqrt{\kappa_w}}\right) - \gamma}, \tag{2.35}$$

and

$$E_{rn}(y) = \tan(l_r \lambda_{rn}) \cos(\lambda_{rn} y) + \sin(\lambda_{rn} y), -l_r \le y \le 0, \tag{2.36a}$$

$$E_{wn}(y) = \frac{k_r}{k_w} \sqrt{\frac{\kappa_w}{\kappa_r}} \left[G(\beta_n) \cos(\lambda_{wn} y) + \sin(\lambda_{wn} y) \right], 0 \le y \le l_w. \tag{2.36b}$$

The plots of the right and left side of the eigenfunction equation with respect to β are shown in Fig. 2.9.

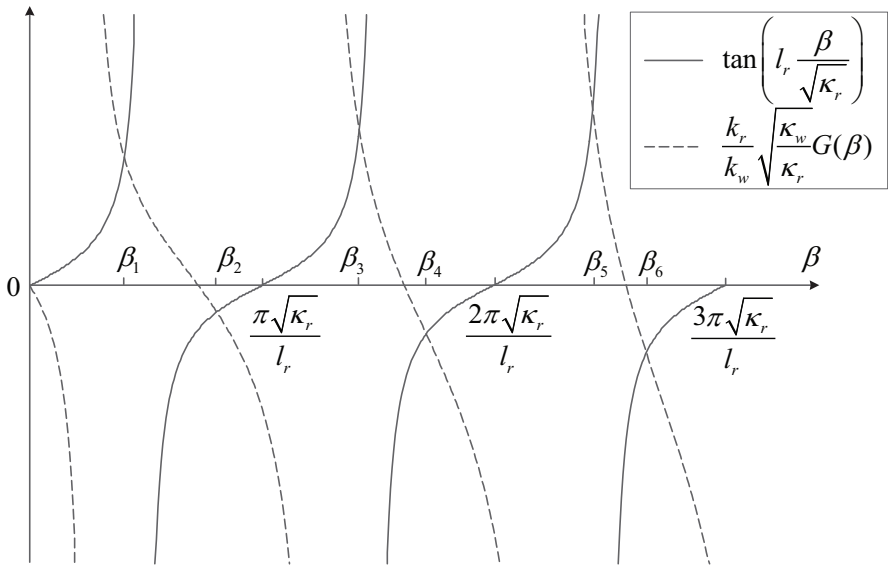

Figure 2.9: Graphs of $\tan\left(l_r \dfrac{\beta}{\sqrt{\kappa_r}}\right)$ and $\dfrac{k_r}{k_w}\sqrt{\dfrac{\kappa_w}{\kappa_r}} G(\beta)$. The abscissas of intersection are the solutions of β, and $G(\beta)$ is defined in (2.35)

2.3 Determination of Eigenvalues

The eigenvalues related to the model in the heat transfer problem are not easy to obtain, usually there is no closed-form expression available. A graphical method is typically used to estimate the eigenvalues, as shown in Fig. 2.8 and 2.9. However, in the graphical method, it is difficult to define "equal". If the numerical tolerance is large, we may miss some intersections; however, we may also have multiple results at one intersection if the tolerance is too small. For periodic functions, there is only one intersection inside each period, so a unique β_n can be found inside each period. However, this method cannot solve for the eigenfunctions which are not periodic.

In this section, a method that combines the value and the derivation of the eigenfunction is described. We study the eigenfunction $f(\beta) = 0$ and define intersections as those points $f(\beta)$ that cross the axis β.

Using a numerical method, some points are shown in Fig. 2.10, where the infinite length is chosen as $\Delta\beta$. If $f(\beta) = 0$, then β is one point we need. If at a point β, $f(\beta)$ and $f(\beta + \Delta\beta)$ have opposite signs, meanwhile $\dot{f}(\beta)$ and $\dot{f}(\beta + \Delta\beta)$ have the same signs (except 0), we can say that f has a zero crossing between β and $\beta + \Delta\beta$. For example, β_o is the zero point we need as $f(\beta_o) = 0$ as shown in the figure. $f(\beta)$ crosses a zero point between β_1 and $\beta_1 + \Delta\beta$ since $f(\beta_1)$ and $f(\beta_1 + \Delta\beta)$ have opposite signs, meanwhile $\dot{f}(\beta_1)$ and $\dot{f}(\beta_1 + \Delta\beta)$ have the same signs. However, for the point β_2, although $f(\beta_2)$ and $f(\beta_2 + \Delta\beta)$ have opposite signs, $f(\beta)$ does not have a zero point but only a pole between β_2 and $\beta_2 + \Delta\beta$, since $\dot{f}(\beta_2)$ and $\dot{f}(\beta_2 + \Delta\beta)$ have the opposite signs. The conditions are summarized in Tab. 2.1.

Once it is identified that there is only one zero point between β and $\beta + \Delta\beta$, the values of the eigenvalue β can be readily obtained based on many numerical root finder methods [69–71].

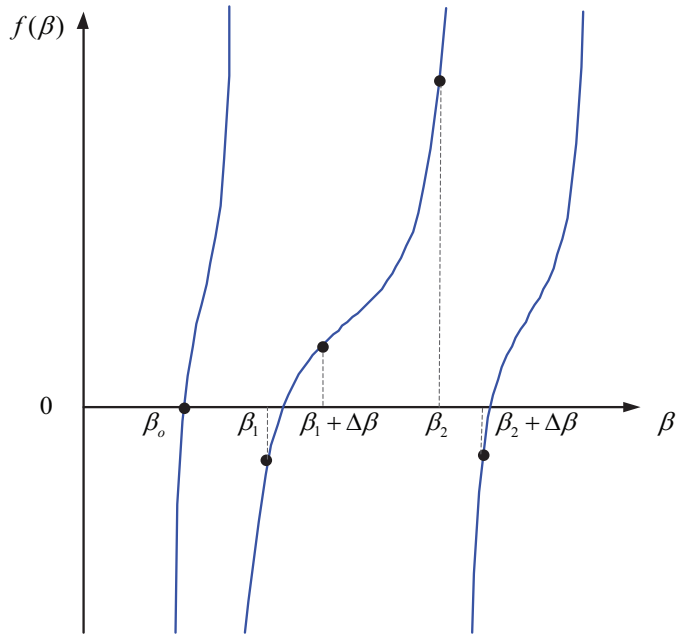

Figure 2.10: Sketch of intersections of eigenfunction $f(\beta) = 0$ and the β axis

Using the method in this section, one can always find the intersections without missing or duplicating them if the tolerance is small enough.

Table 2.1: Criterion of eigenfunction cross zeros point between β and $\beta + \Delta\beta$

Point	$f(\beta)$ and $f(\beta + \Delta\beta)$	$\dot{f}(\beta)$ and $\dot{f}(\beta + \Delta\beta)$
zero	opposite signs	same signs
pole	opposite signs	opposite signs
pole	opposite signs	both are 0

2.4 Determination of Heat Transfer Period

The temperature of the web in each region (ϑ) is a function of y and τ, where τ is the heat transfer period at x, which is different from the time variable t. Consider an infinitesimal slice of web traveling from $x = 0$ to $x = L$, and suppose it starts at $t = 0$. It is heated/cooled while moving, and the heat transfer time is clearly

$\tau = t$. This slice will reach longitudinal position x at time t_d and then passes x, but another slice of web will be at location x. Therefore, after t_d, the heat transfer time at x is determined by the time needed for a infinitesimal slice to travel from 0 to x. If we assume that there is no slip between the roller surface and the web surface, the velocity of the web wrapped on roller is the same as the peripheral velocity of the roller. Denote the web transport velocity on the roller surface by $v_r(t)$ and the velocity of the web in the free web span as $v_F(x_F, t)$. Consider the heat transfer process in a small volume element ΔV which is of length Δx as shown in Fig. 2.1. The distance traveled by a volume element in each region in a time period τ is given by

$$x = \int_{t-\tau}^{t} v(x,t)dt, \tag{2.37}$$

where $v(x,t)$ is either $v_r(t)$ or $v_F(x_F,t)$ depending on the region considered. Rewriting Eqn. (2.37) as $\tau = g(x,t)$, the equation for τ is given by

$$\tau(x,t) = \begin{cases} t, & t \le t_d, \\ g(x,t), & t > t_d. \end{cases} \tag{2.38}$$

Figure 2.11 highlights the procedure for obtaining the time t_d. For example, for a constant web speed $v = \bar{v}$, the expression for τ is

$$\tau(x,t) = \begin{cases} t, & t \le x/\bar{v}, \\ x/\bar{v}, & t > x/\bar{v}. \end{cases} \tag{2.39}$$

In most situations, the true transport velocity is not known in advance and is measured online, thus the form of $g(x,t)$ is unknown. To circumvent this problem, one can consider a numerical iterative procedure to determine the variable τ. The approach for this numerical method is illustrated in Fig. 2.12. First establish a vector of τ based on the axis of x. Suppose there are M intervals in a region of length L along

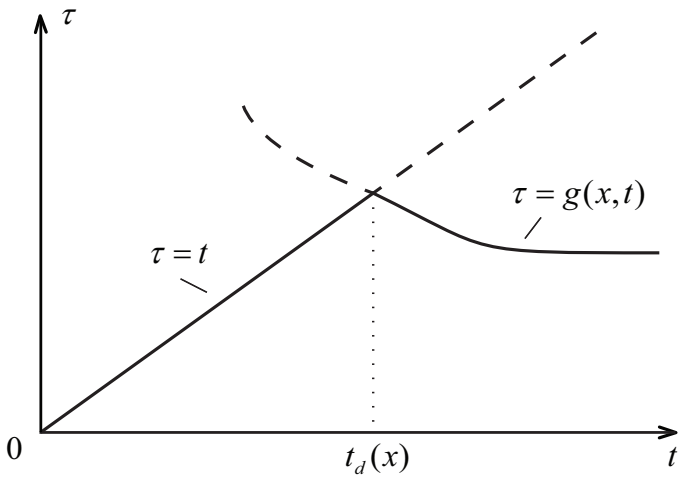

Figure 2.11: Graphs of $\tau(x,t)$, t_d is the abscissa of intersection of $\tau = t$ and $\tau = g(x,t)$

the x-axis, then $M = L/\Delta x$. Assume that at the beginning of the heating/cooling process the time in all the intervals is initialized to zero, so the value of τ in each interval is 0. After $t(1)$ seconds, $K(1)$ intervals enter this region and $K(1)$ intervals leave this region. The entering $K(1)$ intervals have not been heated/cooled yet, so the value of τ inside them are zero and the rest of the intervals have the heat transfer time $t(1)$. Then, after $t(2)$ seconds, $K(2)$ intervals enter this region and $K(2)$ intervals leave. Again, the entering $K(2)$ intervals have the value of 0 and the $K(1)$ intervals after them have been heated/cooled by $t(2)$ seconds, and all the left intervals have the value of $t(2) + t(1)$ (if $K(2) + K(1) \leq M$). Then, the procedure is repeated in this manner for $t(3)$, $t(4)$ and so on. In summary, in time $t(j)$, the form of the vector τ is given by

$$\tau\left[1 : K(j)\right] = 0; \tag{2.40a}$$

$$\tau\left[\sum_{i=j-p}^{i=j} K(i) + 1 : \sum_{i=j-p-1}^{i=j} K(i)\right] = \sum_{i=j-p}^{i=j} t(i), \tag{2.40b}$$

where $p = 0, 1, 2, \ldots, j-1$ and $K(0) = M$. The accuracy of the procedure is improved by choosing a small value for Δx.

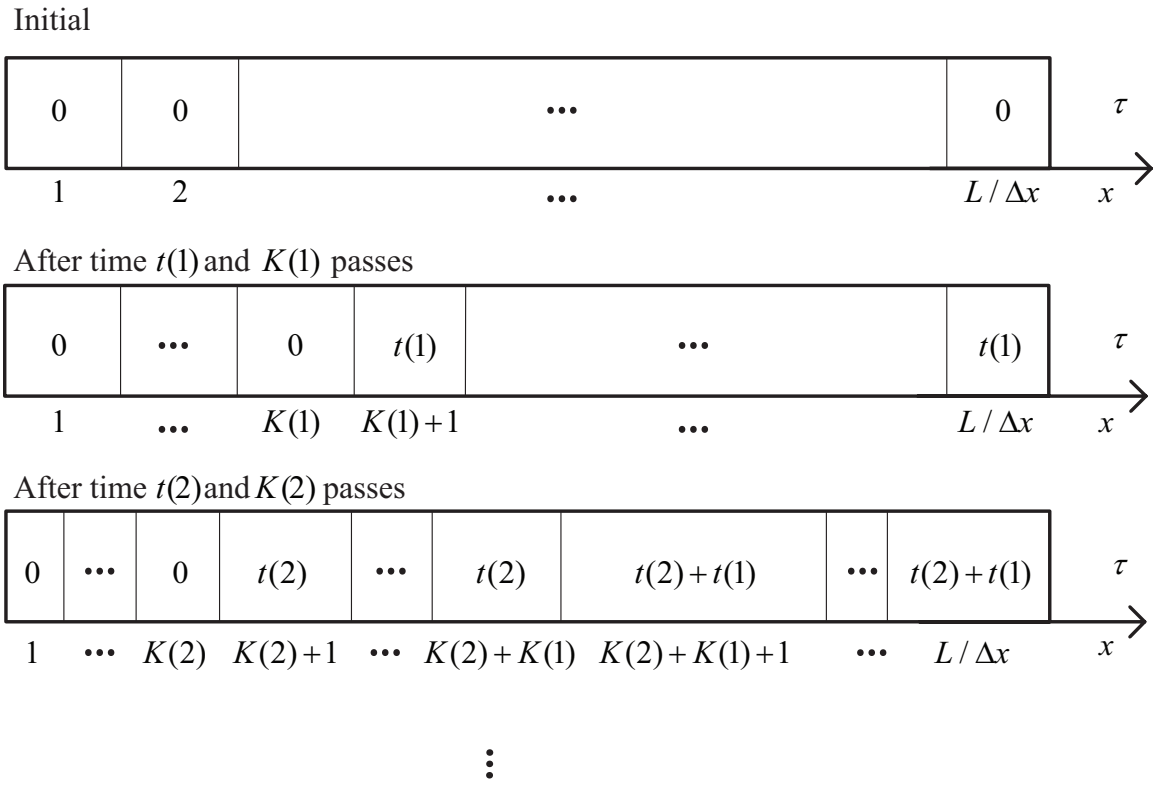

Figure 2.12: Illustration of numerical method to determine τ

One of the most important variables in the convection condition is the coefficient of heat transmission, γ, which could be determined from the Nusselt number, Nu. Although in both the cases when the web is inside the oven and surrounded by steady air the heating process is due to convection by external flow, Nu may vary significantly with different external flow configurations and orientations of the heated web (see Fig. 2.4). Nu is the ratio of convective to conductive heat transfer across the boundary layer, and the thickness and motion of the air boundary layer are determined by the Reynolds number, Re. In the following a procedure to obtain an expression for the coefficient γ in the two cases of the web inside the oven and the web surrounded by steady air is given. Then, an approximation of γ is given for the radiation condition.

2.5 The Coefficient of Heat Transmission of a Web Span Surrounded by Steady Air

For the span surrounded by steady air outside the oven, the air flow is forced by the speed of the web itself and is parallel to the flat web. A sketch of air boundary layer and the heat transfer plot is shown in Fig. 2.13, where x denotes the transport direction of the web. The boundary layer is a region of variable velocity of air built up between the web and the free fluid stream. This model can be applied also to the surface of wrapped web and roller, because the relative convection of surrounding air is forced by the movement of web and roller themselves, and the air flow is also parallel to the surfaces.

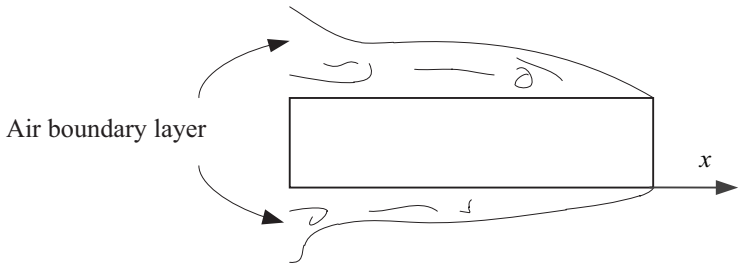

Figure 2.13: Web span surrounded in steady air

For this configuration of parallel flow over a flat plate, the characteristic length of web is the length of the span, L. Thus, the coefficient of heat transmission, γ, could be determined from the Nusselt number:

$$\gamma = \frac{\mathrm{Nu} k_u}{L}. \tag{2.41}$$

The thickness and motion of air boundary layer are determined by Re, which characterizes the relative influence of inertial and viscous forces in a fluid problem:

$$\mathrm{Re} = \frac{v_u x}{\nu}. \tag{2.42}$$

On a flat plate, the critical value of Re for flow to change from laminar regime to turbulent boundary layer is in the range of 3×10^5 to 5×10^5. However, in laboratory experiments the turbulent transition can appear also for Re $\approx 3 \times 10^6$. The above values of the critical Re are related only to flat surfaces [17]. If the surface is curved away from the flow (this may happen in most web handling processes, like the wrapped roller), turbulence might be triggered at much lower values of Re. The value of Nu depends on whether the air boundary layer is in laminar or turbulence state. However, it is difficult to determine the state of the boundary layer considering that the flow does not abruptly pass from laminar to turbulent for a particular value of Re, but this transition occurs gradually. An expression of Nu which can be utilized for both the air boundary layer states is provided in [72] as

$$\mathrm{Nu} = 0.45 + \left(0.3387 T^{1/2}\right) \left\{ 1 + \frac{(T/2600)^{3/5}}{[1 + (T_u/T)^{7/2}]^{2/5}} \right\}^{1/2}, \tag{2.43}$$

where

$$T \equiv \mathrm{RePr}^{2/3} \left[1 + \left(\frac{0.0468}{\mathrm{Pr}} \right)^{2/3} \right]^{-1/2}, \tag{2.44}$$

and T_u is any number between 10^5 and 10^7. An expression for the average Nusselt number can be utilized in the case that the exact value of T_u is difficult to obtain. This average expression is provided in [72], and it is given by

$$\overline{\mathrm{Nu}} = 0.45 + \left(0.6774 T^{1/2}\right) \left\{ 1 + \frac{(T/12500)^{3/5}}{[1 + (T_{um}/T)^{7/2}]^{2/5}} \right\}^{1/2}, \tag{2.45}$$

where $T_{um} \approx 1.875T$, and T is defined in Eqn. (2.44).

The expression for γ in (2.41) is obtained by replacing Nu with $\overline{\mathrm{Nu}}$ in (2.45).

2.5.1 The Coefficient of Heat Transmission of a Web Span Surrounded by Forced Air

Jets are usually employed to produce impinging turbulent air on the web to increase the rate of heat transfer. A sketch is provided in Fig. 2.14. Due to the thin thermal and hydrodynamic boundary layers formed on the web surface, the heat transfer coefficient associated with jet impingement is larger than the one obtained in the case of web surrounded by steady air.

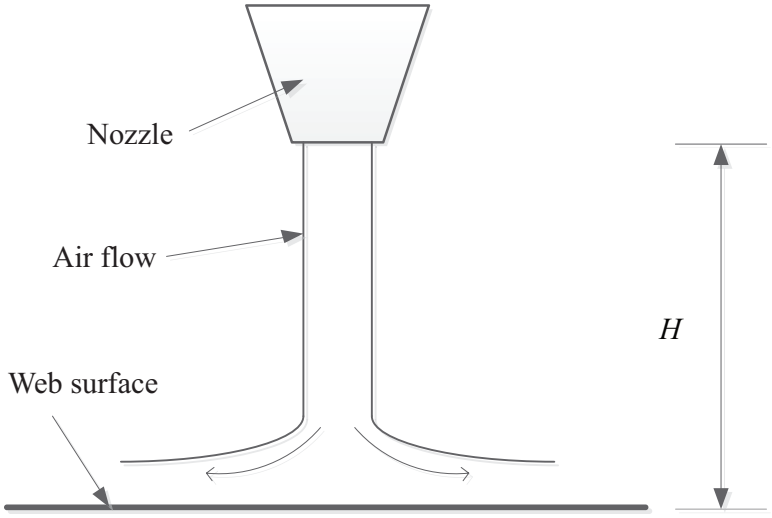

Figure 2.14: Configuration of jet impingement

The air flow is immersed in the same ambient medium, and typically the jet is turbulent at the nozzle exit and can be characterized by a nearly uniform axial velocity profile. The Reynolds number thus can be characterized by this uniform exit velocity [73]:

$$\mathrm{Re} = \frac{v_u D}{\nu}, \tag{2.46}$$

where D corresponds to the characteristic length of the web. An extensive review of heat transfer data for impinging gas jets is provided in [74], and it is suggested that

the following value be used:

$$\gamma = \frac{\mathrm{Nu}k_u}{D}. \tag{2.47}$$

In most cases, an array of slots is used instead of a single slot jet to obtain higher heat transmission coefficient. The configuration of the array is illustrated in Fig. 2.15 where the air flow spurted out from a series of parallel slot nozzles impinges the surface of the web. For the case of array of slot jets, the following average expression

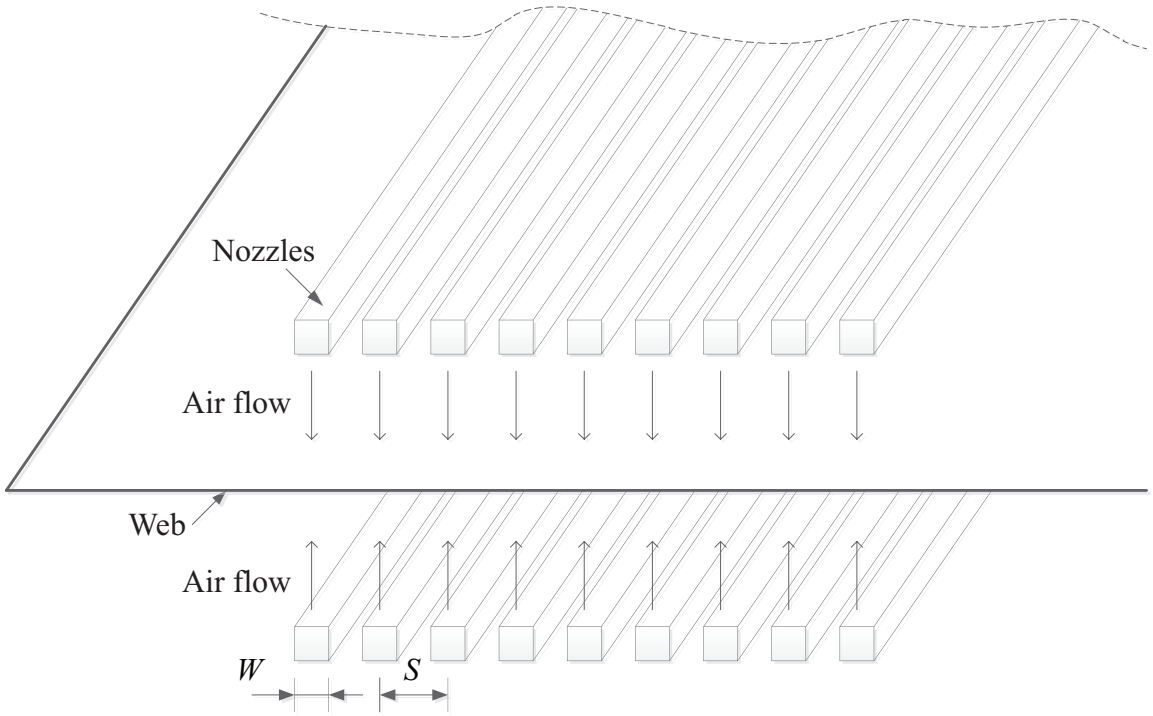

Figure 2.15: Slot jet array configuration

for Nu is provided in [75]:

$$\overline{\mathrm{Nu}} = \frac{2}{3} A_{r,0}^{3/4} \left(\frac{2\mathrm{Re}}{A_r/A_{r,0} + A_{r,0}/A_r} \right)^{2/3} \mathrm{Pr}^{0.42}, \tag{2.48}$$

where

$$A_{r,0} = \left[60 + 4\left(\frac{H}{2W} - 2\right)^2\right]^{-1/2},$$
$$A_r = \frac{W}{S},$$

and Re is obtained using $D = 2W$. The expression for the coefficient γ can be obtained by substituting (2.48) into (2.47).

2.5.2 The Coefficient of Heat Transmission of a Web Heated by Radiation

The radiation effect was omitted in all the previous studies, since it is not obvious for ordinary web or roller. Industries usually place some radiation panels in the process line, parallel to the web. This can be approximated, and classified into the convective boundary condition.

The heat transfer by radiation involves transfer of energy by electromagnetic waves, and the boundary condition is given by

$$-k_w \frac{\partial \vartheta}{\partial y} = \epsilon\varsigma(\vartheta^4 - \theta_u), \tag{2.49}$$

where the temperatures are in Kelvin. This is a nonlinear boundary condition and is typically used in numerical simulations. In a typical environment, the radiation effect is not so significant as in vacuum, thus the boundary condition may be approximated by the first linear term of the Taylor series [66]:

$$-k_w \frac{\partial \vartheta}{\partial y} = 4\epsilon\varsigma\theta_u^3(\vartheta - \theta_u). \tag{2.50}$$

This is mathematically equivalent to the convection boundary condition with

$$\gamma = 4\epsilon\varsigma\theta_u^3. \tag{2.51}$$

The radiator panels are usually placed parallel to the web. For parallel bodies with emissivity ϵ_1 and ϵ_2 respectively, the formula to compute ϵ is

$$\epsilon = \frac{\epsilon_1 \epsilon_2}{\epsilon_1 + \epsilon_2 - \epsilon_1 \epsilon_2}. \tag{2.52}$$

2.5.3 Viscosity and Thermal Conductivity of Air

In order to compute γ in (2.41), (2.47) and (2.51), viscosity and thermal conductivity of air are needed. The following gives a brief summary of computing theses values.

The expression for the viscosity of air is given by [76]

$$\nu = \nu^0(\theta_u) + \nu^r(T, \delta), \tag{2.53}$$

where ν^0 is the dilute gas viscosity, ν^r is the residual gas viscosity, $T = 132.6312/\theta_{ui}$, and $\delta = \rho_u/302.9833$. The dilute gas viscosity is given by

$$\nu^0(\theta_u) = \frac{1.108477 \times 10^{-6}\sqrt{\theta_{ui}}}{\Omega(\theta_u^*)}, \tag{2.54}$$

where $\theta_u^* = \theta_u/103.3$ is the Lennard-Jones energy parameter, and Ω is the collision integral given by

$$\Omega(\theta_u^*) = \exp\left(\sum_{i=0}^{4} b_i [\ln(\theta_u^*)]^i\right). \tag{2.55}$$

The values of the coefficients b_i are given in Tab. 2.2. The residual gas viscosity is given by

$$\nu^r(T, \delta) = \sum_{i=1}^{n} N_i T^{\xi_i} \delta^{d_i} \exp(-\Gamma_i \delta^{\mu_i}), \tag{2.56}$$

where Γ_i is zero when μ_i is zero and one when μ_i is not zero, and the values of the coefficients N_i, ξ_i, d_i and μ_i are given in Tab. 2.3.

The thermal conductivity of air is expressed as a function of temperature and density:

$$k_u = k_u^0(\theta_u) + k_u^r(T, \delta), \tag{2.57}$$

Table 2.2: Coefficients of the collision integral equation (2.55)

i	b_i
0	0.431
1	-0.4623
2	0.08406
3	0.005341
4	-0.00331

where k_u^0 is the dilute gas thermal conductivity, k_u^r is the residual fluid thermal conductivity, $T = 132.6312/\theta_u$, and $\delta = \rho_u/302.9833$.

Table 2.3: Coefficients and exponents of the residual air viscosity equation (2.56)

i	N_i	ξ_i	d_i	μ_i
1	10.72	0.2	1	0
2	1.122	0.05	4	0
3	0.002019	2.4	9	0
4	-8.876	0.6	1	1
5	-0.02916	3.6	8	1

The dilute gas conductivity is given by

$$k_u^0 = N_1 \nu^0(\theta_u) + N_2 T^{\xi_2} + N_3 T^{\xi_3}, \tag{2.58}$$

where ν^0 is the dilute gas viscosity described previously, and the coefficients N_i, ξ_i, d_i and μ_i are given in Tab. 2.4. The residual gas conductivity is given by

$$k_u^r = \sum_{i=4}^{n} N_i T^{\xi_i} \delta^{d_i} \exp(-\Gamma_i \delta^{\mu_i}), \tag{2.59}$$

where $\Gamma_i = 0$ when μ_i is zero and $\Gamma_i = 1$ when μ_i is not zero, and the remaining coefficients are given in Tab. 2.4.

Table 2.4: Coefficients and exponents of the residual air thermal conductivity equation (2.59)

i	N_i	ξ_i	d_i	μ_i
1	1.308			
2	1.405	-1.1		
3	-1.036	-0.3		
4	8.743	0.1	1	0
5	14.76	0.0	2	0
6	-16.62	0.5	3	2
7	3.793	2.7	7	2
8	-6.142	0.3	7	2
9	-0.3778	1.3	11	2

2.6 Summary

A model for the multi-layer temperature distribution in moving webs for different heating/cooling sources is developed in this chapter. This heat transfer model is useful for determining the evolution of the web temperature as it is transported through sections of the web process line where heating/cooling operations are performed on the web. All kinds of heat transfer processes pertaining to the heating/cooling of a moving web are classified into two scenarios: the web wrapped on a heat transfer roller and the web span between two consecutive rollers. The special cases of single layer web heat transfer is also presented in this chapter as they are commonly used in industry. Formulas are given to compute heat transmission under different heating/cooling situations (by steady air, forced air, or radiation).

CHAPTER 3

APPLICATIONS OF TEMPERATURE DISTRIBUTION MODEL

Evaluation of the temperature distribution model on two R2R machine configurations that involve heating/cooling is discussed in this chapter. The first line is an industrial coating and fusion process line, and the second line is an experimental R2R platform for atomic/molecular layer deposition. Model simulations are conducted together with comparison of the model output with the measured data from the coating and fusion line.

3.1 Coating and Fusion Process Line

To evaluate the developed models, model simulation results are compared with experimental data obtained on a production R2R coating and fusion process machine which is used to manufacture flooring materials in web form. In this production R2R machine, the base layer (felt) is first coated by a layer of gel followed by a layer of another clear coating. Then a desired pattern is embossed on the clear coat side of the composite web. The sequential structure of the coating and fusion process machine is illustrated in Fig. 3.1. Measured temperature data were collected for two situations: a heat transfer roller after gel coating and in the embossing section. Corresponding model simulations were conducted for these two situations.

The thermal properties and thickness of the three web layers and the shell of the heat transfer roller are given in Tab. 3.1. The shell of the heat transfer roller is

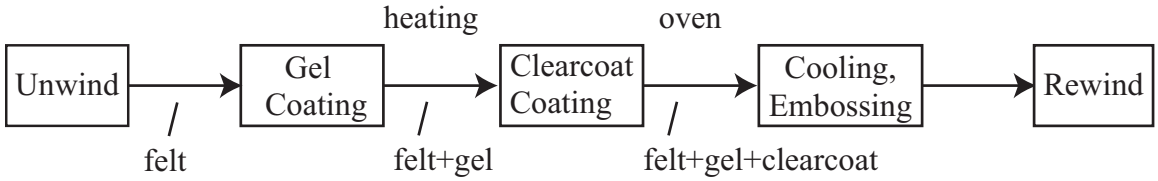

Figure 3.1: Schematic of a coating and fusion process line

made of ASTM A515 grade 55 carbon steel. Felt web materials are made of a mix of Cellulose, Limestone and Styrene-Butadiene-Rubber (SBR) latex. Gel is made of a mix of Polyvinyle Chloride (PVC), Di-Iso Phenyl Pthalate, Limestone, Titanium Dioxide and other process aids. The contact resistance (R) between shell and web is considered to be 0.003 m^2K/W, which is in the range of values suggested in [77, 78]. The heat coefficient of steady room air is taken as 1.7 $W/(m^2K)$. The web width is 3.7 m and transport speed is 0.41 m/s (80 feet per minute). The first 100 eigenvalues are considered in all model simulations.

Table 3.1: Properties of each layer of web and oil drum outer shell

Layer	ρ (kg/m^3)	k ($W/(mK)$)	c ($J/(kg \cdot K)$)	l (mm)
Shell	7850	52	470	12.7
Felt	1072.5963	0.14	2200	0.7112
Gel	1334.8634	0.19	1000	0.2337
Clearcoat	648.2288	0.05	3500	0.1061

3.1.1 Heat Transfer Roller

A heat transfer roller within a section of the R2R machine between the gel and clearcoat coating rollers is considered for temperature measurements and model evaluation. Also, this is the most accessible heat transfer roller in the machine for instru-

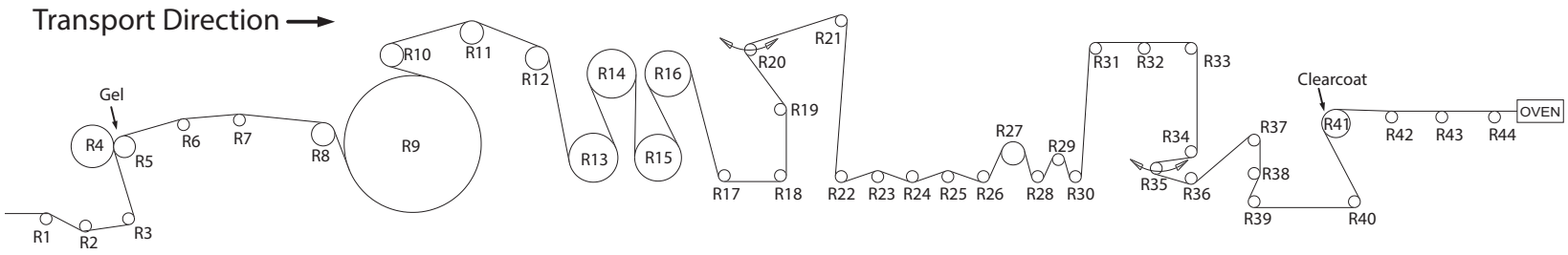

Figure 3.2: Gel and clearcoat section of the R2R machine

menting temperature sensors around the circumference of the roller. A line sketch of this section is shown in Fig. 3.2; R4 is the gel coater, R41 is the clear layer coater, and R9 is the heat transfer roller. Dynamics and friction of the rollers are not considered in the temperature distribution simulation. A sketch of the heat transfer roller (R9) with the transported web around it is shown in Fig. 3.3. The sketch also shows the location of the three temperature sensors labeled as S1, S2 and S3. Hot oil is pumped through the chamber of the heat transfer roller to heat the shell. As the gel layer touches the surface of the heat transfer roller, the sensors at S1, S2 and S3 measure the surface temperature of the felt layer. The outer diameter of the heat transfer roller is 2 m and the angle of wrap of the web around the roller is 286°. The temperatures of the hot oil, ambient air and web before reaching the heat transfer roller surface are 450K (177°C), 297 K (24°C) and 297 K, respectively.

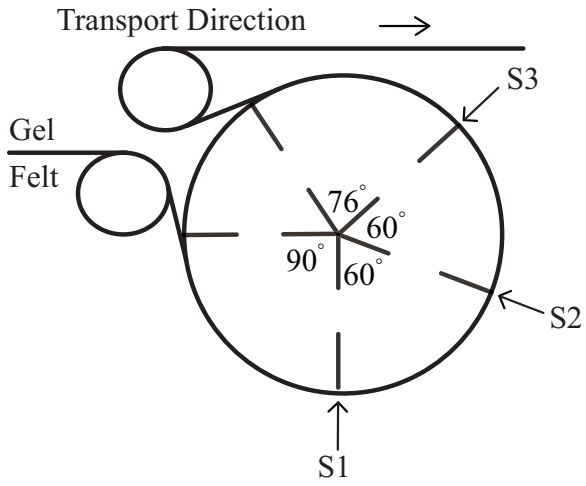

Figure 3.3: Heat transfer roller with wrapped web and temperature sensors

The temperatures of the web measured using the three sensors and model simulations with and without contact resistance are shown in Fig. 3.4. The evolution of temperature measured at S1, S2 and S3 are also shown for thirty minutes in Fig. 3.5. The variations in the recorded temperature are shown as solid bars in Fig. 3.4. It

is evident that the results from model simulations can predict measured data well, and the model simulation data using the contact resistance model is closer to the measured data than the one without considering contact resistance. Figure 3.6 shows the temperature profile for different thicknesses of the multi-layer web.

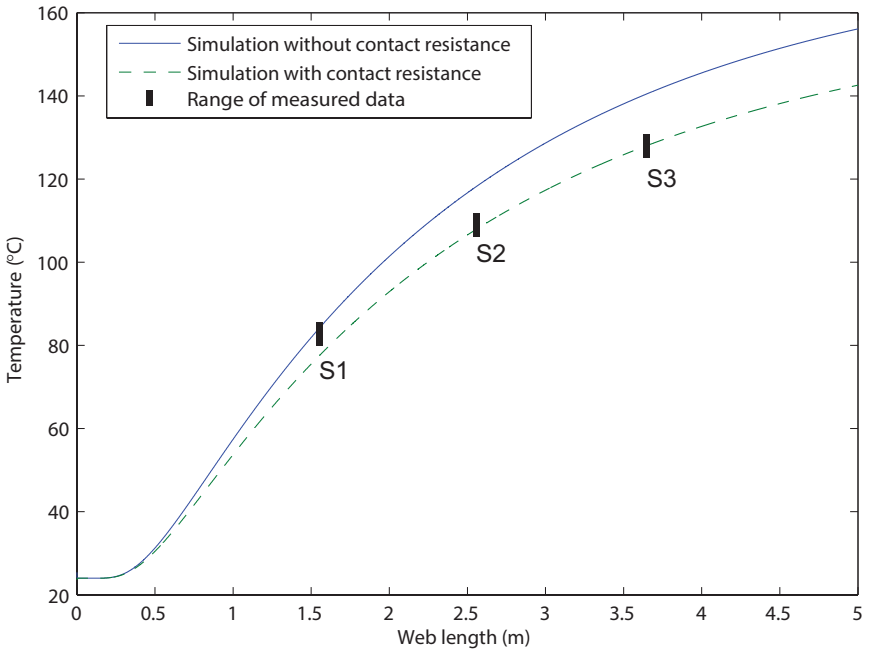

Figure 3.4: Web temperature profile from model simulations and experiments with the heat transfer roller

3.1.2 Embossing Section

The embossing section of the R2R machine is employed to emboss a particular pattern on the clearcoat layer of the multi-layer web. Radiation heating is employed for heating the clearcoat layer prior to being transported over the embossing roller. The embossed web is subsequently cooled by chilled rollers to bring the web to the room temperature prior to winding it onto a roll. Figure 3.7 shows a line sketch of the embossing section where rollers 2, 3, 9, 14, 15, 16 and 17 are heat transfer rollers.

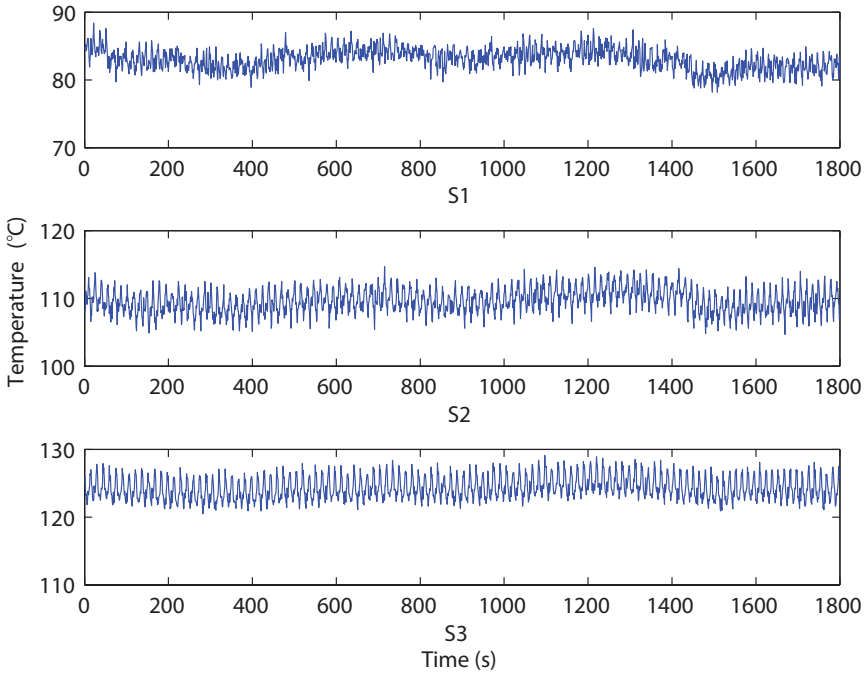

Figure 3.5: Evolution of temperature at S1, S2 and S3 from experiments with the heat transfer roller

Model simulations were conducted for the embossing section shown to evaluate the temperature distribution in the web as it is transported through this section. Two infrared temperature sensors at locations A and B are used to measure web temperature. The diameter of the various rollers, wrap angles, span lengths, and fluid temperature in the heat transfer rollers are given in Tab. 3.2. In the radiation zone between roller R5 and R7, the clearcoat surface of the web is heated by hot filaments which changes the heat transfer coefficient between web and air in that zone. The temperature of the web coming out of the oven and at the beginning of the embossing section is 450K (177°C). The fluid temperature in each of the heat transfer rollers is indicated in the Tab. 3.2 and the set point temperature for the hot filaments of the radiator is 700K (427°C).

Figure 3.8 shows the web temperature as it is transported through the embossing

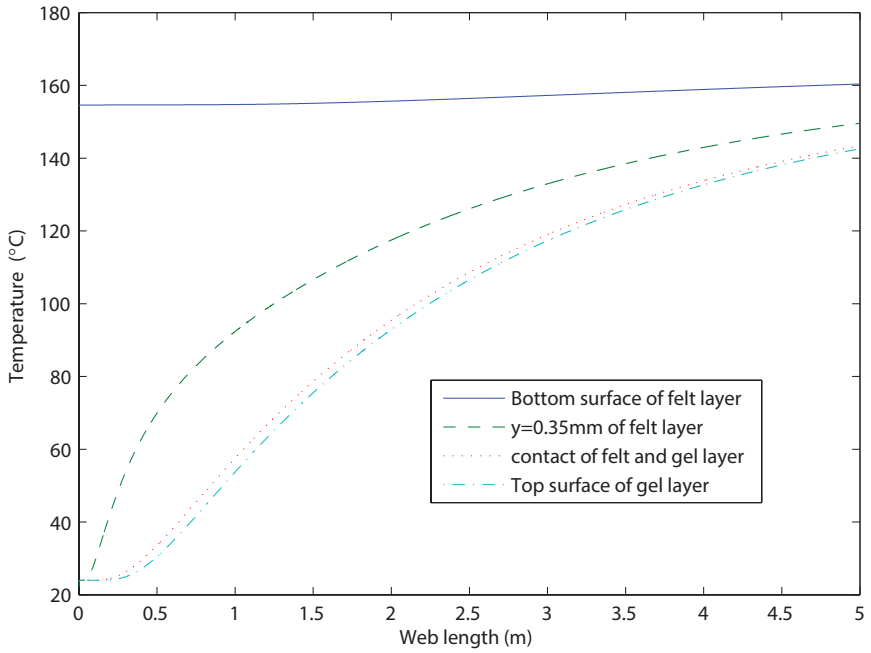

Figure 3.6: Simulation of temperature at different web thicknesses wrapped on the roller

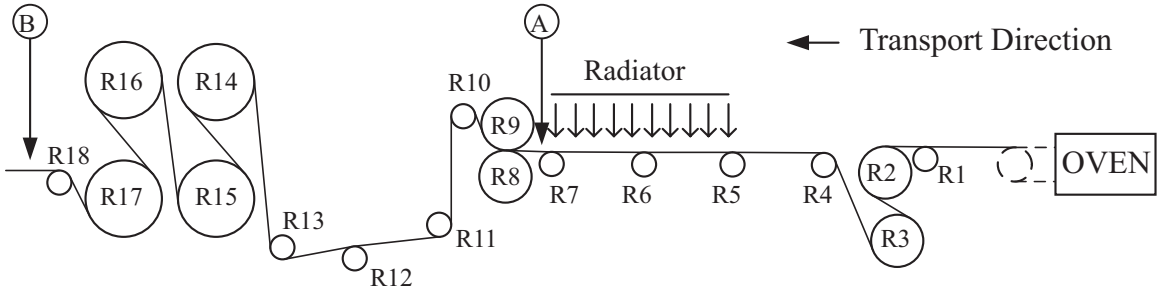

Figure 3.7: A heating/cooling section of an embossing process line with infrared temperature sensors A and B

Table 3.2: Parameters of a heat transfer section of the embossing line

Roller No.	Diameter (m)	Wrap Angle (°)	Span Length (m)	Fluid Temp (°C)
1	0.254	0	0.457	
2	0.610	152	0.483	90
3	0.610	219	1.143	10
4	0.254	67	1.067	
5	0.254	0	1.016	
6	0.254	0	1.041	
7	0.254	0	0.508	
8	0.584	0	NIP	
9	0.584	50	0.279	10
10	0.254	145	1.092	
11	0.254	87	0.965	
12	0.254	5	0.838	
13	0.254	97	1.930	
14	0.890	217	0.991	18
15	0.890	222	1.397	18
16	0.890	216	0.991	18
17	0.890	184	0.432	18
18	0.279	65	NA	

section. The range of measured temperature at locations A and B are shown in addition to the model simulation result for the entire section. Overall, the web is cooled in this section because the temperature of the web decreases steadily as it is transported through the section, except in the region with the radiator just prior to the embosser. The temperature of the web cooled by the chilled rollers decreases much faster when compared to the free web span due to the higher heat transfer by conduction to the chilled rollers. Notice that although Rollers 14 to 17 have the same source fluid temperature, the temperature variations in the web are different. This is due to the decrease in the temperature difference between the web and the rollers.

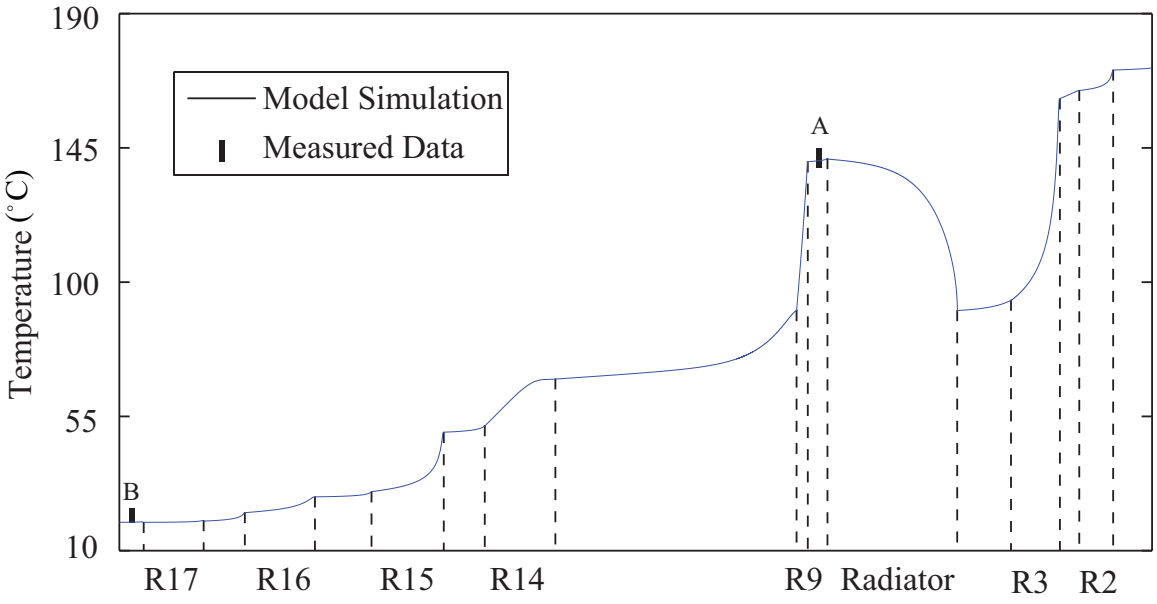

Figure 3.8: Top layer temperature of web in the heating/cooling section of the embossing line

3.2 Roll-to-Roll Machine for Atomic/Molecular Layer Deposition

In batteries manufacturing, to enhance the cycling stability of cathode material, the Atomic/Molecular Layer Deposition method is used to deposit ultrathin and highly

conformal anode coatings onto cathode material [79].

Figure 3.9 shows a web path layout of ALD/MLD machine. The base layer is passing through parallel infrared heating panels to reach desired temperature, and then the electrical material is deposited on the base layer in gas reactor. The infrared

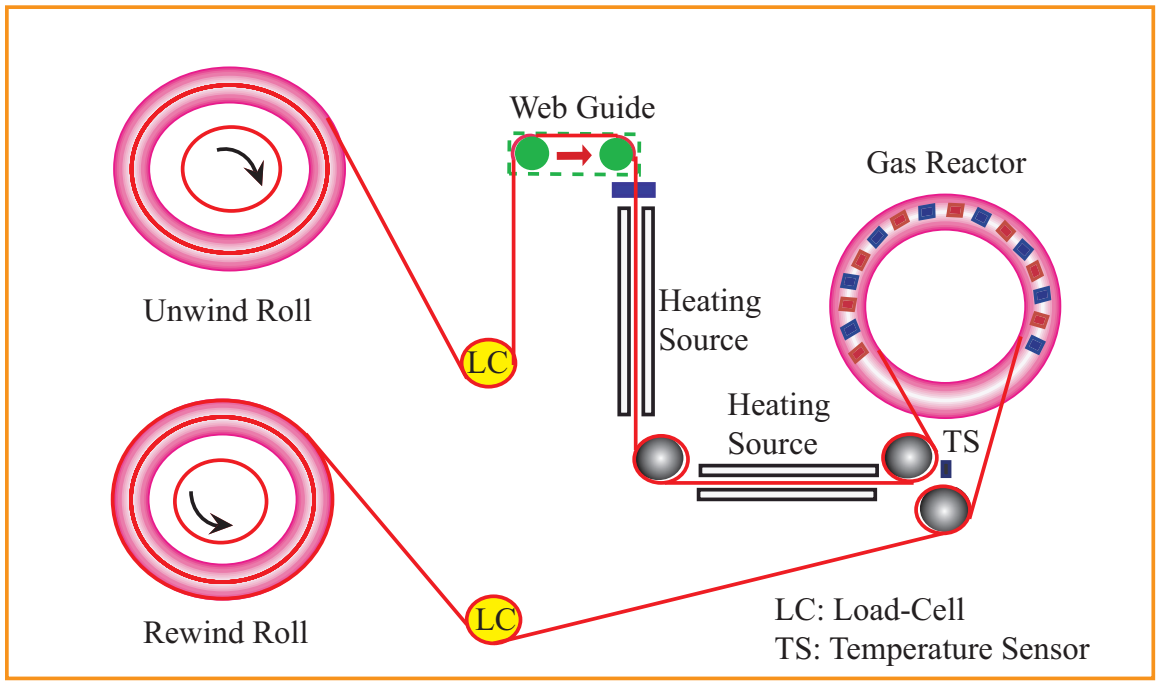

Figure 3.9: ALD/MLD machine web path layout

panel heaters are used parallel to the web to provide steady, uniform heat source. The heated web length is set to be 0.76 m, the distance between the radiator and the first slit of the gas reactor is set to be 0.24 m, and the radiator emissivity is about 0.66. The object is to raise the temperature of top layer web from the room temperature 23 °C to 120 °C before reaching the gas reactor, and the line speed is set to be 20 m/min. Three sets of web materials are simulated: (1) cathode film laminated of Aluminum foil and Nickel-Manganese-Cobalt (NMC), (2) anode film laminated of Copper foil and Graphite, (3) single layer Kapton film. The properties of each layer are shown in Tab. 3.3. In order to design the length of heating radiator, both single radiator and

dual radiators design are simulated and compared.

Table 3.3: Properties of each layer in R2R ALD/MLD machine

Layer	Thermal conductivity k (W/(mK))	Specific heat c (J/(kg · K))	Density ρ (kg/m^3)	Thickness l (micron)	Emissivity ϵ
Al foil	205	910	2700	17	0.04
NMC	12.5	430	8300	80	0.4
Cu foil	401	386	8960	22	0.05
Graphite	380	846	1500	80	0.95
Kapton	0.12	1090	1420	75	0.78

Figure 3.10 shows the average temperature of NMC layer along the web length, the temperature increases in the range of heating radiators, and drops after heating due to convection with ambient room air. It shows that setting the radiator temperature as 420 °C can achieve the goal, the final temperature before reaching the gas reactor is above 120 °C, for both single radiator and dual radiators cases. Similar results are shown in Fig. 3.11 and Fig. 3.12, and the radiator temperature for anode and Kapton films are 280 °C and 250 °C respectively.

3.3 Summary

Temperature distributions are simulated in two machine lines: coating and fusion process line and Atomic/Molecular Layer Deposition machine. In the coating and fusion process line, heating and cooling processes are simulated and compared with experiment results. In the ALD/MLD machine, temperature distribution is simulated to design the length and heating temperature of radiator.

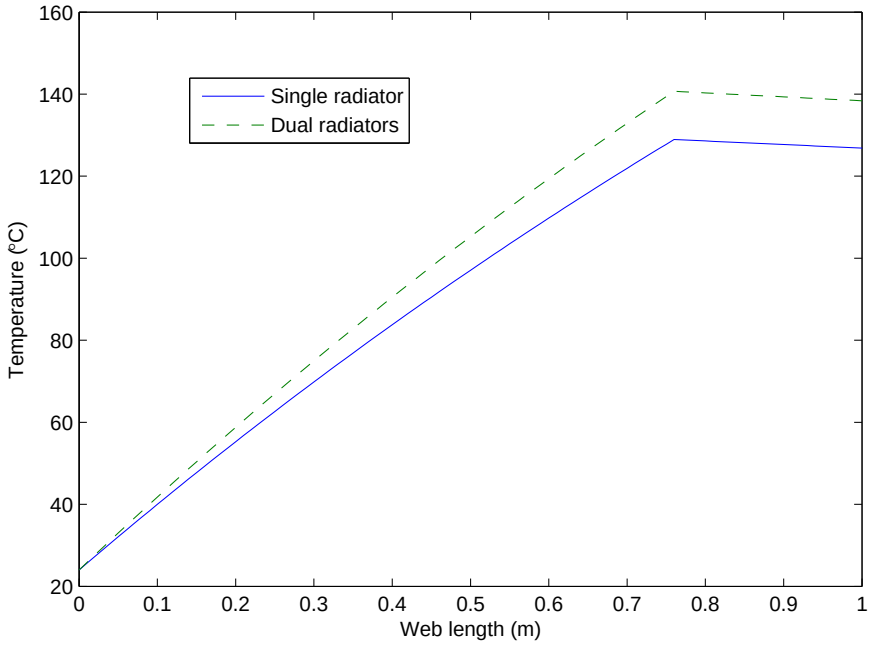

Figure 3.10: Simulation of the average temperature of NMC layer with radiator of 420 °C

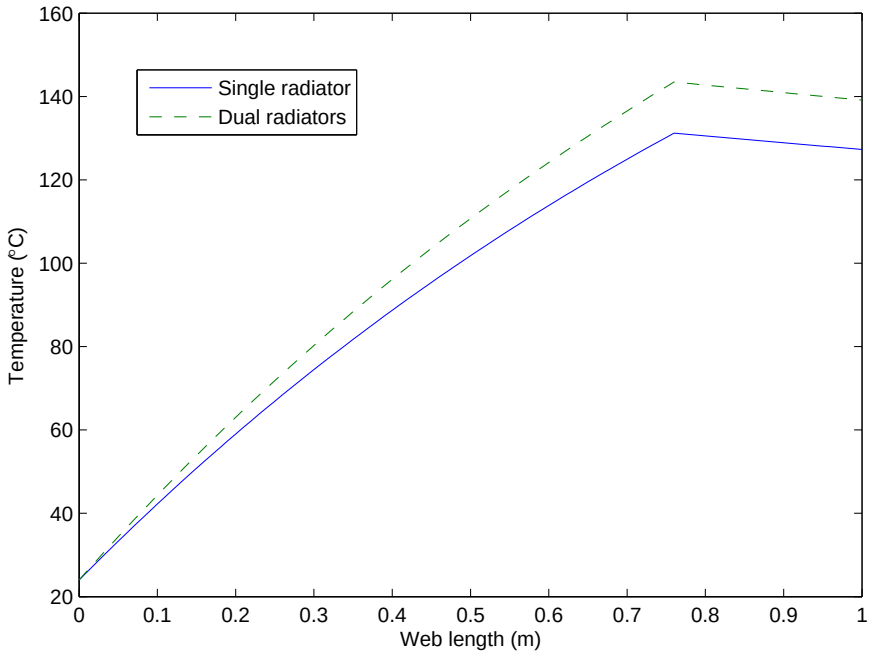

Figure 3.11: Simulation of the average temperature of graphite layer with radiator of 280 °C

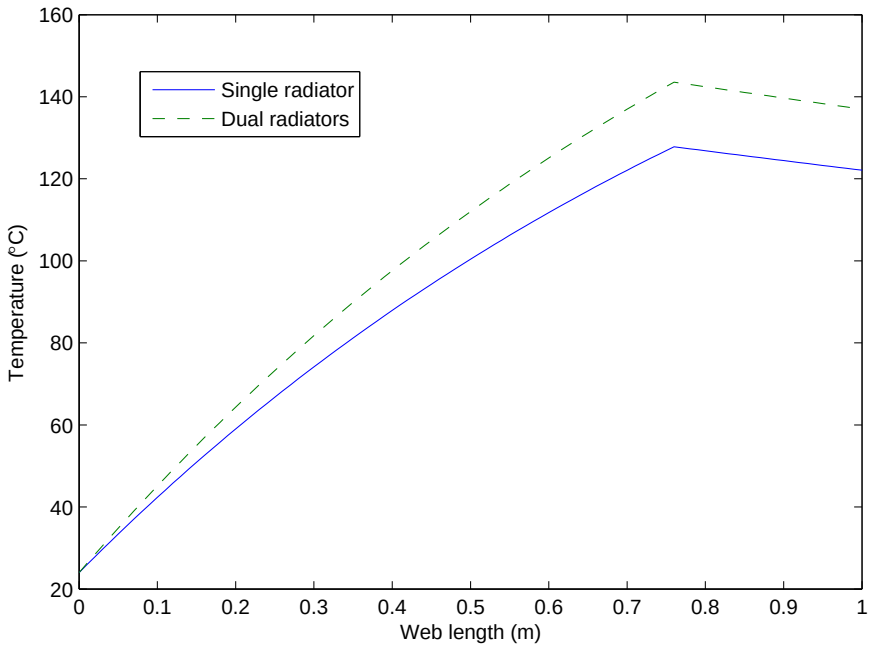

Figure 3.12: Simulation of the average temperature of Kapton with radiator of 250 °C

CHAPTER 4

STRAIN AND TENSION GOVERNING EQUATIONS AND CONTROL

In this chapter, strain and tension governing equations of web considering temperature effects are developed first. An adaptive nonlinear dual-loop tension controller is developed for a tension zone. Further, experiments are conducted on a modular R2R machine that contains heat transfer rollers.

Based on the temperature distribution model, a governing equation for mechanical strain by considering thermal strain as part of the total strain is first developed. Both the elastic modulus and thermal strain are affected by the temperature distribution in the web. The law of conservation of mass in a control volume is used to form the mechanical strain governing equation. Then, an elastic constitutive relation between strain and tension is considered to develop a governing equation for tension in a web span (the temperature range of elastic relation vary for different materials). Using the governing equations for tension in a span and web velocity, one can form the governing equations for the entire R2R process line.

For the development of a tension controller, one tension zone is considered; a tension zone is the web between any two driven rollers. For one tension zone, a state space model resulting from tension and velocity governing equations in the nonlinear block controllable form is used for control design. Since the temperature dependent elastic modulus is not well known, an adaptive controller is designed together with an estimator of the modulus-dependent parameter. This strategy is applied to a modular

R2R experiment platform to evaluate the proposed scheme, and a representative sample of the experimental results are presented and discussed.

4.1 Governing Equations for Web Strain and Tension Considering Temperature Effects

In this section, we derive a governing equation for web strain behavior which includes strain induced by thermal effects in addition to the elastic strain. The thermal distribution model is utilized for the derivation of the strain governing equation.

The temperature distribution expressions obtained from Chapter 2 are functions of y and τ, where τ is the heat transfer period at x, thus ϑ is a function of x, y and t, depending on the velocity function $v(x,t)$ of web. When the line speed is maintained in the R2R machine (an example of the machine is shown in Fig. 4.6) at the desired value, under the assumption that the web velocity variations around its reference value are small, one can simplify the temperature function by using the reference velocity, thus $\tau = x/v_R$ and ϑ is expressed as $\vartheta(x,y)$.

The elastic modulus and thermal strain are dependent on the web temperature. Given the temperature distribution equation, one can obtain the elastic modulus as $E(\vartheta)$ and the thermal strain as $\varepsilon^{\vartheta} = \alpha[\vartheta - \vartheta(t=0)]$. Therefore, both the elastic modulus and thermal strain are functions of x and y.

For developing a model for the web process machine, the machine is typically divided into different sections, each section specifying a tension zone which is the web between two driven rollers. A depiction of an R2R machine into several tension zones is shown in Fig. 4.1. It consists of $N+1$ driven rollers numbered from 0 to N, including the unwind material roll (0^{th} roll) and the rewind material roll (N^{th} roll), which result in N tension zones between the rollers. There could be one or

more non-driven rollers between each set of driven rollers to support and transport the web through different processes. Some of the idle rollers are also mounted on load cells to provide web tension via the measurement of roller reaction forces. The angular motion of the idle rollers is provided by the tension in the web. For controller development purposes, the model development follows by ignoring the idle rollers and utilizing the notion of the tension zone which is the web between two driven rollers. This approach is extensively used in the industry [37] and results in a model that is amenable to controller design. We will also assume that the web is elastic and there is no slip between the web and roller surfaces.

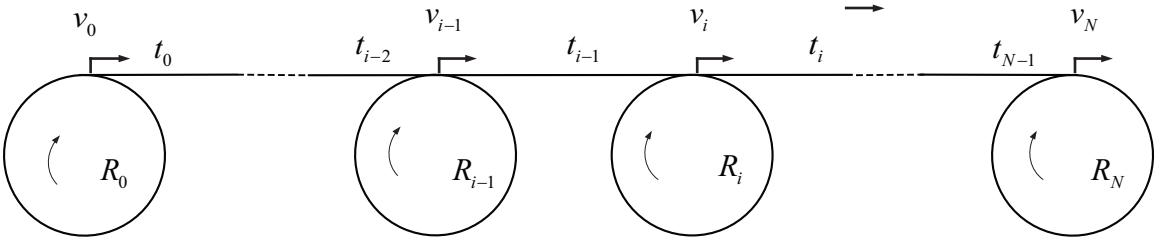

Figure 4.1: Driven rollers and web spans

4.1.1 Governing Equation for Web Strain and Tension

Typically the entire web line is divided into several tension zones, with each tension zone given by two successive driven rollers. Since the free roller dynamics have a significant effect on the web tension only during the transients due to acceleration/deceleration of the web line, under constant line speed operation the dynamics of the idle rollers are ignored. The temperature distribution in each tension zone can be written as a continuous function of the displacement along the transport direction in the region. The total length is defined as $L = L_C + L_F$, where L_C is the length of the web wrapped on the heat transfer roller and L_F is the length of the free web span. The i^{th} tension zone is shown in Fig. 4.2.

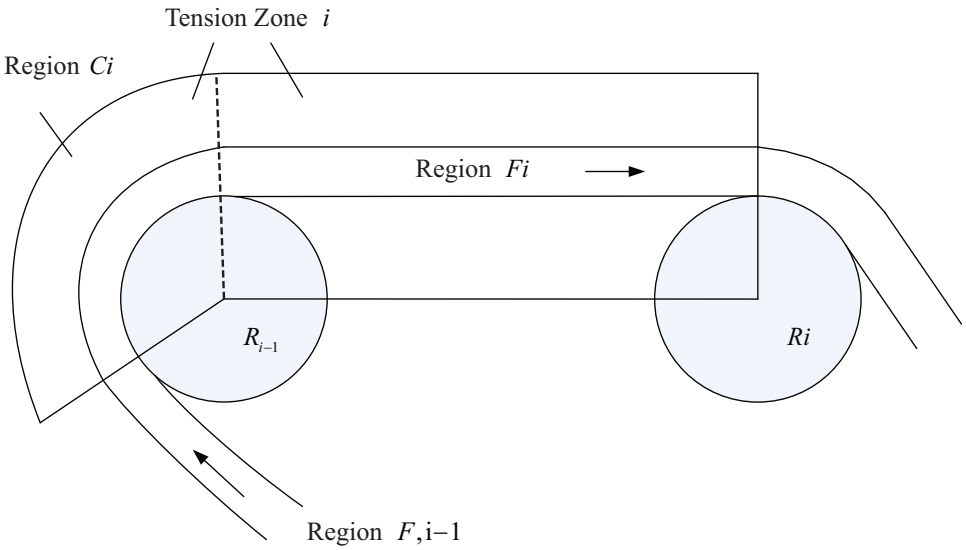

Figure 4.2: Tension zone with two rollers and web span

The law of conservation of mass in a control volume which includes the volume of web in the C region and the F span is used to derive the governing equation for web strain. The mass of the unstretched and stretched web are given by $m = \rho A \Delta x$ and $m_s = \rho_s A_s \Delta x_s$, respectively, where $\Delta x_s = (1 + \varepsilon(x,t))\Delta x$. Since $m_s = m$, and assuming $A_s = A$,

$$\frac{\rho_s A_s}{\rho A} = \frac{\rho_s}{\rho} = \frac{\Delta x}{\Delta x_s} = \frac{1}{1+\varepsilon(x,t)}. \tag{4.1}$$

The continuity equation [80] applied to the web tension zone gives

$$\frac{\partial \rho}{\partial t} + \frac{\partial (\rho v)}{\partial x} = 0. \tag{4.2}$$

Using Eqn. (4.2), integrating over the control volume V shown in Fig. 4.2 gives

$$\int_V \frac{\partial}{\partial t}\left(\frac{1}{1+\varepsilon}\right) dV = -\int_V \frac{\partial}{\partial x}\left(\frac{v}{1+\varepsilon}\right) dV. \tag{4.3}$$

Assuming a constant web cross section, $dV = A dx$, one can rewrite (4.3) as

$$\int_0^L \frac{\partial}{\partial t}\left(\frac{1}{1+\varepsilon}\right) dx = -\int_0^L \frac{\partial}{\partial x}\left(\frac{v}{1+\varepsilon}\right) dx. \tag{4.4}$$

Equation (4.4) can be simplified by assuming that web strain is small (that is, $\varepsilon << 1$). In particular, this allows the following approximation: $1/(1+\varepsilon) \approx (1-\varepsilon^2)/(1+\varepsilon) = 1-\varepsilon$. The use of the small strain approximation prior to the evaluation of the integral results in the following equation:

$$\frac{\partial}{\partial t}\int_0^L [1-\varepsilon(x,t)]dx = -v(x,t)\,[1-\varepsilon(x,t)]\,|_{x=0}^{L}. \tag{4.5}$$

Rewriting (4.5) for the i^{th} tension zone gives

$$\frac{\partial}{\partial t}\int_0^{L_i} [1-\varepsilon_i(x,t)]dx = v_{i-1}(t)[1-\varepsilon_{i-1}(L_{i-1},t)] - v_i(t)[1-\varepsilon_i(L_i,t)], \tag{4.6}$$

or

$$\frac{\partial}{\partial t}\int_0^{L_i} \varepsilon_i(x,t)dx = -v_{i-1}(t) + v_i(t) + \varepsilon_{i-1}(L_{i-1},t)v_{i-1}(t) - \varepsilon_i(L_i,t)v_i(t). \tag{4.7}$$

The total web strain is composed of two terms: tension-dependent, ε^e; and temperature-dependent, ε^ϑ; i.e., $\varepsilon = \varepsilon^e + \varepsilon^\vartheta$. By assuming that only thermal strain changes in the tension zone, and considering that ε^e is function of time only, we can obtain the equation for the elastic strain from Eq. (4.7) as

$$L_i\dot{\varepsilon}_i^e(t) = -v_{i-1}(t) + v_i(t) + \varepsilon_{i-1}(L_{i-1},t)v_{i-1}(t) - \varepsilon_i^e(t)v_i(t) - \varepsilon_i^\vartheta(L_i)v_i(t), \tag{4.8}$$

where the temperature-dependent strain used here is the average value given by $\varepsilon^\vartheta(x) = (1/l)\int_0^l \varepsilon^\vartheta(x,y)dy$. Once the uniform elastic strain is obtained, one can compute the total strain as a function of the spatial coordinates and time by $\varepsilon(x,y,t) = \varepsilon^e(t) + \varepsilon^\vartheta(x,y)$.

To obtain a governing equation for tension in the i^{th} zone from the strain equation, we assume that the web is linearly elastic and relate them according to

$$t_i(t) = E_{ei}A\varepsilon_i^e(t), \tag{4.9}$$

where A is the cross section area of web, E_{ei} is the equivalent elastic modulus of one tension zone, which is given by [19]

$$E_e = \frac{L}{\int_0^L \frac{1}{E(x)} dx}. \tag{4.10}$$

The relation between elastic modulus and temperature is different for different materials, and one example of polypropylene is shown in Fig. 4.3 [81].

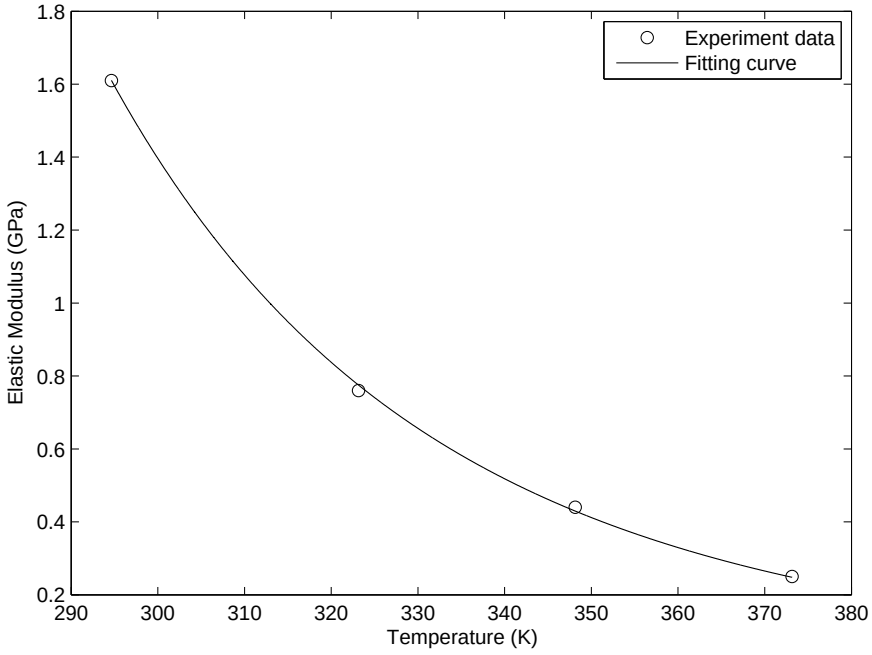

Figure 4.3: Effect of temperature on elastic modulus of polypropylene

Therefore, using (4.8) and (4.9), the governing equation for tension is obtained as

$$\begin{aligned} \dot{t}_i(t) = &- \frac{AE_{ei}}{L_i} v_{i-1}(t) + \frac{AE_{ei}}{L_i} v_i(t) + \frac{E_{ei}}{L_i E_{e,i-1}} t_{i-1}(t) v_{i-1}(t) \\ &+ \frac{AE_{ei}}{L_i} \varepsilon_{i-1}^{\vartheta}(L_{i-1}) v_{i-1}(t) - \frac{t_i(t)}{L_i} v_i(t) - \frac{AE_{ei}}{L_i} \varepsilon_i^{\vartheta}(L_i) v_i(t). \end{aligned} \tag{4.11}$$

Let $c_{1i} = \frac{AE_{ei}}{L_i}$, $c_{2i} = 1 - \varepsilon_{i-1}^{\vartheta}(L_{i-1})$, $c_{3i} = 1 - \varepsilon_i^{\vartheta}(L_i)$ and $c_{4i} = \frac{E_{ei}}{L_i E_{e,i-1}}$. The tension governing equation (4.11) can be rewritten as

$$\dot{t}_i = c_{1i}(-c_{2i} v_i + c_{3i} v_{i+1}) + c_{4i} t_{i-1} v_i - \frac{t_i v_{i+1}}{L_i}. \tag{4.12}$$

Note that if the web is not heated or cooled, the tension governing equation (4.11) is the same as the one given in [37]:

$$L_i\dot{t}_i = AE(v_{i+1} - v_i) + t_{i-1}v_i - t_iv_{i+1}. \tag{4.13}$$

4.1.2 Governing Equation for Roller Speed

The governing equation for web transport speed on the unwind roll is given by [37]

$$\frac{J_0}{R_0}\dot{v}_0 = t_0R_0 - n_0u_0 - \frac{b_{f0}}{R_0}v_0 - \frac{d_w}{2\pi R_0}\left(\frac{J_0}{R_0^2} - 2\pi\rho_w w_w R_0^2\right)v_0^2. \tag{4.14}$$

The governing equation for web transport speed on the i^{th} driven roller is given by

$$\frac{J_i}{R_i}\dot{v}_i = (t_i - t_{i-1})\,R_i + n_iu_i - \frac{b_{fi}}{R_i}v_i, \tag{4.15}$$

where n_i is the gear ratio between the i^{th} motor shaft and roll shaft, b_{fi} is the coefficient of friction in the i^{th} roll shaft, and u_i is the control torque from the i^{th} motor. Similar to the transport speed equation on the unwind roll, one can obtain the web transport speed equation for the rewind roll as

$$\begin{aligned}\frac{J_N}{R_N}\dot{v}_N = &- t_{N-1}R_N + n_Nu_N - \frac{b_{fN}}{R_N}v_N \\ &+ \frac{d_w}{2\pi R_N}\left(\frac{J_N}{R_N^2} - 2\pi\rho_w w_w R_N^2\right)v_N^2.\end{aligned} \tag{4.16}$$

In the general form, Equations (4.14) to (4.16) can be written as

$$\dot{v}_i = \begin{cases} F_0 - \frac{R_0}{J_0}n_0u_0, \ i = 0, \\ F_i + \frac{R_i}{J_i}n_iu_i, \ i = 1, 2, \cdots, N, \end{cases} \tag{4.17}$$

where

$$F_0 = t_0 \frac{R_0^2}{J_0} - \frac{b_{f0}}{J_0} v_0 - \frac{d_w}{2\pi J_0} \left(\frac{J_0}{R_0^2} - 2\pi \rho_w w_w R_0^2 \right) v_0^2, \tag{4.18a}$$

$$F_i = (t_i - t_{i-1}) \frac{R_i^2}{J_i} - \frac{b_{fi}}{J_i} v_i, \ i = 2, 3, \cdots, N-1, \tag{4.18b}$$

$$\begin{aligned} F_N = & - t_{N-1} \frac{R_N^2}{J_N} - \frac{b_{fN}}{J_N} v_N \\ & + \frac{d_w}{2\pi J_N} \left(\frac{J_N}{R_N^2} - 2\pi \rho_w w_w R_N^2 \right) v_N^2. \end{aligned} \tag{4.18c}$$

Depending on the number of driven rollers between the unwind and rewind rolls for a particular R2R process machine, one can compose the dynamic model corresponding to the given machine configuration from these governing equations.

4.2 Adaptive Nonlinear Control Design

It is common in industrial R2R process machines to employ a speed-based tension control strategy where there is an inner speed loop to control the web transport speed and an outer tension loop that provides a trim to the speed reference of the inner loop. The typical structure of such a dual loop control scheme to simultaneously control transport speed and tension is shown in Fig. 1.2. Each tension zone utilizes this control system. In processes where the web is heated and cooled, the material properties are changing from one tension zone to the other. Therefore, a controller that utilizes the nonlinear governing equations instead of linearized equations would provide better control of tension in those tension zones.

Define the following web transport speed and tension errors: $e_v = v_i - v_{Ri}$ and $e_t = t_i - t_{Ri}$, where t_{Ri} is the constant tension reference and v_{Ri} is the corrected transport speed reference. Note that we have defined the errors without the subscript i for ease of presentation. We consider the following control law for the driven roller

torques:

$$u_i = \begin{cases} \frac{-\dot{v}_{R0}+F_0+K_v e_v - c_{1i}c_{2i}e_t + c_{4i}t_{i-1}e_t}{R_0 n_0/J_0}, \ i=0, \\ \frac{\dot{v}_{Ri}-F_i-K_v e_v + c_{1i}c_{2i}e_t - c_{4i}t_{i-1}e_t}{R_i n_i/J_i}, \ i=1,2,\cdots,N, \end{cases} \tag{4.19}$$

where K_v is a positive gain and the corrected reference speed v_{Ri} is given by

$$v_{Ri} = \frac{\dot{t}_{Ri} - c_{1i}c_{3i}v_{i+1} + \frac{t_i v_{i+1}}{L_i} - K_t e_t}{-c_{1i}c_{2i} + c_{4i}t_{i-1}}, \tag{4.20}$$

where K_t is a positive gain. Note that one must have $t_{i-1} \neq c_{1i}c_{2i}/c_{4i}$ for the corrected reference speed to be bounded. This is satisfied in all practical cases because c_{2i} is close to unity (thermal strain is much smaller than unity) and $c_{1i}/c_{4i} = AE_{i-1}$ is much larger than the reference tension under which the web is transported.

With the control law given by (4.19), the governing equations for speed error and tension error are given by

$$\dot{e}_v = -K_v e_v + c_{1i}c_{2i}e_t - c_{4i}t_{i-1}e_t \tag{4.21}$$

and

$$\dot{e}_t = -c_{1i}c_{2i}v_i + c_{1i}c_{3i}v_{i+1} + c_{4i}t_{i-1}v_i - \frac{t_i v_{i+1}}{L_i} - \dot{t}_{Ri}. \tag{4.22}$$

To show the stability of the solutions $e_v = 0$ and $e_t = 0$, we define the following Lyapunov function candidate

$$V = \frac{1}{2}e_t^2 + \frac{1}{2}e_v^2, \tag{4.23}$$

whose derivative is given by

$$\begin{aligned} \dot{V} =& e_t\dot{e}_t + e_v\dot{e}_v \\ =& \left(-c_{1i}c_{2i}v_i + c_{1i}c_{3i}v_{i+1} + c_{4i}t_{i-1}v_i - \frac{t_i v_{i+1}}{L_i} - \dot{t}_{Ri}\right) e_t \\ & + \left(-K_v e_v + c_{1i}c_{2i}e_t - c_{4i}t_{i-1}e_t\right) e_v \\ =& \left(-c_{1i}c_{2i}e_v + c_{4i}t_{i-1}e_v - K_t e_t\right) e_t + \left(-K_v e_v + c_{1i}c_{2i}e_t - c_{4i}t_{i-1}e_t\right) e_v \\ =& -K_t e_t^2 - K_v e_v^2. \end{aligned} \tag{4.24}$$

Therefore, one can guarantee exponential convergence of e_t and e_v to zero.

The above controller requires accurate knowledge of all the parameters. Note that the parameters c_1 and c_4 are dependent on the elastic modulus which is not readily available when the webs are heated/cooled during transport. To account for uncertainties in the elastic modulus, estimation of the parameters c_1 and c_4 is considered. Denote $\tilde{c}_1 = c_1 - \hat{c}_1$ and $\tilde{c}_4 = c_4 - \hat{c}_4$. Rewrite (4.20) with the estimated parameter values as

$$v_{Ri} = \frac{-\hat{c}_{1i}c_{3i}v_{i+1} + \dfrac{t_i v_{i+1}}{L_i} - K_t e_t}{-\hat{c}_{1i}c_{2i} + \hat{c}_{4i}t_{i-1}}, \tag{4.25}$$

and the control torque to the i^{th} roller is given by

$$u_i = \begin{cases} \frac{-\dot{\hat{v}}_{R0} + F_0 + K_v e_v - \hat{c}_{1i}c_{2i}e_t + \hat{c}_{4i}t_{i-1}e_t}{R_0 n_0 / J_0}, \ i = 0, \\ \frac{\dot{\hat{v}}_{Ri} - F_i - K_v e_v + \hat{c}_{1i}c_{2i}e_t - \hat{c}_{4i}t_{i-1}e_t}{R_i n_i / J_i}, \ i = 1, 2, \cdots, N. \end{cases} \tag{4.26}$$

Applying (4.26) into the roller velocity dynamics (4.17) yields

$$\dot{e}_v = -K_v e_v + \hat{c}_{1i}c_{2i}e_t - \hat{c}_{4i}t_{i-1}e_t. \tag{4.27}$$

Now, define the following modified Lyapunov function candidate

$$V = \frac{1}{2}e_t^2 + \frac{1}{2}e_v^2 + \frac{1}{2}K_1\tilde{c}_{1i}^2 + \frac{1}{2}K_4\tilde{c}_{4i}^2, \tag{4.28}$$

where K_1 and K_4 are the positive parameter estimator gains. The derivative of (4.28)

is given by

$$\begin{aligned}
\dot{V} =& e_t\dot{e}_t + e_v\dot{e}_v + K_1\tilde{c}_{1i}\dot{\tilde{c}}_{1i} + K_4\tilde{c}_{4i}\dot{\tilde{c}}_{4i} \\
=& \left(-c_{1i}c_{2i}v_i + c_{1i}c_{3i}v_{i+1} + c_{4i}t_{i-1}v_i - \frac{t_i v_{i+1}}{L_i} - \dot{t}_{Ri}\right) e_t \\
&+ \left(-K_v e_v + \hat{c}_{1i}c_{2i}e_t - \hat{c}_{4i}t_{i-1}e_t\right) e_v + K_1\tilde{c}_{1i}\dot{\tilde{c}}_{1i} + K_4\tilde{c}_{4i}\dot{\tilde{c}}_{4i} \\
=& \left(-c_{1i}c_{2i}e_v - \tilde{c}_{1i}c_{2i}v_{Ri} + \tilde{c}_{1i}c_{3i}v_{i+1} + \tilde{c}_{4i}t_{i-1}e_v + \hat{c}_{4i}t_{i-1}e_v + \tilde{c}_{4i}t_{i-1}v_{Ri} - K_t e_t\right) e_t \\
&+ \left(-K_v e_v + \hat{c}_{1i}c_{2i}e_t - \hat{c}_{4i}t_{i-1}e_t\right) e_v - K_1\tilde{c}_{1i}\dot{\hat{c}}_{1i} - K_4\tilde{c}_{4i}\dot{\hat{c}}_{4i} \\
=& -\tilde{c}_{1i}c_{2i}e_t e_v - \tilde{c}_{1i}c_{2i}v_{Ri}e_t + \tilde{c}_{1i}c_{3i}v_{i+1}e_t + \tilde{c}_{4i}t_{i-1}e_v e_t \\
&+ \tilde{c}_{4i}t_{i-1}v_{Ri}e_t - K_t e_t^2 - K_t e_v^2 - K_1\tilde{c}_{1i}\dot{\hat{c}}_{1i} - K_4\tilde{c}_{4i}\dot{\hat{c}}_{4i}.
\end{aligned} \tag{4.29}$$

By choosing the following adaptation laws for the estimated parameters

$$\dot{\hat{c}}_{1i} = \left(-c_{2i}e_v - c_{2i}v_{Ri} + c_{3i}v_{i+1}\right) e_t/K_1, \tag{4.30a}$$

$$\dot{\hat{c}}_{4i} = \left(t_{i-1}e_v + t_{i-1}v_{Ri}\right) e_t/K_4, \tag{4.30b}$$

we obtain

$$\dot{V} = -K_t e_t^2 - K_v e_v^2. \tag{4.31}$$

This implies asymptotic convergence of e_v and e_t to zero. Note that although parameter estimates are not guaranteed to converge to their true values, the adaptive control algorithm provides a way to estimate the parameter values during transport of the web through heating/cooling processes. It is difficult to obtain the true values of the parameters as this entails obtaining the material physical and mechanical properties under the conditions in which the web is transported. To obtain mechanical properties for a range of elevated temperatures, one can conduct elevated temperature tensile tests on the base webs that are utilized to obtain the final product. The control strategy developed in this section is concluded and shown in Fig. 4.4.

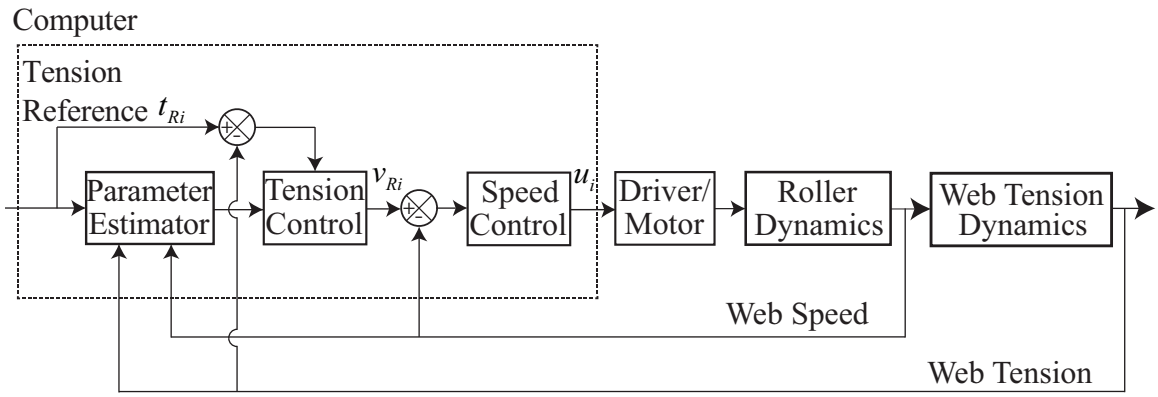

Figure 4.4: Control strategy with dual-loop adaptive nonlinear controller

4.3 Experiments on a Modular Roll-to-Roll Machine

A line schematic of a modular R2R machine is shown in Fig. 4.5. A picture of the machine is shown in Fig. 4.6. The unwind roll, rewind roll, S-wrap rolls, heating roll and cooling roll are all driven rollers.

Both the heating roller and cooling roller consist of an outer shell, an inner shell and a liquid chamber between the two. Hot oil is pumped through the chamber for heating and chilled water for cooling, which provides steady surface temperature, and the heat transfer condition is 'conduction + convection' as discussed in [10]. Two idle rollers mounted with load cells are used for measuring web tension in the unwind tension zone and the process zone between the heating and cooling rollers. The line sketch also shows the location of the two temperature sensors, at the beginning and ending of the heating zone.

The diameters of all the idle rollers are 2 inches (0.0508 m), and the diameters and angles of wrap of the driven rollers are given in Table 4.1. Note that the diameters of unwind and rewind rollers are core diameters without the web. The initial diameter with the roll of web is 12 inches (0.3048 m). The inertia of both heating and cooling rollers reflected to the motor side is 1.1378 kg m^2 (27 lb ft^2). The inertia of the

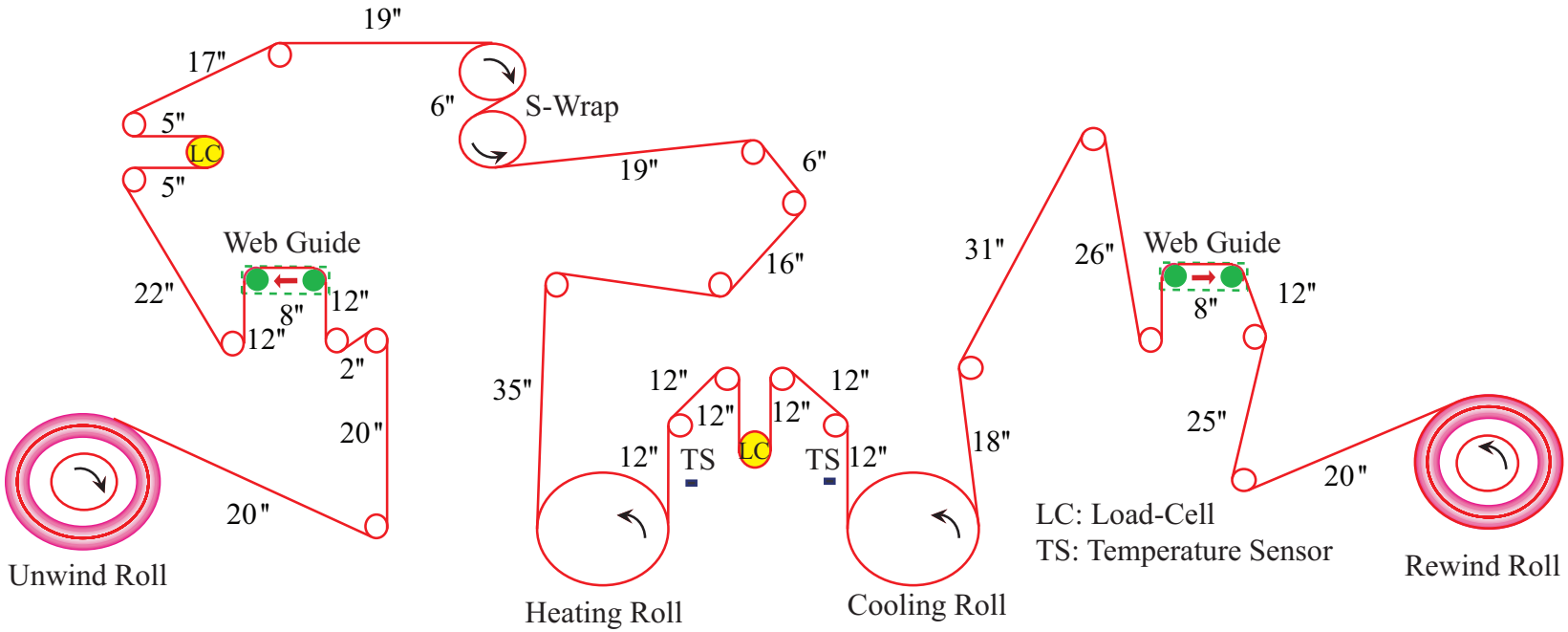

Figure 4.5: Line schematic of the experimental platform

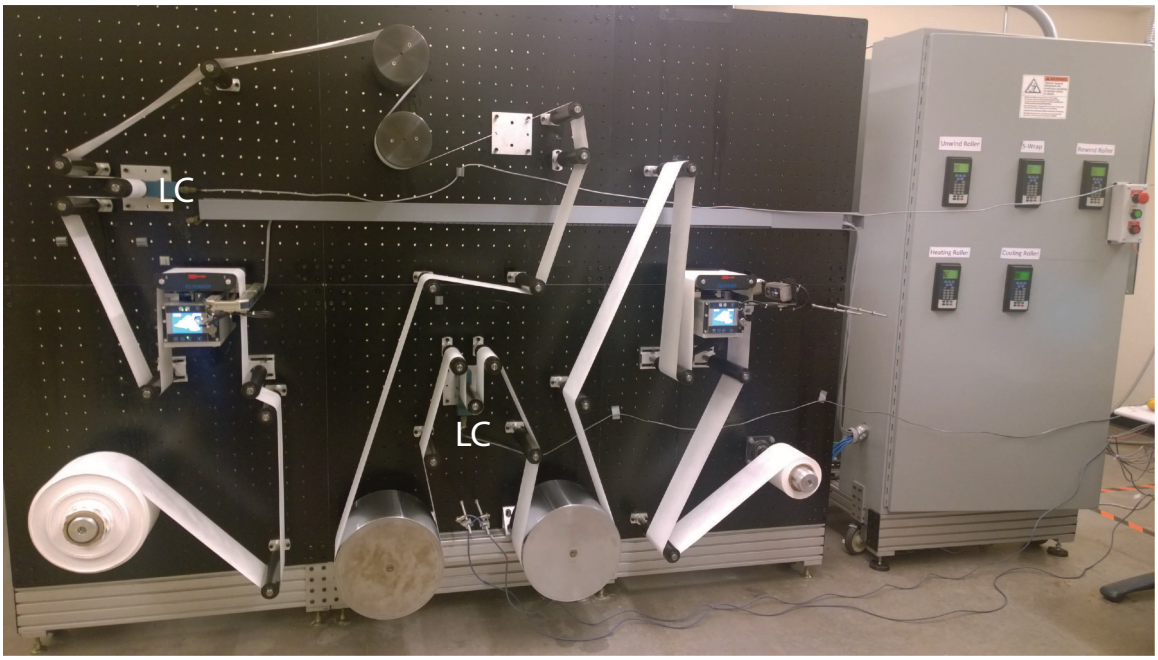

Figure 4.6: Picture of the experimental platform

S-wrap rollers reflected to the motor side is 0.0527 kg m^2 (1.25 lb ft^2). The inertia of the unwind material roller with the core reflected to the motor side is given by

$$J_0(t) = n_0^2 J_{c0} + \frac{\pi}{2} w_w \rho_w (R_0^4 - R_{c0}^4), \tag{4.32}$$

where $J_{c0} = 0.0527$ kg m^2 (0.5 lb ft^2) is the inertia of the driven shaft and the core mounted on it, and R_{c0} is 0.0445 m (1.75 inches). The inertia of the rewind roll reflected to the motor is given by

$$J_N(t) = n_N^2 J_{cN} + \frac{\pi}{2} w_w \rho_w (R_N^4 + R_{cN}^4), \tag{4.33}$$

where $J_{cN} = 0.0527$ kg m^2 (0.5 lb ft^2) is the inertia of the driven shaft and the core mounted on it, and R_{c0} is 0.0445 m (1.75 inches).

The web material is Tyvek, a flashspun nonwoven High-density Polyethylene (HDPE) fiber made by DuPont. The web width is 0.152 m (6 inches) and the thickness is 0.127 mm (0.005 inches). The heating roll is made of type 1026 mild carbon

Table 4.1: Diameters and wrap angles of driven rollers

Roller	Diameter (in)	Wrap angle (°)
Unwind roll	3.5 (core)	NA
S-Wrap rolls (pair)	6	180
Heating roll	12.5	240
Cooling roll	12.5	240
Rewind roll	3.5 (core)	NA

steel, with width of 0.152 m (6 inches) and outer shell thickness of 0.01 m (0.39 inches). The material properties of steel roll [82] and HDPE web [83] are shown as below: $k_r = 52$ W/(mK), $c_r = 470$ J/(kgK), $\rho_r = 7850$ kg/m^3, $k_w = 0.52$ W/(mK), $c_w = 2200$ J/(kgK), $\rho_w = 965$ kg/m^3, and $\alpha_w = 200 \times 10^{-6}$.

4.3.1 Pure Speed Control Experiments

Speed control experiments were conducted with zero percent draw with and without heating of the web. The temperature of heating oil is 94 °C (200 °F), and the speed reference to all the driven rollers is 0.05 m/s (10 fpm). The tension feedback of the load cell roller before the heating roll is shown in Fig. 4.7. The solid plot shows web tension without heating and the dashed plot shows web tension when heating the web. First, note that without any heating under pure speed control tension is not regulated at any specific reference value. Second, when the web is heated, the tension in the unwind zone is also affected as its value decreases when the web is heated in the downstream tension zone. Therefore tension regulation is required in the unwind zone.

Figure 4.8 shows the tension measurement in the heating zone, that is, the load

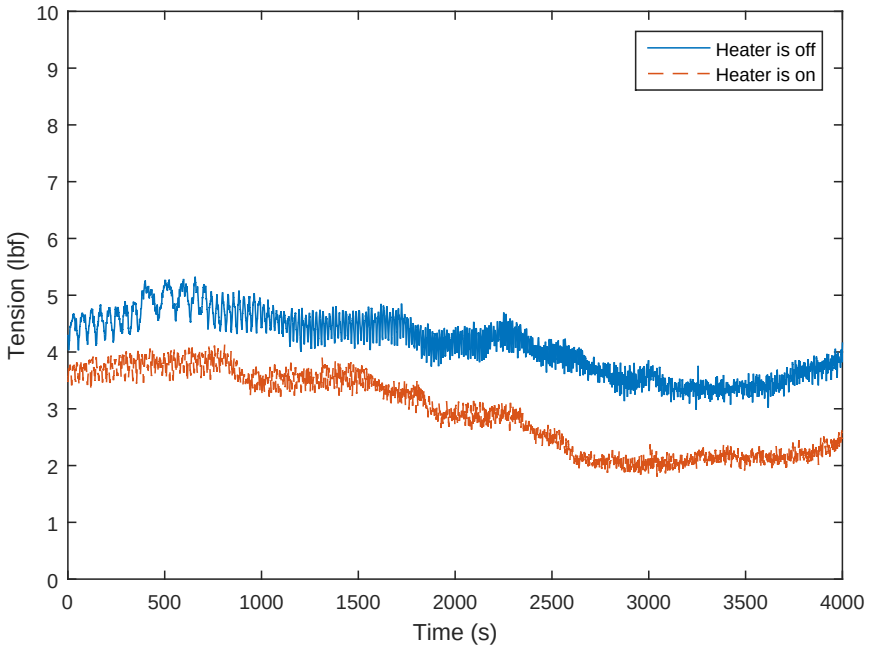

Figure 4.7: Web tension in the unwind zone with and without heating from pure speed control experiments

cell roller located in the tension zone between the heating and cooling roller. Under pure speed control it is clear that web tension is not regulated. Further, one can also notice a reduction in web tension when the web is heated indicating a drop in the elastic modulus of the web with heating.

When thermal strain change is not significant, the dominant cause of web tension change is the change in the elastic modulus, according to the tension formula $t = EA\varepsilon^e$. The specific relationship between the elastic modulus and temperature of Tyvek is not well known, but some tests of general HDPE material are reported in [1]; the measured data is shown as squares in Fig. 4.9. Since web is assumed to be elastic, this data is taken as providing the nominal values for elastic modulus of Tyvek at different temperatures. The following functional relation shows a simple fit

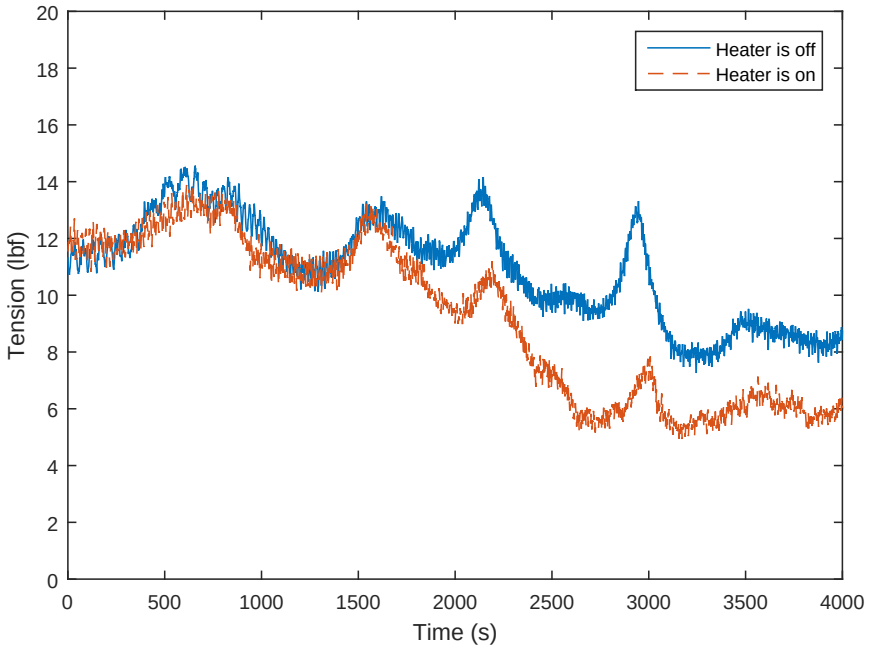

Figure 4.8: Web tension in the heating zone with and without heating from pure speed control experiments

for the data:

$$E = 1300(\text{MPa})\text{e}^{-0.018\vartheta(^\circ\text{C})}. \tag{4.34}$$

In the case of our experiments, the web reaches about 52 °C on the heating roll, and the average temperature in the web zone after heating is about 40 °C. From elastic modulus curve as a function of temperature, it is clear that the modulus drops about 20% from room temperature to 40 °C, which roughly agrees with the tension drop observed in Fig. 4.8.

4.3.2 Tension Control Experiments

Experiments were conducted by implementing the nonlinear tension control scheme discussed in the preceding section. The temperature of the heating oil that is circulated through the heating roller is 94 °C (200 °F), and the speed reference to all driven

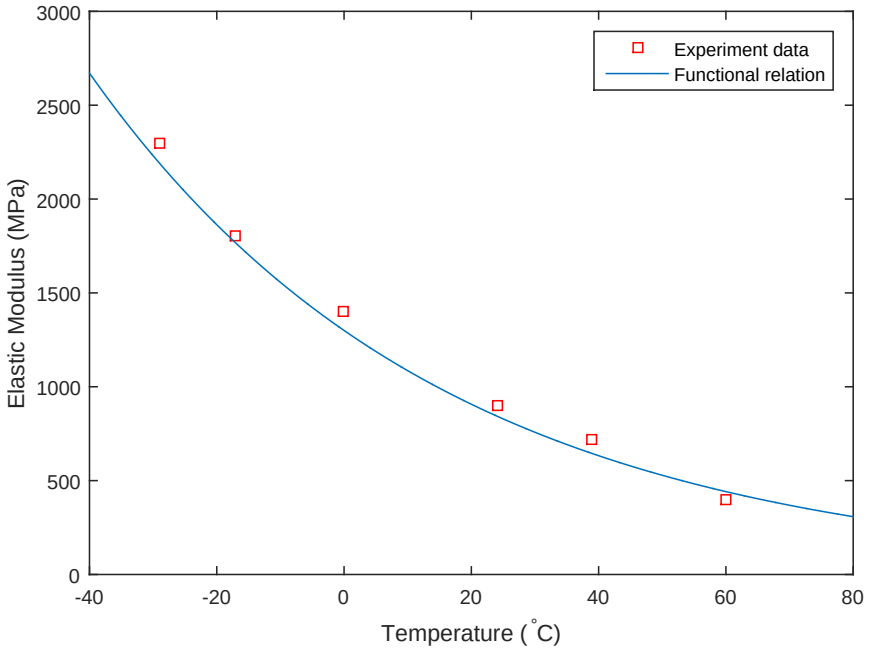

Figure 4.9: Elastic modulus vs. temperature for HDPE [1]

rollers is 0.05 m/s (10 fpm). To evaluate the performance of the control scheme, two different constant reference values are tested: 22.24 N (5 lbf) and 44.48 N (10 lbf).

The web from the unwind roll to the heating roll is not heated, and as a result the system parameters in this section do not change. The following control gain values are chosen: $K_t = 10$, $K_v = 10$, and $K_1 = K_4 = 1$. From Fig. 4.9, the elastic modulus of web at room temperature is about 0.8 GPa. Let TZ1 be the the tension zone from the unwind roll to the heated roll and TZ2 be the tension zone from the heated roller to the cooling roller. The following are the approximate values of the parameters at the room temperature for TZ1 and TZ2. TZ1: $c_1 \approx 2574$, $c_2 \approx 1$, $c_3 \approx 1$, $c_4 \approx 0.1667$. TZ2: $c_1 \approx 8437$, $c_2 \approx 1$, $c_3 \approx 1$, $c_4 \approx 0.5464$. However, the initial values of the estimated parameters in both tension zones are simply chosen to be $\hat{c}_1(0) = 2000$ and $\hat{c}_4(0) = 0.2$. Note that in both conditions, the reference tension is much smaller than the product of elastic modulus and cross-section area.

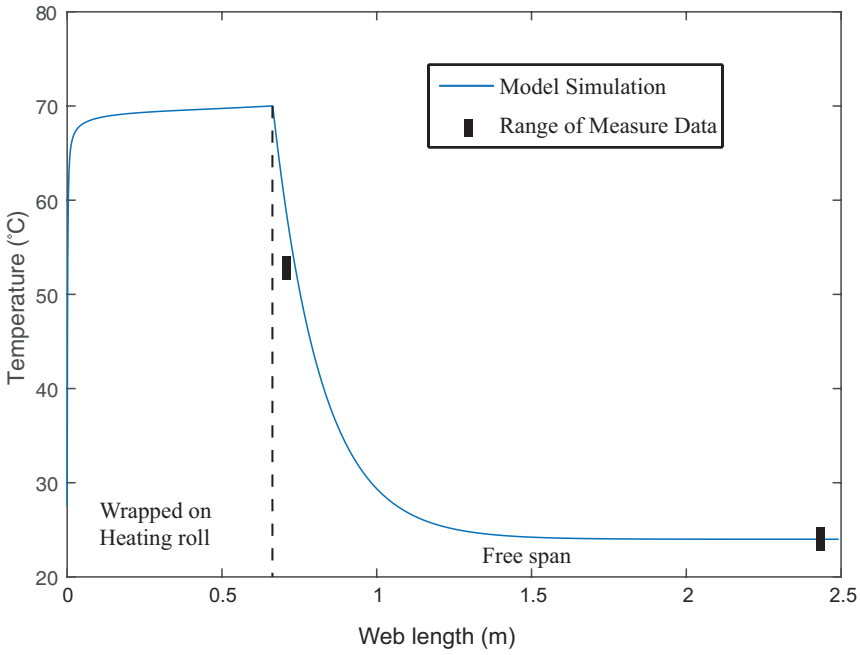

Figure 4.10: Web temperature distribution in the heating zone

When hot oil is pumped through the heating roller, the web experiences thermal strain as well as changes in the elastic modulus. Using the models in [10] with thermal contact resistance between the heated roller and web surface as 0.003 m^2K/W [77], the web temperature as it is transported on the heating roll and TZ2 from model simulations is shown in Fig. 4.10. The range of measured temperature using infrared temperature sensors at the two locations indicated in Fig. 4.5 are shown in addition to the model simulation result in Fig. 4.10. The web is first heated by conduction on the heating roll, then cooled by convection to the ambient air, and the average temperature in this tension zone is about 39 °C (102 °F). Tensile test data shown in Fig. 4.9 indicates the modulus to be $E_e = 0.6$ GPa, only about 70% compared to the modulus at room temperature, and the actual parameters c_1 and c_4 should drop to about 70%. Therefore, in the heating case, the parameters of the span before heating roll are not affected. However, the modulus dependent parameters, c_1 and

c_4, change significantly for TZ2. The approximate values of the parameters at the average temperature of 39°C (102 °F) are given by: $c_1 \approx 5898$, $c_2 \approx 0.9940$, $c_3 \approx 1$, $c_4 \approx 0.3819$.

For reference tension 5 lbf, Figs. 4.11 and 4.12 show the tension response in the unwind zone. It is clear that the controller is able to follow the desired tension references, either with or without heating of the web. Using the same gain values, the tension response in the heating zone is shown in Figs. 4.13 and 4.14. In this tension zone also, it is clear that the controller is able to follow the desired tension references, either with or without heating of the web. The estimate of c_1 in the heating zone is shown in Fig. 4.15. Note that $c_{1i} = Ae_{ei}/L_i$, and the web temperature increases in the heating zone, thus c_{1i} decreases. The estimate of c_1 in the unwind zone is shown in Fig. 4.16, and the parameter also decreases when compared to when the heater is off. However this decrease is not as much as in the heating zone.

For reference tension 10 lbf, similar results are shown in Figures 4.17 to 4.22.

4.4 Summary

In this chapter, a governing equation for web tension is developed by considering thermal strain and web elastic modulus as functions of temperature in the web. A model-based nonlinear tension controller is designed for control of tension in each tension zone of an R2R machine. Experiments are conducted on a modular unwind-rewind R2R experimental platform consisting of a heating and a cooling roller. It is shown that tension is not regulated at any particular value if only pure speed control is employed. Experimental results show that the proposed nonlinear control scheme is capable of regulating tension in the heating zone at any desired level specified by the user.

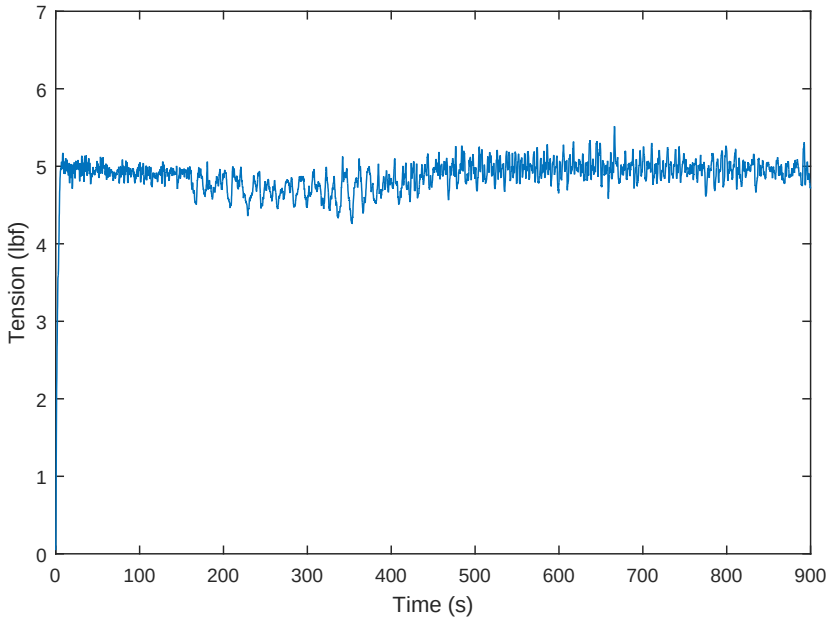

Figure 4.11: Tension in unwind zone with heater off under reference 5 lbf from tension control experiments

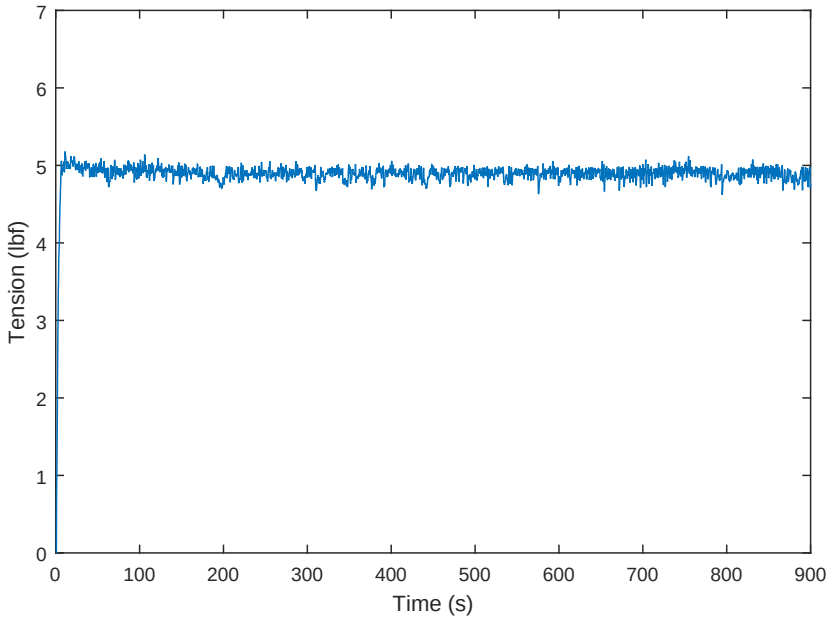

Figure 4.12: Tension in unwind zone with heater on under reference 5 lbf from tension control experiments

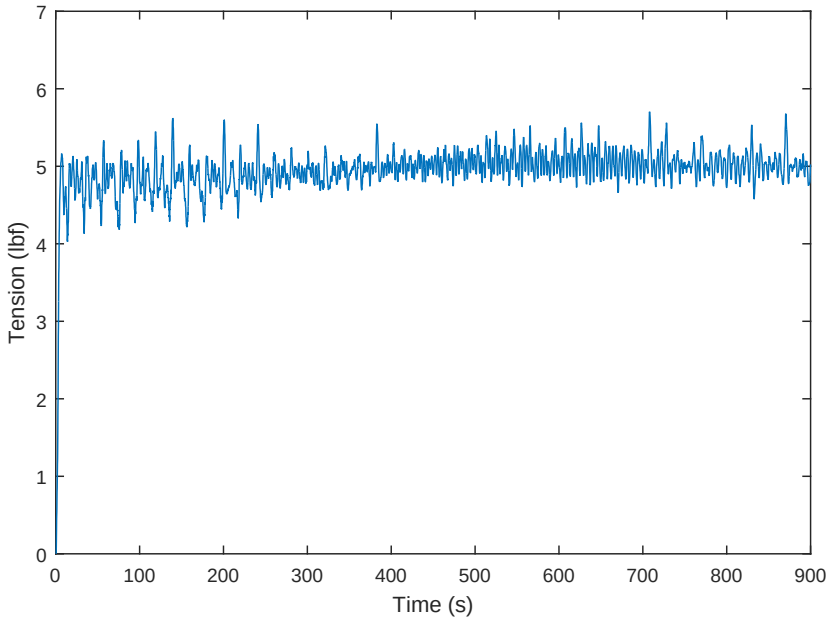

Figure 4.13: Tension in heating zone with heater off under reference 5 lbf from tension control experiments

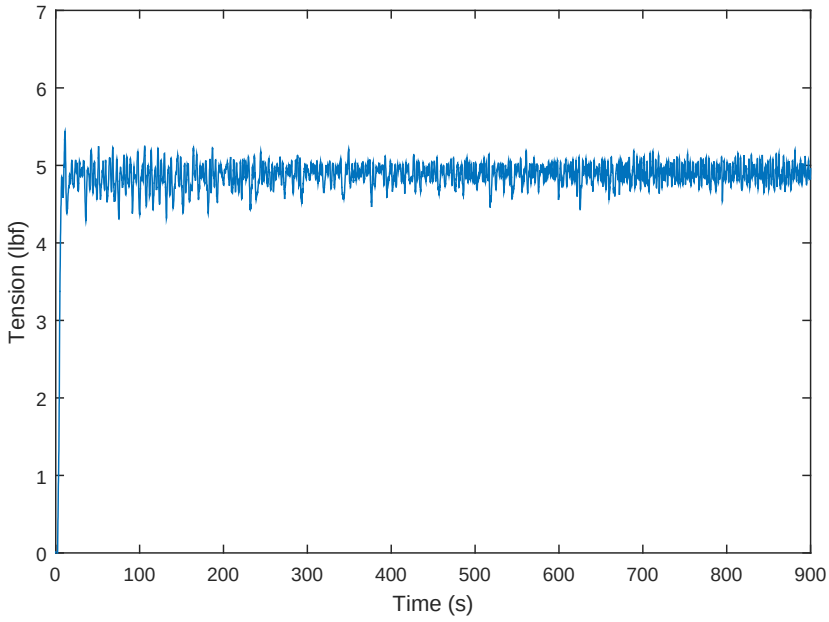

Figure 4.14: Tension in heating zone with heater on under reference 5 lbf from tension control experiments

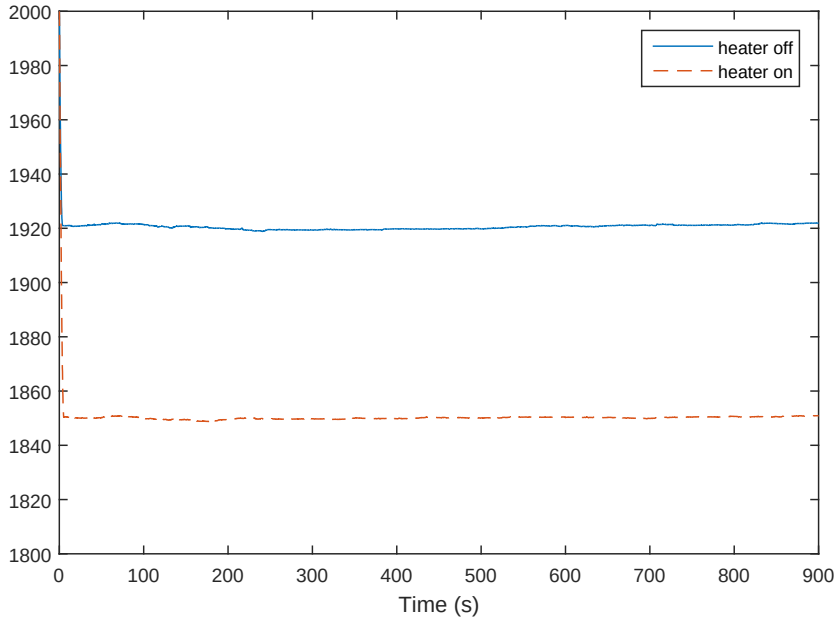

Figure 4.15: Estimate of c_1 in the heating zone under reference 5 lbf from tension control experiments

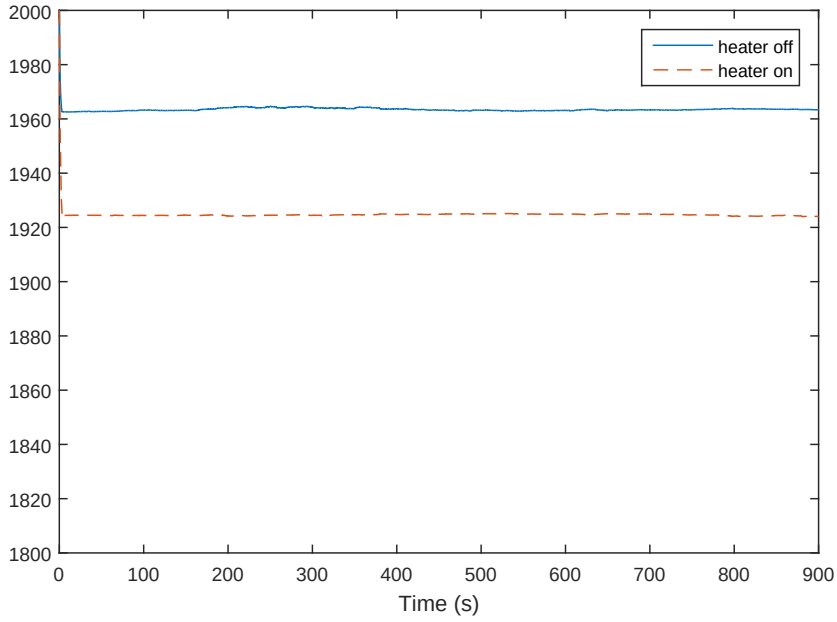

Figure 4.16: Estimate of c_1 in the unwind zone under reference 5 lbf from tension control experiments

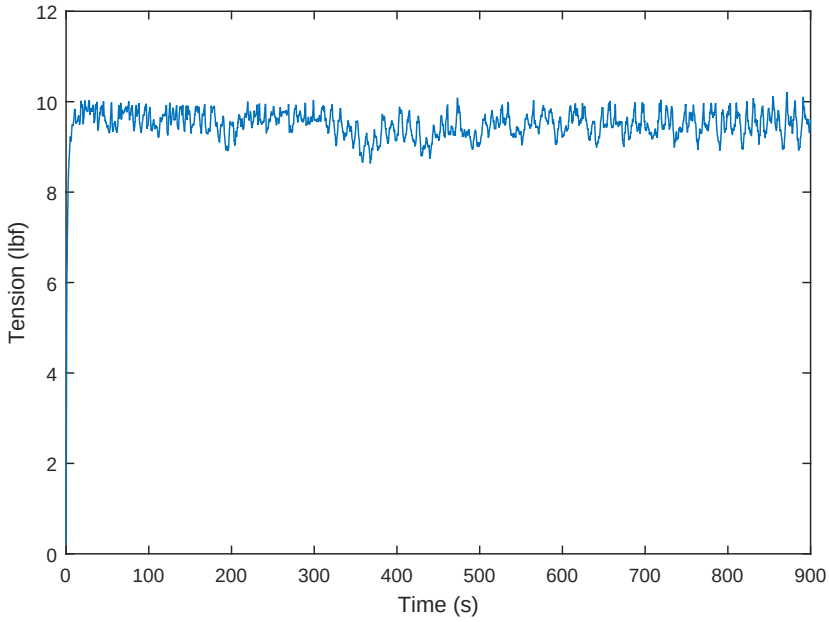

Figure 4.17: Tension in unwind zone with heater off under reference 10 lbf from tension control experiments

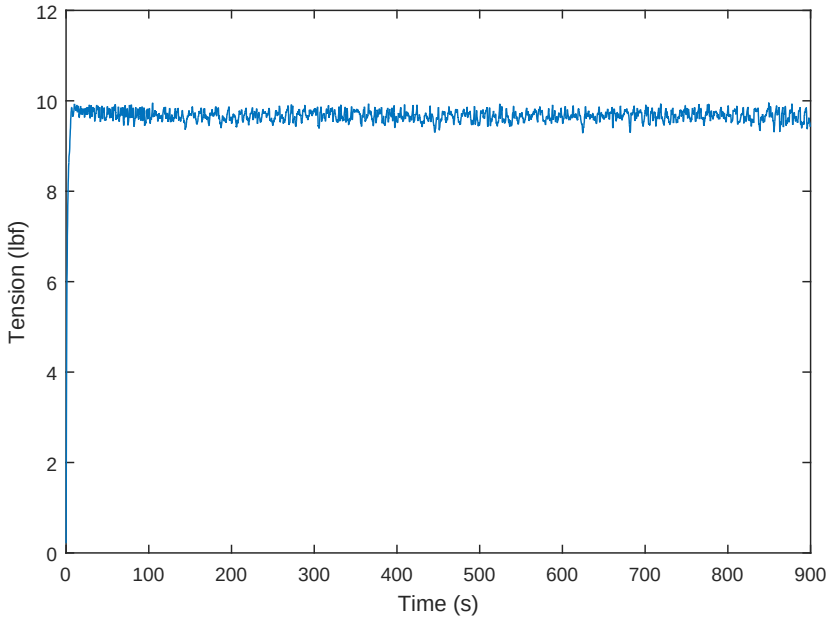

Figure 4.18: Tension in unwind zone with heater on under reference 10 lbf from tension control experiments

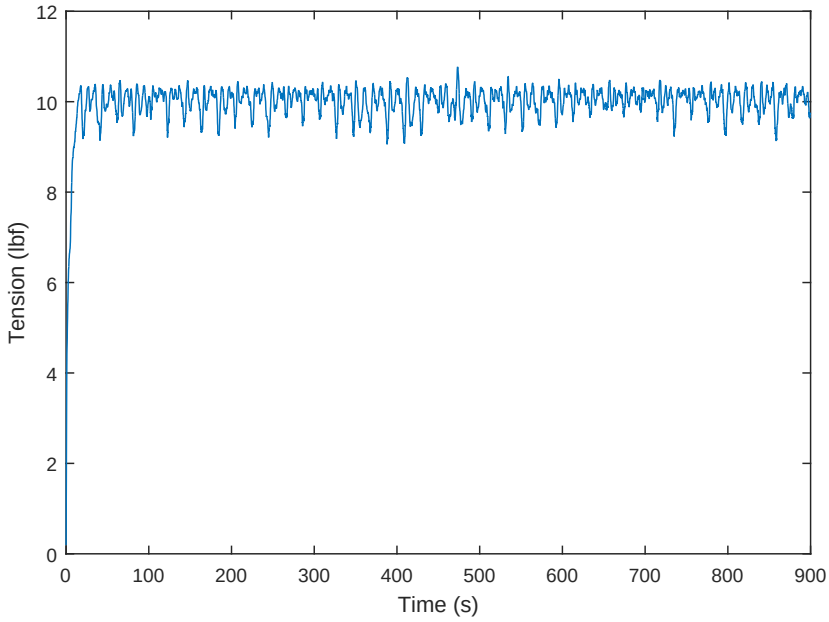

Figure 4.19: Tension in heating zone with heater off under reference 10 lbf from tension control experiments

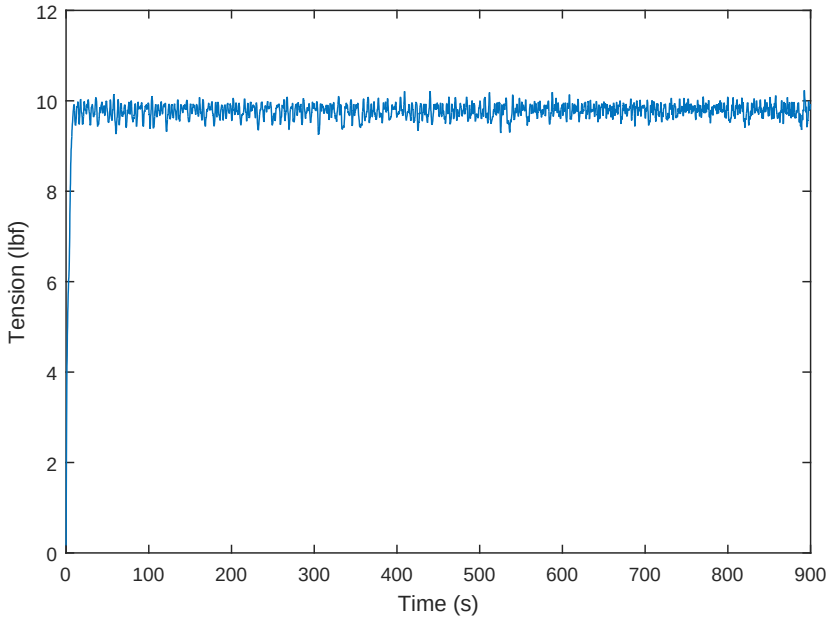

Figure 4.20: Tension in heating zone with heater on under reference 10 lbf from tension control experiments

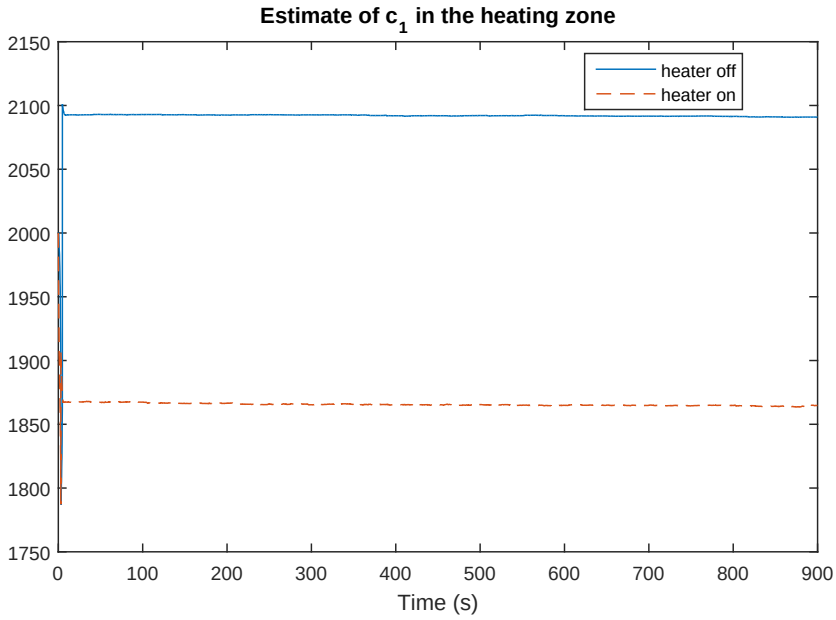

Figure 4.21: Estimate of c_1 in the heating zone under reference 10 lbf from tension control experiments

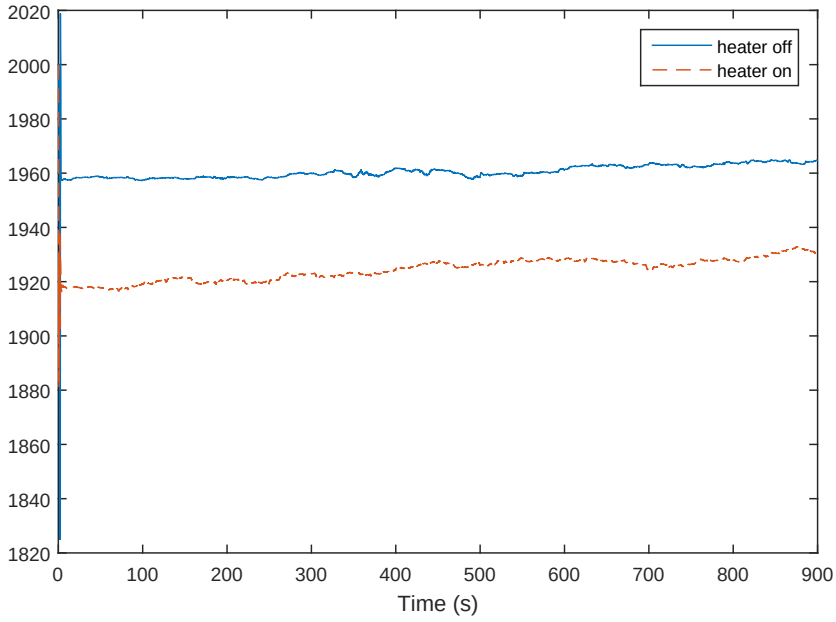

Figure 4.22: Estimate of c_1 in the unwind zone under reference 10 lbf from tension control experiments

CHAPTER 5

TENSION OBSERVER DESIGN AND MODELING OF ROLL TO ROLL LAMINATION PROCESS

Two important problems are studied in this chapter: (i) control of strip tension in the heating/cooling sections of continuous annealing lines using model-based tension estimation; and (ii) modeling and control of Roll-to-Roll lamination process . Both involve the dynamic models and control strategies obtained in previous chapters.

5.1 Tension Observer Design for Steel Strip Processing Line

The goal is to develop a tension control strategy for control of tension in the steel strip transported through the heating and cooling sections of continuous steel processing lines, such as continuous annealing lines (CAL) and continuous galvanizing lines (CGL). A model-based control design strategy will be considered to develop a tension control system that can precisely control tension when there are disturbing forces on the strip due to heating/cooling of the web and machine imperfections. An important aspect to consider in the model development is the incorporation of thermal strain induced in the steel strip as a result of heating/cooling of the web. Since thermal strain affects the transport behavior and tension in particular, a nonlinear governing equation for tension that includes the temperature distribution in the steel strip will be considered.

It is critical to control the strip tension in a stable manner within the acceptable

tolerance range in the steel strip processing lines. There are many factors that may lead to poor tension control. For example, due to heating/cooling of the strip during transport, there are changes to the physical and mechanical properties of the strip material that must be accounted for in the design of tension control systems. In particular, changes in the strip elastic modulus due to heating/cooling of the web can result in poorly performing tension control systems if fixed gain controllers such as the traditional PI controllers are employed.

Another aspect is the slip between the steel strip and the roller surfaces can cause severe defects such as scratches on the surface of the steel strip. This may be either due to an unresponsive tension control system or tension variations induced by a variety of process or machine conditions, including the heating/cooling process, non-ideal rollers, friction, etc. Even a small amount of slip over a long period of time in an annealing furnace can cause very small but severe dent marks which result due to the clod of strip constituent elements. It may be possible to avoid slip by increasing reference tension, but this is not desirable as conservative high tension operation reduces the life cycle of the equipment used to transport the strip. Conservative high tension operation is believed to have the merit of minimizing slip under tension control transient conditions. But high tension aggravates the sink roll grove marks on the steel strip as well as reduction of durable life of the sink roll bearing due to aggravated wear. Ensuring that there is minimal slip with proper tension control is necessary to prolong the life cycle of the equipment and produce defect-free exposed quality steel strips, such as those used for automotive steel products. Therefore, it is essential to select an optimal tension reference level and design a precise tension control system that can achieve the tension reference in the face of many material property changes and dynamic conditions.

A precise model that is capable of predicting the transport tension behavior will

significantly assist in the analysis of transport behavior and development of tension control systems. Since the strip is undergoing changes during transport, an adaptive tension control system that can adapt to these changes in real-time while maintaining precise strip tension reference level has the potential to significantly improve performance over what is currently achievable with the existing tension control systems.

5.1.1 Analysis of Continuous Galvanizing/Annealing Lines Furnace

Continuous galvanizing/annealing lines are highly productive manufacturing lines used by steel making companies for the manufacture of thin steel sheet products. In these lines, the steel strip is continuously heated and cooled depending on the heat processing cycle required for a particular product. The heating/cooling cycle plays a critical role in programming the material properties of sheet products. The annealing furnace is the main processing section of a CGL/CAL and is divided into several heat transfer sections, such as heating section (HS), soaking section (SS), rapid cooling section (RCS), and cooling section (CS) as illustrated in Figure 5.1. By transporting the steel strip through the annealing furnace, concentrated uneven stress in the strip resulting from the cold rolling process is relieved and new material property specifications, such as tensile strength, yield strength or ductile strength, are obtained for the steel strip depending on customer orders. To obtain the designed material properties with good productivity and quality, steel web transport system, which comprises of driving motors for roller, strip tension measurement equipment, and heating and cooling equipment, has to be designed and controlled with the consideration of various key factors that aid in efficient transport of the steel strip through the annealing furnace without defects.

During transport of the steel strip in the annealing furnace, the strip experiences heating and rapid cooling that is called quenching. In the heating section, the strip

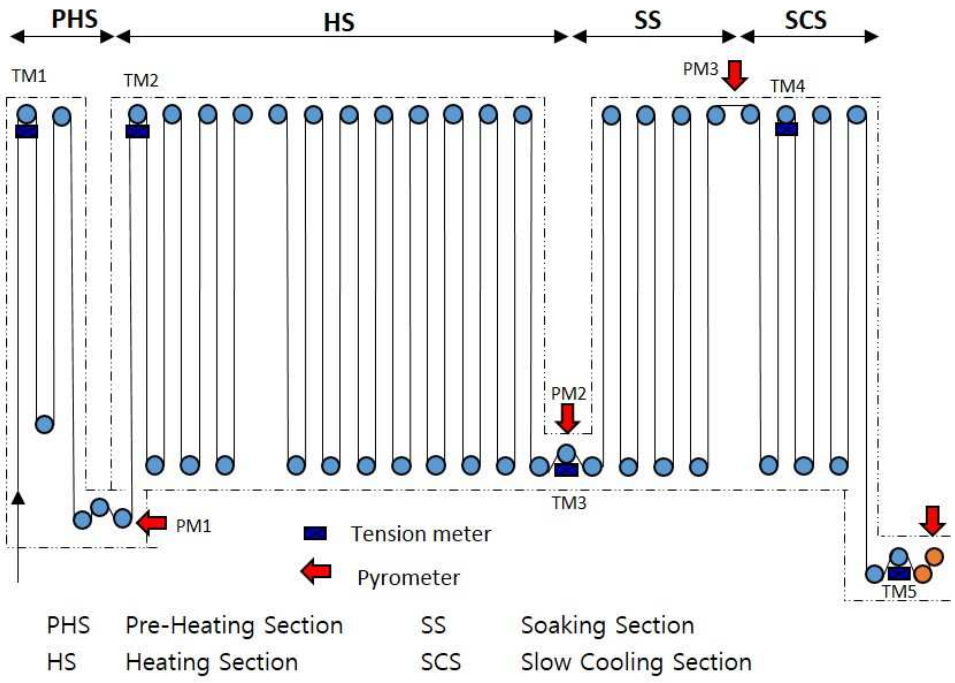

Figure 5.1: Sketch of heating/cooling sections of an annealing furnace

temperature may reach up to 800 °C which makes the strip soft during transport and reduces its mechanical strength. As a result the strip properties and its transport behavior are sensitive to tension fluctuations. Because of this sensitivity to tension fluctuations, the strip tension in the heating section and other high temperature sections is maintained as low as possible but adequate enough to facilitate transport. Even in low tension transport, there are many possibilities for generating scratches on the strip surface due to slip between the strip and the roll surface. To avoid such surface defects, an electro-mechanical roll driving system comprising of combination of roll driving motors and tension measurement sensors is used. In the past, driven rollers were sparsely installed in the driving system, for example one motor for every 4 rolls. Since the idle rollers are driven by the energy from the strip, they cause tension fluctuations, and as a result it is not difficult to find furnace roll driving systems that drive every roll in the furnace using motors as shown in figure 5.1. By attaching a

motor to every roll, it is possible to obtain high speed operation of over 500 meters per minute (MPM) due to the improved speed control synchronization performance between the roll and strip. Because it is not practical to install measurement sensors in every span, the control systems must cope with the unknown disturbances and delay due to the inability of sensing the feedback signal close to where the signal is controlled. A speed based tension control system is employed for each driven roller within the heating section with an ability to adjust the control system for each roller with information from control systems of other rollers within the zone, as shown in Figure 5.2.

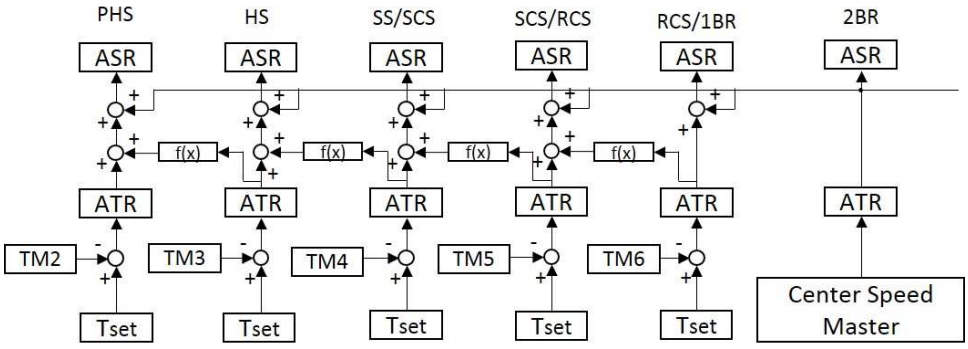

Figure 5.2: CGL/CAL Control block diagram

In the annealing process, strip heating is necessary to soften the material that is very hard just before its entry into the furnace. To obtain the strip target temperature, direct or indirect heating methods are used. In older facilities, direct heating method that uses direct fire flame was applied. But in continuous annealing lines developed in recent times, indirect heating such as radiant tube heating is employed to obtain high quality surface even with low energy consumption. In the heating section, many heating tubes are packed in between strip and rolls to heat up the strip temperature. Because it is expensive to install many temperature sensors in each strip span of the heating section, only the strip temperature at the exit of the zone

is measured by a temperature sensor installed at the exit point. Even though it is possible to estimate the temperature of each span by theoretical heat transfer models based on the type of heat sources used to heat the strip, simplified interpolated temperature calculation will be used in this study for modeling of the temperature distribution and associated thermal strain.

Cooling of the strip in the furnace is critical for adjusting or programming its mechanical properties. To cool the strip, cooling chambers which are also packed in between the strip space are used. Cooling chambers attached with specially designed nozzles injecting cooling agents like HN gas or water mist are typically employed. In this situation also, the strip temperature at specific locations within the furnace can be predicted using theoretical heat transfer models, but interpolated strip temperature based on measured section exit temperature will be used in the models. A typical desired temperature map for the various sections of the annealing furnace is shown in figure 5.3. Note that the desired strip temperature at the exit of each zone is typically given and indicated by the solid dots in the figure; in this illustration, a linear interpolation is used to join these desired temperature set points. The temperature profile in the steel strip within each zone is highly dependent on the type and location of heating sources within the zone and need not follow the linear profile shown in the temperature map.

5.1.2 Tension Observer Design for Strip in a Single Span

The procedure for designing a model-based observer is illustrated with a single span (i^{th} span). It is assumed that the tension in the $(i-1)^{\text{th}}$ and $(i+1)^{\text{th}}$ spans is measured. Later in the report this observer will be extended to the multiple span case where the entry and exit tensions into the multiple-span sections are measured.

The tension governing equation in a tension zone is obtained in (4.12), and the

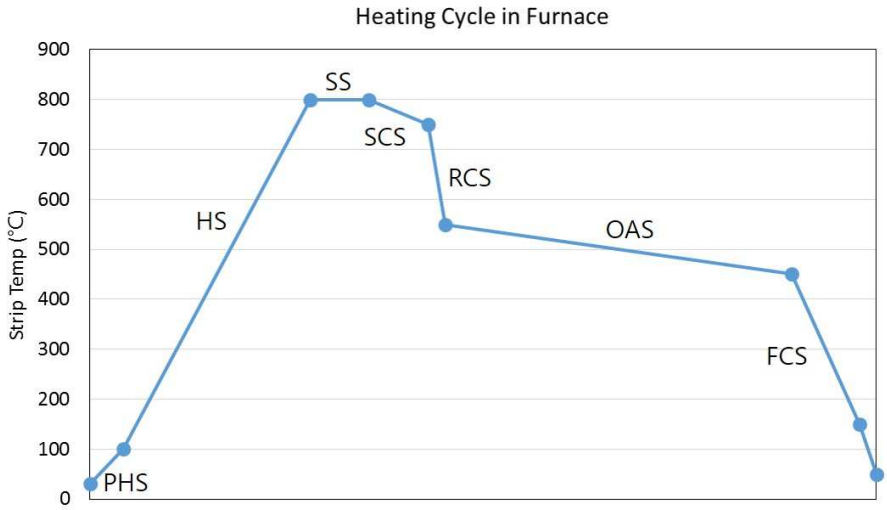

Figure 5.3: Temperature Map within Annealing Furnace

governing equation for the angular velocity of the roller is given by (4.17). The same coefficient notations c_1 to c_4 are used in this chapter, and define $c_1 = E_{ei}$, $c_2 = \dfrac{A}{L_i}\left(1 - \varepsilon_{i-1}^{\vartheta}(L_{i-1})\right)$, $c_3 = \dfrac{A}{L_i}\left(1 - \varepsilon_{i}^{\vartheta}(L_{i})\right)$, $c_4 = \dfrac{E_{ei}}{E_{e,i-1}}$, $c_5 = \dfrac{R_i^2}{J_i}$, $c_6 = \dfrac{n_i R_i}{J_i}$, and $c_7 = \dfrac{b_{fi}}{J_i}$. Since observer is required for the spans inside the furnace, the unwind and rewind roller dynamics are not considered in this section. Note that since only one zone is considered, index i is not used on these parameters; in subsequent sections for multi-span design, the parameters will be replaced by c_{i1} through c_{i7}. With these definitions, the web tension and speed equations are given by

$$\begin{aligned} \dot{t}_i &= c_1\left(-c_2 v_i + c_3 v_{i+1}\right) + c_4 t_{i-1} v_i - \frac{t_i v_{i+1}}{L_i}, \\ \dot{v}_i &= c_5\left(t_i - t_{i-1}\right) + c_6 u_i - c_7 v_i. \end{aligned} \tag{5.1}$$

The dynamical systems will be transformed to the following stand forms for ob-

server design:

$$\dot{v}_i = f_1(t, v_i, t_i), \tag{5.2a}$$

$$\dot{t}_i = f_2(t, v_i, t_i) + \phi(t, v_i, t_i)q, \tag{5.2b}$$

where f_1, f_2 and ϕ are required to be locally Lipschitz in $v_i \in K_v$, $t_i \in K_t$ uniformly in $t \in \mathbb{R}$, $q \in K_q$ is a vector of constant, uncertain parameters, and $K_v \subset \mathbb{R}^m$, $K_t \subset \mathbb{R}^n$ and $K_q \subset \mathbb{R}^p$ are compact sets.

If there exist a differentiable Lyapunov function of $\tilde{t}_i$ and $f_v(t, v_i, \hat{t}_i)$ such that

$$f_1(t, v_i, t_i) - f_1(t, v_i, \hat{t}_i) = f_v(t, v_i, \hat{t}_i) \left(\frac{\partial V_z}{\partial \hat{t}_i} \right)^T, \tag{5.3}$$

the observers and parameter estimators will be designed using the following theorem [84]

Theorem 5.1 *Suppose $\eta(t, v_i, \hat{t}_i)$ is a solution to the partial differential equation*

$$-\phi^T(t, v_i, \hat{t}_i) = \left(\frac{\partial \eta}{\partial v_i}(t, v_i, \hat{t}_i) + \frac{\partial \eta}{\partial \hat{t}_i}(t, v_i, \hat{t}_i) \frac{\partial \beta}{\partial v_i}(t, v_i, \xi) \right) f_v(t, v_i, \hat{t}_i). \tag{5.4}$$

Then, the adaptive observer is

$$\dot{\xi} = \psi(t, v_i, \xi) + \left(\frac{\partial \beta}{\partial \xi} \right)^{-1} \phi(t, v_i, \xi)\hat{q}, \tag{5.5}$$

$$\hat{t}_i = \beta(t, v_i, \xi), \tag{5.6}$$

$$\begin{aligned} \dot{\hat{\sigma}} =& \Gamma \frac{\partial \eta}{\partial t}(t, v_i, \hat{t}_i) + \Gamma \frac{\partial \eta}{\partial v_i}(t, v_i, \hat{t}_i) f_1(t, v_i, \hat{t}_i) \\ &+ \Gamma \frac{\partial \eta}{\partial \hat{t}_i}(t, v_i, \hat{t}_i) \left(\frac{\partial \beta}{\partial t}(t, v_i, \xi) + \frac{\partial \beta}{\partial v_i}(t, v_i, \xi) f_1(t, v_i, \hat{t}_i) \right. \\ &\left. + \frac{\partial \beta}{\partial \xi}(t, v_i, \xi)\psi(t, v_i, \xi) + \phi(t, v_i, \hat{t}_i)\hat{q} \right), \end{aligned} \tag{5.7}$$

$$\hat{q} = \hat{\sigma} - \Gamma \eta(t, v_i, \hat{t}_i), \tag{5.8}$$

where $\Gamma = \Gamma^T > 0$, provides the following properties for the error dynamics: all solutions starting in

$$B = \left\{ (\hat{t}_i, \hat{q}) \in \mathbb{R}^n \times \mathbb{R}^p | V_z(t, \hat{t}_i) + \frac{1}{2}\hat{q}^T \Gamma^{-1} \hat{q} \leq c_z \right\} \tag{5.9}$$

are uniformly bounded and $\lim_{t\to\infty}\tilde{t}_i = 0$*, and* $c_z > 0$ *is a design constant.*

Rewrite the system (4.17) and (4.12) into the following form

$$\dot{v}_i = c_5(t_i - t_{i-1}) + c_6 u_i - c_7 v_i, \tag{5.10a}$$

$$\dot{t}_i = -\frac{t_i v_{i+1}}{L_i} + \begin{bmatrix} -c_2 v_i + c_3 v_{i+1} & t_{i-1} v_i \end{bmatrix} \begin{bmatrix} c_1 \\ c_4 \end{bmatrix}, \tag{5.10b}$$

where $i = 1, 2, \cdots, N$. To be consistent with the notation we rewrite (5.10) into the form of (5.2) by defining

$$\begin{aligned} f_1 &= c_5(t_i - t_{i-1}) + c_6 u_i - c_7 v_i, \\ f_2 &= -\frac{t_i v_{i+1}}{L_i}, \\ \phi &= \begin{bmatrix} -c_2 v_i + c_3 v_{i+1} & t_{i-1} v_i \end{bmatrix}, \\ q &= \begin{bmatrix} c_1 \\ c_4 \end{bmatrix}. \end{aligned}$$

In the known parameter case a reduced order observer of system (5.10) is given by

$$\hat{t}_i = \beta(v_i, \xi) = \xi - K_o v_i, \tag{5.11}$$

$$\begin{aligned} \dot{\xi} &= \psi + \phi(\hat{t}_i) q \\ &= f_2(\hat{t}_i) + K_o f_1(\hat{t}_i) + \phi(\hat{t}_i) q \\ &= -\frac{v_{i+1}\hat{t}_i}{L_i} + K_o f_1(\hat{t}_i) + \phi(\hat{t}_i) q, \end{aligned} \tag{5.12}$$

and $\partial\beta/\partial\xi = 1$. The estimation error $\tilde{t}_i = t_i - \hat{t}_i$. To verify the stability condition,

take the derivative of (5.11) with respect to time, use (5.10), giving

$$\begin{aligned}\dot{\tilde{t}}_i &= \dot{t}_i - \dot{\hat{t}}_i \\ &= -\frac{v_{i+1}t_i}{L_i} + \frac{v_{i+1}\hat{t}_i}{L_i} - K_o c_5 t_i + K_o c_5 \hat{t}_i \\ &= -\frac{v_{i+1}}{L_i}\tilde{t}_i - K_o c_5 \tilde{t}_i. \end{aligned} \tag{5.13}$$

Taking $V_z = (1/2)\tilde{t}_i^2$, we get

$$\dot{V}_z = \dot{\tilde{t}}_i \tilde{t}_i = -\frac{v_i}{L_i}\tilde{t}_i^2 - K_o c_5 \tilde{t}_i^2. \tag{5.14}$$

Using the fact that v_i and L_i are all positive values, the stability is ensured when K_o is chosen that $K_o c_5 > 0$, that is, $K_o > 0$.

We select $f_v = -c_5$ to satisfy (5.3). To apply Theorem 5.1, one needs a function $\eta(t, v_i, \hat{t}_i)$ satisfying (5.4), and that is

$$-\begin{bmatrix} -c_{2i}v_i + c_{3i}v_{i+1} \\ t_{i-1}v_i \end{bmatrix} = -c_5 \left(\frac{\partial \eta}{\partial v_i} - K_o \frac{\partial \eta}{\partial \hat{t}_i} \right). \tag{5.15}$$

To satisfy (5.15), the form of η has several options, and one possible choice is:

$$\eta = \frac{1}{c_5} \begin{bmatrix} \frac{c_3}{2}v_{i+1}^2 + \frac{c_2}{K_o}v_i\hat{t}_i \\ -\frac{1}{K_o}t_{i-1}v_i\hat{t}_i \end{bmatrix}. \tag{5.16}$$

Then, the adaptive observer with parameter estimator are eqs. (5.5) to (5.8) with the form of (5.7) as

$$\begin{aligned}\dot{\hat{\sigma}} =& \frac{\Gamma}{c_5} \begin{bmatrix} c_3 v_{i+1} \\ 0 \end{bmatrix} f_1(\hat{t}_i) + \frac{\Gamma}{c_5} \begin{bmatrix} \frac{c_2}{K_o}v_i \\ -\frac{1}{K_o}t_{i-1}v_i \end{bmatrix} \\ & \times \left(-K_o f_1(\hat{t}_i) + f_2(\hat{t}_i) + K_o f_1(\hat{t}_i) + \phi\hat{q} \right). \end{aligned} \tag{5.17}$$

In this estimation algorithm, the derivative of the estimates depend on both the measured output (v_i) and the estimated tension (t_i).

5.1.3 Tension Observer Design for Multiple Spans

Consider a N span system. For the adaptive observer design, the relevant variables for the multiple span case defined by the standard form (5.2) are given by

$$V = \begin{bmatrix} v_1 \\ v_2 \\ \vdots \\ v_N \end{bmatrix}, \quad T = \begin{bmatrix} t_1 \\ t_2 \\ \vdots \\ t_N \end{bmatrix},$$

$$q = \begin{bmatrix} c_{11} & c_{41} & \dots & c_{1i} & c_{4i} & \dots & c_{1N} & c_{4N} \end{bmatrix}^T,$$

$$f_1(V,T) = \begin{bmatrix} c_{51}(t_2 - t_1) + c_{61}u_1 - c_{71}v_1 \\ \vdots \\ c_{5i}(t_{i+1} - t_i) + c_{6i}u_i - c_{7i}v_i \\ \vdots \\ c_{5N}(t_{N+1} - t_N) + c_{6N}u_N - c_{7N}v_N \end{bmatrix}, \quad f_2(V,T) = \begin{bmatrix} -\frac{v_1 t_1}{L_1} \\ \vdots \\ -\frac{v_i t_i}{L_i} \\ \vdots \\ -\frac{v_N t_N}{L_N} \end{bmatrix},$$

$$\phi(V,T) = \begin{bmatrix} -c_{21}v_0 + c_{31}v_1 & & & & & & \\ t_0 v_0 & & & & & & \\ & \ddots & & & & & \\ & & -c_{2i}v_{i-1} + c_{3i}v_i & & & & \\ & & t_{i-1}v_{i-1} & & & & \\ & & & \ddots & & & \\ & & & & -c_{2N}v_{N-1} + c_{3N}v_N & \\ & & & & t_{N-1}v_{N-1} & \end{bmatrix}.$$

Note that V, T, f_1, f_2 are all $N \times 1$ vectors, ϕ is a $2N \times N$ matrix, and q is an $2N \times 1$ vector.

In the known parameter case a reduced order observer is given by

$$\hat{T} = \xi - K_o V, \tag{5.18}$$

$$\dot{\xi} = f_2(V, \hat{T}) + K_o f_1(V, \hat{T}) + \phi(V, \hat{T})^T q, \tag{5.19}$$

where K_o is a diagonal matrix of gains and is given by $K_o = \text{diag}\{K_1, K_2, \cdots, K_N\}$. The governing equation for the estimation error vector $\tilde{T} = T - \hat{T}$ can be derived as follows:

$$\begin{aligned}
\dot{\tilde{T}} &= -\begin{bmatrix} \frac{v_1}{L_1}\tilde{t}_1 \\ \vdots \\ \frac{v_i}{L_i}\tilde{t}_i \\ \vdots \\ \frac{v_N}{L_N}\tilde{t}_N \end{bmatrix} + \begin{bmatrix} 0 & v_0\tilde{t}_0 & & & & & \\ & \ddots & & & & & \\ & & 0 & v_{i-1}\tilde{t}_{i-1} & & & \\ & & & & \ddots & & \\ & & & & & 0 & v_{N-1}\tilde{t}_{N-1} \end{bmatrix} q \\
&\quad + K_o \begin{bmatrix} c_{51}(-\tilde{t}_1 + \tilde{t}_2) \\ \vdots \\ c_{5i}(-\tilde{t}_i + \tilde{t}_{i+1}) \\ \vdots \\ c_{5N}(-\tilde{t}_N + \tilde{t}_{N+1}) \end{bmatrix} \\
&= -\begin{bmatrix} \frac{v_1}{L_1}\tilde{t}_1 \\ \vdots \\ \frac{v_i}{L_i}\tilde{t}_i \\ \vdots \\ \frac{v_N}{L_N}\tilde{t}_N \end{bmatrix} + \begin{bmatrix} v_0 c_{41}\tilde{t}_0 + K_1 c_{51}(-\tilde{t}_1 + \tilde{t}_2) \\ \vdots \\ v_{i-1}c_{4i}\tilde{t}_{i-1} + K_i c_{5i}(-\tilde{t}_i + \tilde{t}_{i+1}) \\ \vdots \\ v_{N-1}c_{4N}\tilde{t}_{N-1} + K_N c_{5N}(-\tilde{t}_N + \tilde{t}_{N+1}) \end{bmatrix},
\end{aligned} \tag{5.20}$$

where $\tilde{t}_0 = 0$ and $\tilde{t}_{N+1} = 0$ because measurement of tension is assumed in both the entry span (0^{th} span) and the exit span $(N+1)^{\text{th}}$ span). Considering the Liapunov function candidate $V_z = (1/2)\tilde{t}^T\tilde{t}$ and using the fact that $-\dfrac{v_i}{L_i}\tilde{t}_i^2 \leq 0$ since v_i and L_i are all positive, we get

$$\begin{aligned}
\dot{V}_z =& \sum_{i=1}^{N}\left\{-\frac{v_i}{L_i}\tilde{t}_i + v_{i-1}c_{4i}\tilde{t}_{i-1} + K_i c_{5i}(-\tilde{t}_i + \tilde{t}_{i+1})\right\}\tilde{t}_i \\
=& -\sum_{i=1}^{N}\frac{v_i}{L_i}\tilde{t}_i^2 + \sum_{i=1}^{N}\left\{v_{i-1}c_{4i}\tilde{t}_{i-1}\tilde{t}_i - K_i c_{5i}\tilde{t}_i^2 + K_i c_{5i}\tilde{t}_i\tilde{t}_{i+1}\right\} \\
\leq& -\sum_{i=1}^{N}\frac{v_i}{L_i}\tilde{t}_i^2 + \sum_{i=1}^{N}\left\{v_{i-1}c_{4i}\frac{\tilde{t}_{i-1}^2 + \tilde{t}_i^2}{2} - K_i c_{5i}\tilde{t}_i^2 + K_i c_{5i}\frac{\tilde{t}_i^2 + \tilde{t}_{i+1}^2}{2}\right\} \\
=& -\sum_{i=1}^{N}\frac{v_i}{L_i}\tilde{t}_i^2 + \sum_{i=1}^{N}\left\{\frac{v_{i-1}c_{4i}}{2}\tilde{t}_{i-1}^2 + \frac{v_{i-1}c_{4i} - K_i c_{5i}}{2}\tilde{t}_i^2 + \frac{K_i c_{5i}}{2}\tilde{t}_{i+1}^2\right\} \\
=& -\sum_{i=1}^{N}\frac{v_i}{L_i}\tilde{t}_i^2 + \sum_{i=1}^{N}\frac{1}{2}(v_{i-1}c_{4i} + v_i c_{4,i+1} + K_{i-1}c_{5,i-1} - K_i c_{5i})\tilde{t}_i^2. \qquad (5.21)
\end{aligned}$$

One can make $\dot{V}_z \leq 0$ by choosing the observer gains K_i such that

$$\begin{aligned}
&K_1 \geq v_1 c_{42}, \\
&K_2 \geq \frac{v_1 c_{42} + v_2 c_{43} + K_1 c_{51}}{c_{52}}, \\
&\vdots \\
&K_i \geq \frac{v_{i-1}c_{4i} + v_i c_{4,i+1} + K_{i-1}c_{5,i-1}}{c_{5i}}, \\
&\vdots \\
&K_N \geq \frac{v_{N-1}c_{4N}K_{N-1}c_{5,N-1}}{c_{5N}}.
\end{aligned}$$

The recursive form of the conditions for the observer gains is given by

$$K_i \geq \frac{v_{i-1}c_{4i} + v_i c_{4,i+1} + K_{i-1}c_{5,i-1}}{c_{5i}}, \quad i = 1, 2, \cdots, N. \qquad (5.22)$$

Denote $L = \text{diag}\{L_1, L_2, \cdots, L_N\}$, the parameter adaptation algorithm for the multi-span case is given below:

$$\hat{T} = \xi - K_o V, \tag{5.23a}$$

$$\dot{\xi} = -\frac{V\hat{T}}{L} + K_o f_1(V, \hat{T}) + \phi\hat{q}, \tag{5.23b}$$

$$\dot{\hat{\sigma}} = \Gamma\frac{\partial\eta}{\partial V} f_1(V, \hat{T}) + \Gamma\frac{\partial\eta}{\partial\hat{T}}\left(f_2(V, \hat{T}) + \phi(V, \hat{T})^T\hat{q}\right), \tag{5.23c}$$

$$\hat{q} = \hat{\sigma} - \Gamma\eta(V, \hat{T}), \tag{5.23d}$$

where η is given in (5.24).

5.1.4 Model Simulations of Continuous Annealing Line

A program in MATLAB/Simulink was developed and simulation parameters that mimic the real plant operation are considered as given in Table 5.1. In heating sections of continuous annealing lines, the strip temperature is raised up to 800 °C in order to soften the material. To raise the strip temperature, heating devices are installed in a furnace that provides an insulated controlled heating environment. For the effective heating, a heating device is installed in each strip span. By applying the same amount of heat from each heating device, the strip temperature rises gradually as it passes through the spans of the heating section so that the heat transfer appears in the form of sum of each span temperature as the web is transported from one span to another span up to the exit of the section. In this simulation, strip temperature rises by 30 °C as it passes through each roll span. The total temperature rise after passing through five spans is 120 °C, so that the exit span temperature would be 620 °C.

$$\eta = \begin{bmatrix}
\frac{c_{31}}{2c_{51}}v_1^2 + \frac{c_{21}v_0}{K_1c_{51}}\hat{t}_1 & \frac{c_{21}v_0 - c_{31}v_1}{K_2c_{52}}\hat{t}_2 & \cdots & \cdots & \cdots & \cdots & \cdots & \frac{c_{21}v_0 - c_{31}v_1}{K_Nc_{5N}}\hat{t}_N \\
-\frac{t_0v_0}{K_1c_{51}}\hat{t}_1 & -\frac{t_0v_0}{K_2c_{52}}\hat{t}_2 & \cdots & \cdots & \cdots & \cdots & \cdots & -\frac{t_0v_0}{K_Nc_{5N}}\hat{t}_N \\
 & \ddots & \cdots & \cdots & \cdots & \cdots & \cdots & \vdots \\
 & \ddots & \cdots & \cdots & \cdots & \cdots & \cdots & \vdots \\
 & & \frac{c_{3i}}{2c_{5i}}v_i^2 + \frac{c_{2i}v_{i-1}}{K_ic_{5i}}\hat{t}_i & \frac{c_{2i}v_{i-1} - c_{3i}v_i}{K_{i+1}c_{5,i+1}}\hat{t}_{i+1} & \cdots & \frac{c_{2i}v_{i-1} - c_{3i}v_i}{K_jc_{5j}}\hat{t}_j & \cdots & \frac{c_{2i}v_{i-1} - c_{3i}v_i}{K_Nc_{5N}}\hat{t}_N \\
 & & -\frac{\hat{t}_{i-1}v_{i-1}}{K_ic_{5i}}\hat{t}_i & -\frac{\hat{t}_{i-1}v_{i-1}}{K_{i+1}c_{5,i+1}}\hat{t}_{i+1} & \cdots & -\frac{\hat{t}_{i-1}v_{i-1}}{K_jc_{5j}}\hat{t}_j & \cdots & -\frac{\hat{t}_{i-1}v_{i-1}}{K_Nc_{5N}}\hat{t}_N \\
 & & & \ddots & \cdots & \cdots & \cdots & \vdots \\
 & & & \ddots & \cdots & \cdots & \cdots & \vdots \\
 & & & & \ddots & \cdots & \cdots & \vdots \\
 & & & & \ddots & \cdots & \cdots & \vdots \\
 & & & & & \ddots & \cdots & \vdots \\
 & & & & & \ddots & \cdots & \vdots \\
 & & & & & & \ddots & \vdots \\
 & & & & & & \ddots & \vdots \\
 & & & & & & & \frac{c_{3N}}{2c_{5N}}v_N^2 + \frac{c_{2N}v_{N-1}}{K_Nc_{5N}}\hat{t}_N \\
 & & & & & & & -\frac{t_{N-1}v_{N-1}}{K_Nc_{5N}}\hat{t}_N
\end{bmatrix}. \tag{5.24}$$

Table 5.1: Simulation parameters

Parameter	Value
Strip thickness	0.7 mm
Strip width	1500 mm
Strip span length	20 m
Line speed	300 mpm
Strip temperature	500 $\sim$ 800 °C

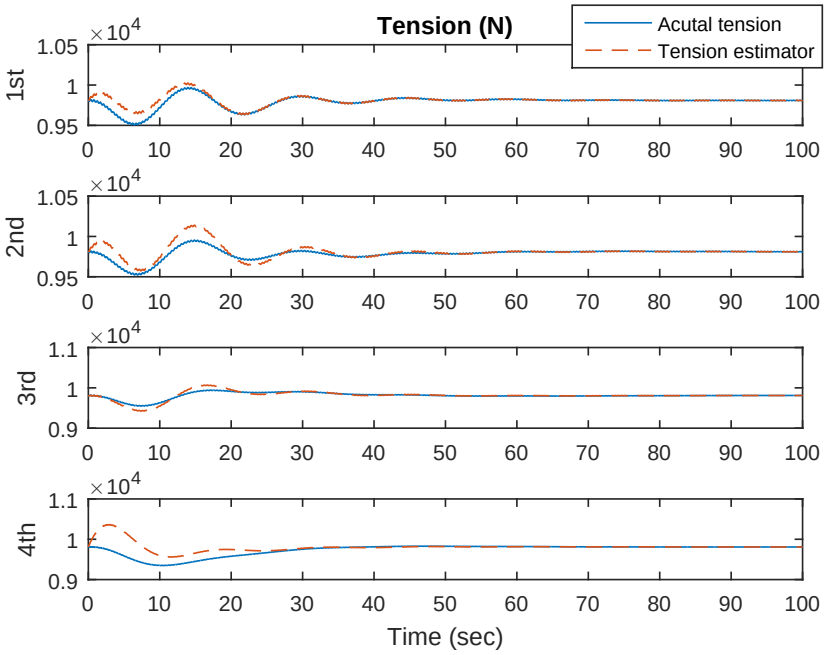

Figure 5.4: Simulation of tension response and estimate of multi-span with controller and observer

The observer discussed in aforementioned section is simulated in MATLAB/Simulink for a section of multi-span strips. The tension in the target spans are not measured but only the tension in the entry and exit spans are measured. The implementation of

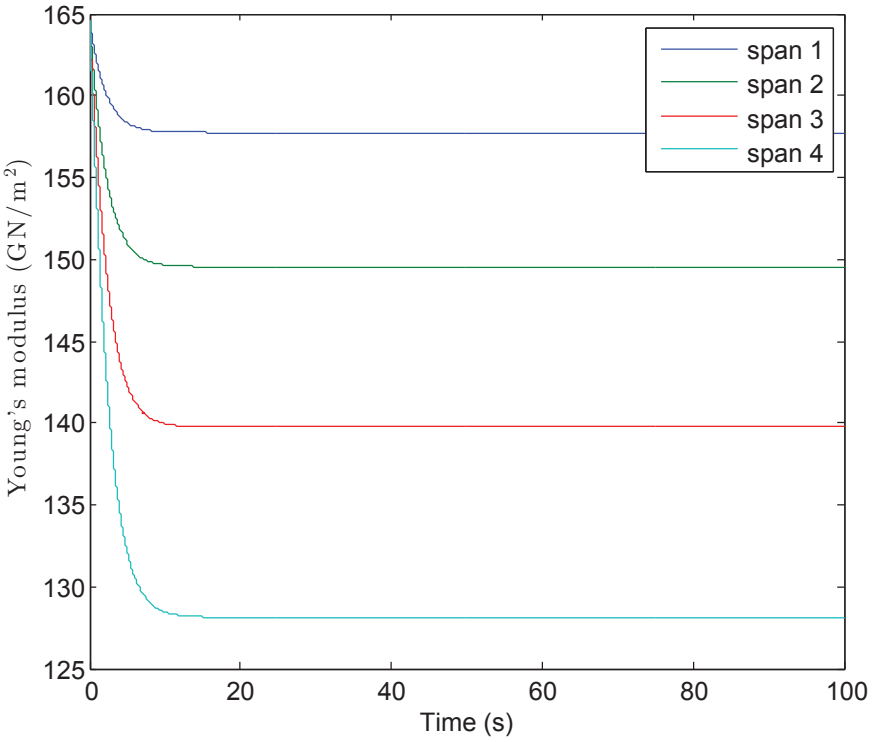

Figure 5.5: Simulation of modulus in different spans

the tension controller uses the tension estimate from the observer. The inner speed-loop is based on measured speed and the outer-tension loop is based on the estimate from the observer. Multi-span strips with known time-varying parameters case observer with PID controller is presented and 4 spans are simulated. The simulation results are shown in Fig. 5.4. The initial values of tension in spans 1 through 4 are 9610 N, 9218 N, 8630 N, and 7943 N. The initial estimates of tension in the observer were taken to be equal to the reference tension which is 9800 N. The time-varying modulus for different spans is shown in Figure 5.5.

5.2 Modeling and Control of Roll-to-Roll Lamination Process

Lamination of two or more webs to form a composite web is an important process in R2R manufacturing. The lamination process typically involves transporting multiple layers of web into a loaded nip roller system to form a single composite web. The mechanical and physical properties of the constituent materials dictate the properties of the composite material. Further, the properties of the laminated web also depend on the upstream transport conditions of the constituent webs. For example, if the final product of the laminate that is produced in rolled form is to be cut into flat rectangular sheets, then one would require that the resulting laminate in the unstretched state be flat without curling. One way to ensure this is to maintain equal strains in the individual layers prior to lamination.

The dynamic behavior of the individual webs upstream of the lamination roller, the physical and mechanical properties of the materials forming the laminate, and the lamination process play critical roles in forming a composite web with desirable properties. Although web lamination is a common process in many web processing industries, web tension behavior during and after the process of lamination is not well understood.

The goal of this section is to develop a governing equation for web tension in the laminated web span and investigate efficient methods to control the lamination process. Based on the transport behavior of single webs with thermal effects and properties of the composite web, tension and velocity governing equations for the laminated web span are derived. An algorithm to control the lamination strain is then developed and model simulations are conducted to verify the models and the control design procedure.

5.2.1 Lamination Process and Governing Equations for Single Layer Webs

Figure 5.6 provides an illustration of the lamination process of two webs, where webs A and B are laminated into one composite web C. Typically an R2R system is divided into several tension zones; a web between two successive driven rollers is called a tension zone. Both R_{0A} and R_{0B} are driven rollers. There is usually only one driven roller in the pair of nip Rollers 1, and we assume R_{1A} to be the driven roller and R_{1B} to the idle nip roller.

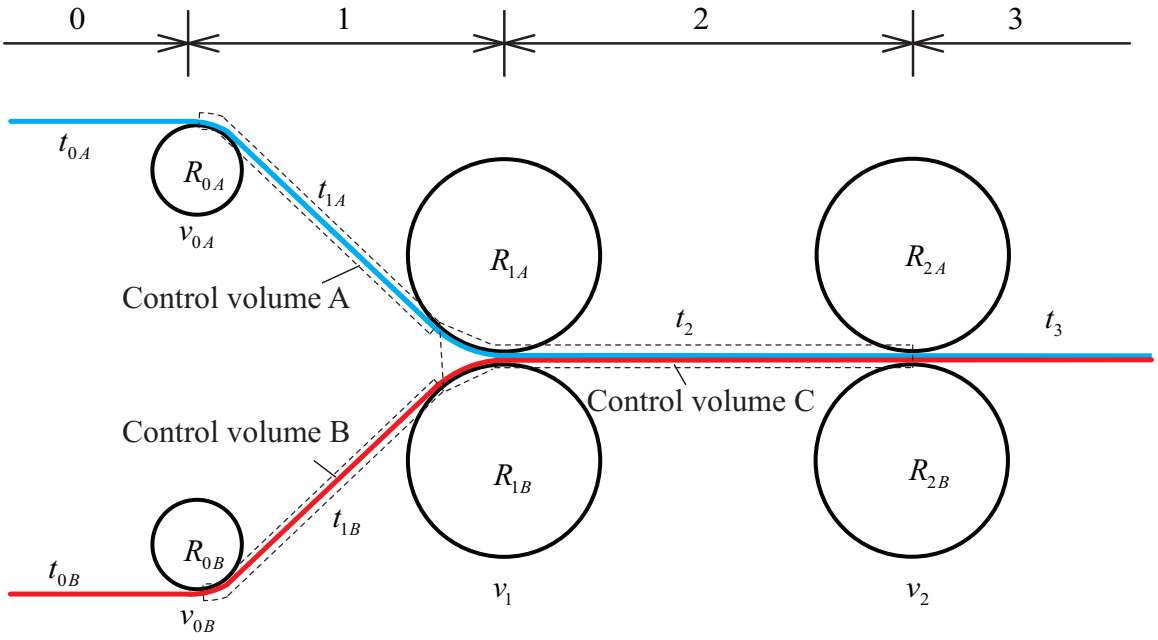

Figure 5.6: Sketch of lamination process

Although a heat transfer mechanism is not shown for the individual webs prior to joining at the laminator, heating/cooling sources are used to heat/cool one or more of the individual webs prior to lamination. A single layer temperature distribution model is considered in webs A and B. The following are the tension and velocity

governing equations for spans and rollers immediately upstream of the laminator.

$$\dot{t}_{1A}(t) = -\frac{AE_{e,1A}}{L_{1A}}v_{0A}(t) + \frac{AE_{e,1A}}{L_{1A}}v_{1A}(t) + \frac{AE_{e,1A}}{L_{1A}}\varepsilon_{0A}(L_{0A},t)v_{0A}(t) - \frac{t_{1A}(t)}{L_{1A}}v_{1A}(t) - \frac{AE_{e,1A}}{L_{1A}}\varepsilon^{\vartheta}_{1A}(L_{1A})v_{1A}(t), \tag{5.25}$$

$$\dot{t}_{1B}(t) = -\frac{AE_{e,1B}}{L_{1B}}v_{0B}(t) + \frac{AE_{e,1B}}{L_{1B}}v_{1B}(t) + \frac{AE_{e,1B}}{L_{1B}}\varepsilon_{0B}(L_{0B},t)v_{0B}(t) - \frac{t_{1B}(t)}{L_{1B}}v_{1B}(t) - \frac{AE_{e,1B}}{L_{1B}}\varepsilon^{\vartheta}_{1B}(L_{1B})v_{1B}(t), \tag{5.26}$$

$$\frac{J_{0A}}{R_{0A}}\dot{v}_{0A}(t) = (t_{1A}(t) - t_{0A}(t))R_{0A} + n_{0A}u_{0A} - \frac{b_{f,0A}}{R_{0A}}v_{0A}(t), \tag{5.27}$$

$$\frac{J_{0B}}{R_{0B}}\dot{v}_{0B}(t) = (t_{1B}(t) - t_{0B}(t))R_{0B} + n_{0B}u_{0B} - \frac{b_{f,0B}}{R_{0B}}v_{0B}(t). \tag{5.28}$$

5.2.2 Mechanical and Physical Properties of Web Laminates

To derive the governing equations for the composite web C, the physical properties of laminated web should be determined first. The web lamina C consisting of two materials A and B is shown in Fig. 5.7. A simple rule-of-mixtures approach is used to develop the mechanical and physical properties of the laminate.

A constant stress or constant strain condition can be used to determine the modulus of elasticity of the web lamina in the x direction. Since a uniform displacement is observed, and required, in the machine direction (x-direction) for perfect bonding between the two layers, a constant strain approximation is considered for determining the modulus of elasticity in the machine direction. Since the width of the two layers is the same, the total stress in the lamina in the transport direction is given by

$$\sigma_C = \frac{\sigma_A l_A + \sigma_B l_B}{l_A + l_B}. \tag{5.29}$$

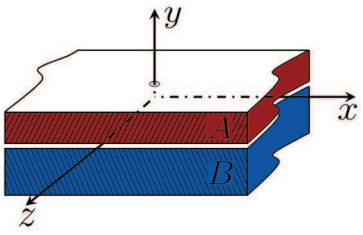

Figure 5.7: Lamination of two webs

Assuming uniform strain model in the x direction gives $\varepsilon_C = \varepsilon_A = \varepsilon_B$. The stress in individual layers can be expressed as $\sigma_A = E_A\varepsilon_A$ and $\sigma_B = E_B\varepsilon_B$. Therefore the modulus of elasticity of the lamina in the transport direction is given by

$$E_C = \frac{\sigma_C}{\varepsilon_C} = \frac{E_A l_A + E_B l_B}{l_A + l_B}. \tag{5.30}$$

The physical properties such as the density and thermal expansion coefficients are derived in a similar manner using the rule of mixtures. The equivalent density of the lamina is given by

$$\begin{aligned}\rho_C &= \frac{\text{Total mass per unit length}}{\text{Total volume per unit length}} = \frac{\rho_A l_A w + \rho_B l_B w}{(l_A + l_B)w} \\ &= \frac{\rho_A l_A + \rho_B l_B}{l_A + l_B}.\end{aligned} \tag{5.31}$$

For a lamina consisting of isotropic layers, the thermal expansion coefficients are given by [85]

$$\alpha_C = \frac{E_A\alpha_A l_A + E_B\alpha_B l_B}{E_A l_A + E_B l_B}. \tag{5.32}$$

5.2.3 Governing Equations for Laminated Web

The governing equations for the laminated web are derived in this section, using similar methods as those employed in developing the single layer equations. Applying the law of conservation of mass to a control volume of the laminated web span between two rollers (see Fig. 5.6) results in

$$\frac{d}{dt}\left[\int_0^{L_2}\rho_{Cs}A_{Cs}dx\right]=[\rho_{As}A_{As}v_1(t)\ +\rho_{Bs}A_{Bs}v_1(t)]-\rho_{Cs}A_{Cs}v_2(t). \tag{5.33}$$

The equations corresponding to (4.1) for the individual web layers and the composite web are

$$\frac{\rho_{As}A_{As}}{\rho_A A_A}=\frac{1}{1+\varepsilon_{1A}(x,t)},\quad \frac{\rho_{Bs}A_{Bs}}{\rho_B A_B}=\frac{1}{1+\varepsilon_{1B}(x,t)},$$

and

$$\frac{\rho_{Cs}A_{Cs}}{\rho_C A_C}=\frac{1}{1+\varepsilon_2(x,t)}. \tag{5.34}$$

Therefore, Eqn. (5.33) can be written as

$$\frac{d}{dt}\Big[\int_0^{L_2}\frac{\rho_C A_C}{1+\varepsilon_2(x,t)}dx\Big]=\frac{\rho_A A_A v_1(t)}{1+\varepsilon_{1A}(L_{1A},t)}+\frac{\rho_B A_B v_1(t)}{1+\varepsilon_{1B}(L_{1B},t)}-\frac{\rho_C A_C v_2(t)}{1+\varepsilon_2(L_2,t)}. \tag{5.35}$$

Assuming small stain, $1-\varepsilon^2\approx 1$,

$$\begin{aligned}\rho_c A_c\frac{d}{dt}\Big[\int_0^{L_2}(1-\varepsilon_2(x,t))dx\Big]=&\rho_A A_A v_1(t)[1-\varepsilon_{1A}(L_{1A},t)]\\&+\rho_B A_B v_1(t)[1-\varepsilon_{1B}(L_{1B},t)]\\&-\rho_C A_C v_2(t)[1-\varepsilon_2(L_2,t)].\end{aligned} \tag{5.36}$$

Expansion of the above equation with $\varepsilon_2(x,t)=\varepsilon_2^e(t)+\varepsilon_2^\vartheta(x)$, and simplifying result in the following equation:

$$\begin{aligned}\rho_C A_C L_2\dot{\varepsilon}_2^e(t)=&-\rho_A A_A v_1(t)+\rho_A A_A v_1(t)\varepsilon_{1A}(L_{1A},t)\\&-\rho_B A_B v_1(t)+\rho_B A_B v_1(t)\varepsilon_{1B}(L_{1B},t)\\&+\rho_C A_C v_2(t)[1-\varepsilon_2^e(t)-\varepsilon_2^\vartheta(L_2,t)].\end{aligned} \tag{5.37}$$

Applying $A=lw$ and (5.31) into (5.37) yields the strain dynamics for ε_2^t:

$$\begin{aligned}L_2\dot{\varepsilon}_2^e(t)=&-v_1(t)+\frac{\rho_A l_A}{\rho_A l_A+\rho_B l_B}v_1(t)\varepsilon_{1A}(L_{1A},t)\\&+\frac{\rho_B l_B}{\rho_A l_A+\rho_B l_B}v_1(t)\varepsilon_{1B}(L_{1B},t)\\&+v_2(t)[1-\varepsilon_2^e(t)-\varepsilon_2^\vartheta(L_2)].\end{aligned} \tag{5.38}$$

Assuming the laminate to be linearly elastic, the web tension dynamics in the laminated span is given by

$$\begin{aligned}\dot{t}_2(t) = &-\frac{E_{e,2}A_C}{L_2}v_1(t) - \frac{v_2(t)t_2(t)}{L_2} + \frac{E_{e,2}A_C}{L_2}v_2(t)[1-\varepsilon_2^{\vartheta}(L_2)] \\ &+ \frac{E_{e,2}A_C}{L_2}\frac{v_1(t)}{\rho_A l_A + \rho_B l_B}[\rho_A l_A \varepsilon_A(L_{1A},t) + \rho_B l_B \varepsilon_B(L_{1B},t)],\end{aligned} \tag{5.39}$$

where $A_C = (l_A + l_B)w$. The tension dynamic model is complete in the sense that it contains both the thermal effect in the individual web layers as well as the composite web. Since the developed model is transparent in terms of different effects, based on a specific process, the machine designer/engineer can selectively choose thermal effects in certain spans of the web line.

The web velocity dynamics on roller 2 is given by [37]

$$\frac{J_2}{R_2}\dot{v}_2(t) = (t_3(t) - t_2(t))R_2 + n_2 u_2 - \frac{b_{f2}}{R_2}v_2(t). \tag{5.40}$$

To determine the governing equation for web velocity v_1 on the laminator rollers, consider the two webs forming the composite web as shown in Fig. 5.8, where F is the internal bonding friction force between the two webs. η is a factor so that ηt_2 applies on roller A and $(1-\eta)t_2$ applies on roller B. Input torque u_1 applies on roller A since it is the driven roller. The velocity governing equations in each separated layers are:

$$\frac{J_{1A}}{R_{1A}}\dot{v}_1 = (\eta t_2 - t_{1A} - F)R_{1A} + n_1 u_1 - \frac{b_{f1A}}{R_{1A}}v_1, \tag{5.41}$$

$$\frac{J_{1B}}{R_{1B}}\dot{v}_1 = ((1-\eta)t_2 - t_{1B} + F)R_{1B} + 0 - \frac{b_{f1B}}{R_{1B}}v_1. \tag{5.42}$$

Summing up (5.41) and (5.42), and assuming the two laminator rollers are identical with inertia J_1 and radius R_1, the web velocity dynamics on roller 1 are

$$\frac{2J_1}{R_1}\dot{v}_1 = (t_2 - t_{1A} - t_{1B})R_1 + n_1 u_1 - \frac{b_{f1}}{R_1}v_1. \tag{5.43}$$

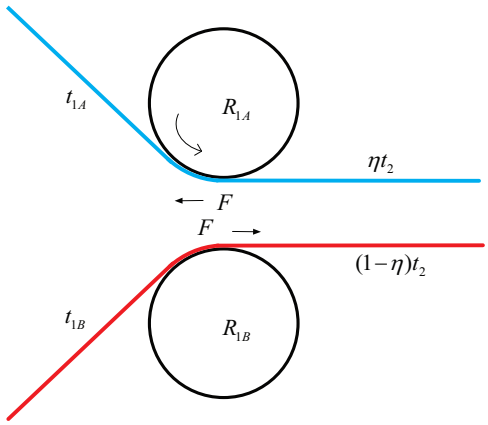

Figure 5.8: Separation of laminated webs

5.2.4 Control Algorithm of Lamination Process

The upstream conditions of the individual webs in the process line that form the laminate are crucial for the lamination process (webs A and B in tension zone 1). For example, if the final product of the laminate that is produced in the rolled form is to be cut into flat rectangular sheets, then one would require that the resulting laminate in the unstretched state be flat without curling. One way to ensure this is to maintain equal strains in the incoming web layers, that is, ensure that the strains in the two individual webs prior to the lamination roller satisfy $\varepsilon_{1A}(L_{1A}, t) = \varepsilon_{1B}(L_{1B}, t)$.

Applying the relation into Eqn. (5.39) yields

$$\dot{t}_2 = \frac{E_{e2}A_C}{L_2}v_1 - \frac{v_2 t_2}{l_2} + \frac{E_{e2}A_C}{L_2}v_2\left[1 - \varepsilon_2^{\vartheta}(L_2)\right] + \frac{E_{e2}A_C}{L_2}v_2\varepsilon_{1A}(L_{1A}, t). \tag{5.44}$$

Replacing t_2 and v_2 with reference values and simplifying (5.44) results in the following reference tension for web A:

$$t_{1A,R} = \left[\frac{L_2\dfrac{\dot{t}_{2R}}{E_{e2}A_C} + v_1 - v_{2R} + v_{2R}\dfrac{t_{2R}}{E_{e2}A_C} + v_{2R}\varepsilon_2^{\vartheta}(L_2)}{v_1} - \varepsilon_{1A}^{\vartheta}(L_{1A})\right] E_{e,1A}A_A. \tag{5.45}$$

Similarly, the reference tension for web B is

$$t_{1B,R} = \left[\frac{L_2 \dfrac{\dot{t}_{2R}}{E_{e2}A_C} + v_1 - v_{2R} + v_{2R}\dfrac{t_{2R}}{E_{e2}A_C} + v_{2R}\varepsilon_2^{\vartheta}(L_2)}{v_1} - \varepsilon_{1B}^{\vartheta}(L_{1B}) \right] E_{e,1B}A_B. \tag{5.46}$$

The following control strategy is employed for driven rollers adjacent to the laminator; an illustration of this strategy is provided in Fig. 5.9. Rollers R_{0A} and R_{0B} are under speed based tension control to regulate tensions in spans 1A and 1B to their reference values of $t_{1A,R}$ and $t_{1B,R}$, respectively. This would facilitate equal strains in spans $1A$ and $1B$. The driven laminators rollers R_{1B} is under pure speed control. The driven roller R_{2B} is under speed based tension control and regulates tension t_2 in the composite web.

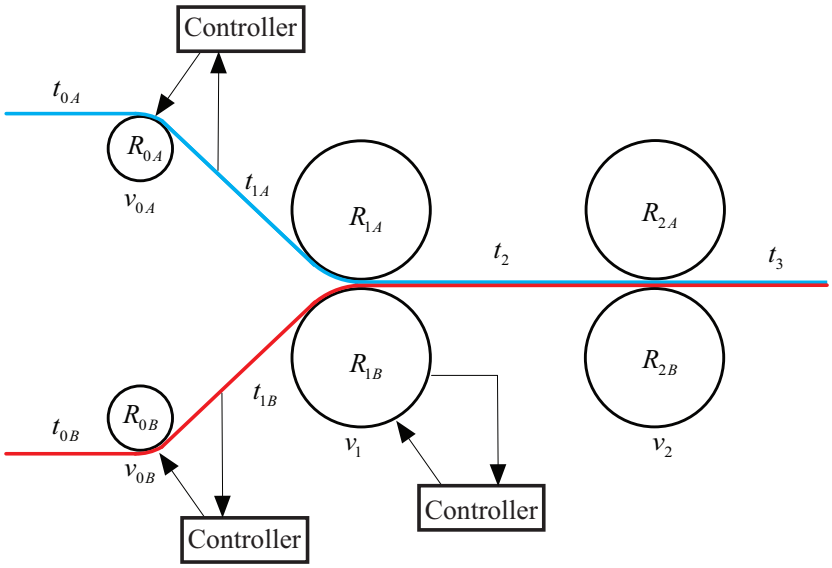

Figure 5.9: Control strategy for two driven rollers upstream of laminator

5.2.5 Model Simulations off Lamination Process

Numerical simulations were conducted to evaluate the governing equations and control strategy shown in Fig. 5.9. Two candidate materials, Polyethylene terephthalate (PET) and Polyethylene naphthalate (PEN), that are employed in R2R manufacturing of solar films, OLEDs are considered for the study. PET is typically used as substrate material, and PEN is used as barrier material to encapsulate the substrate [3] after active layers are deposited.

In this study web layer A is chosen as PET and web layer B as PEN. The key physical properties and simulation parameters for the two webs are shown in Tab. 5.2. The width of all webs is w= 0.35 m, set the reference velocity for all rollers to be 0.02 m/s, and suppose only web A is heated by a radiator with 450 K heating source temperature in tension zone 1A, and the initial temperature of web is at room temperature. With these conditions, the average temperature of web A in tension zone 1A is shown in Fig. 5.10.

Table 5.2: Properties and parameters of webs

	A	B
Material	PET	PEN
k (W/(m·K))	0.2	0.15
ρ (kg/m^3)	1380	1360
c (J/(kg·K))	1000	2250
h (mm)	0.1	0.1
L (m)	0.5	0.5
α (10^{-6}/K)	23	19

The elastic modulus' dependence with temperature of PET and PEN are reported in [86], and the equivalent elastic modulus can be obtained as $E_{e,1A}$ = 3.25 GPa,

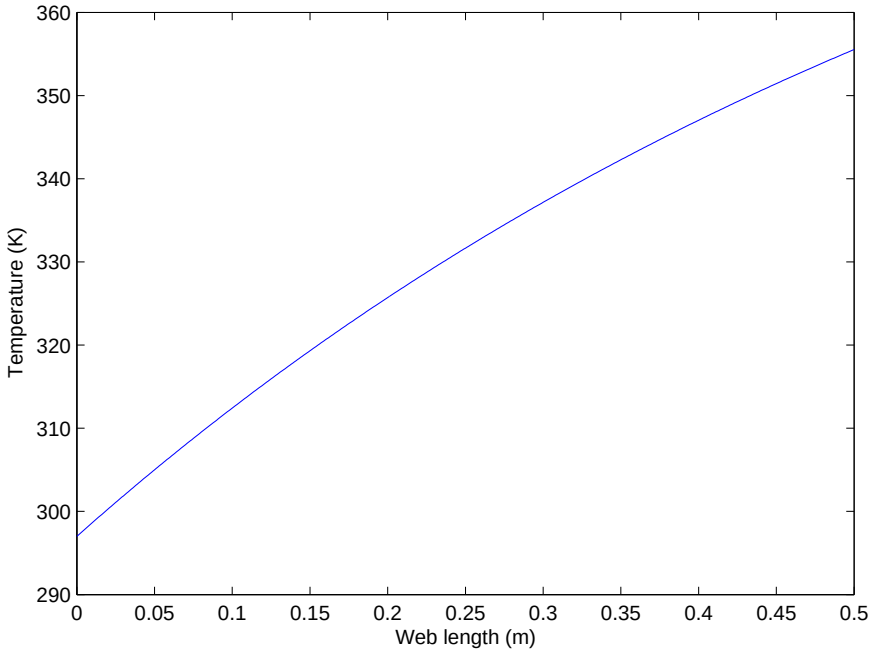

Figure 5.10: Simulation of average temperature of web in tension zone 1A

$E_{e,1B} = 5$ Gpa, $E_{e,2A} = 3.25$ GPa, and $E_{e,2B} = 4.5$ Gpa. The reference tension for laminated web is chosen as $t_{2R} = 500$ N, and choose $n_1 = n_2 = 0.1$, $b_{f1} = b_{f2} = 0.1$, $r_1 = r_2 = 0.1$ m and $J_1 = J_2 = 0.02$ kg·m^2. Using the control strategy shown in Fig. 5.9 and PI controllers for speed and tension, the tensions t_{1A} and t_{1B} are shown in Fig. 5.11, and the strains $\varepsilon_{1A}(L_{1A}, t)$ and $\varepsilon_{1B}(L_{1B}, t)$ are shown in Fig. 5.12. It is clear that the tension in webs A and B are controlled to different value, but the strains in the two individual webs prior to lamination achieve the same value.

5.3 Summary

In this chapter, tension control of a steel strip transported through heating/cooling sections of a continuous annealing and modeling of R2R lamination process are investigated.

A nonlinear model-based tension observer is developed to estimate tension in

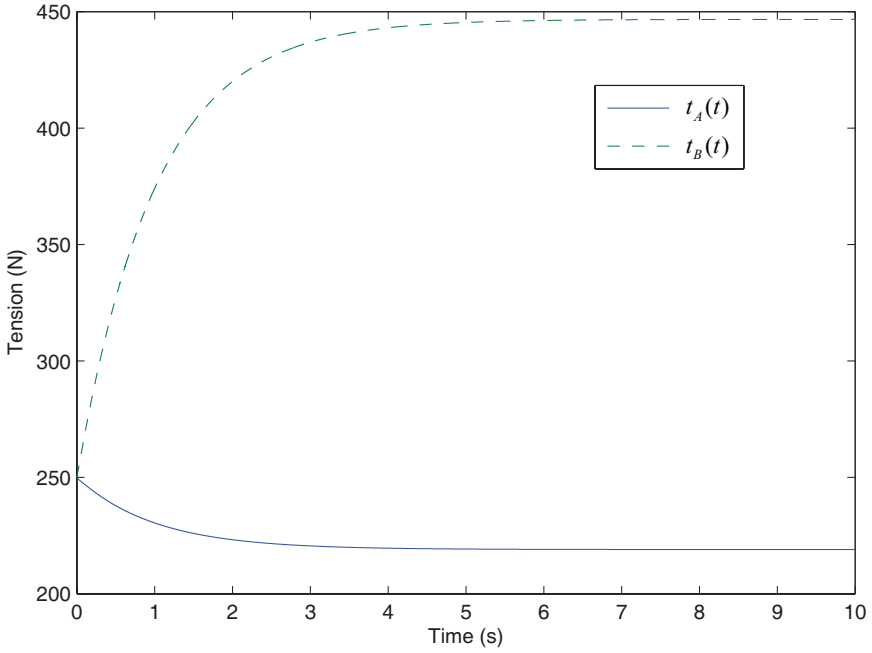

Figure 5.11: Simulation of tensions in the individual webs prior to lamination

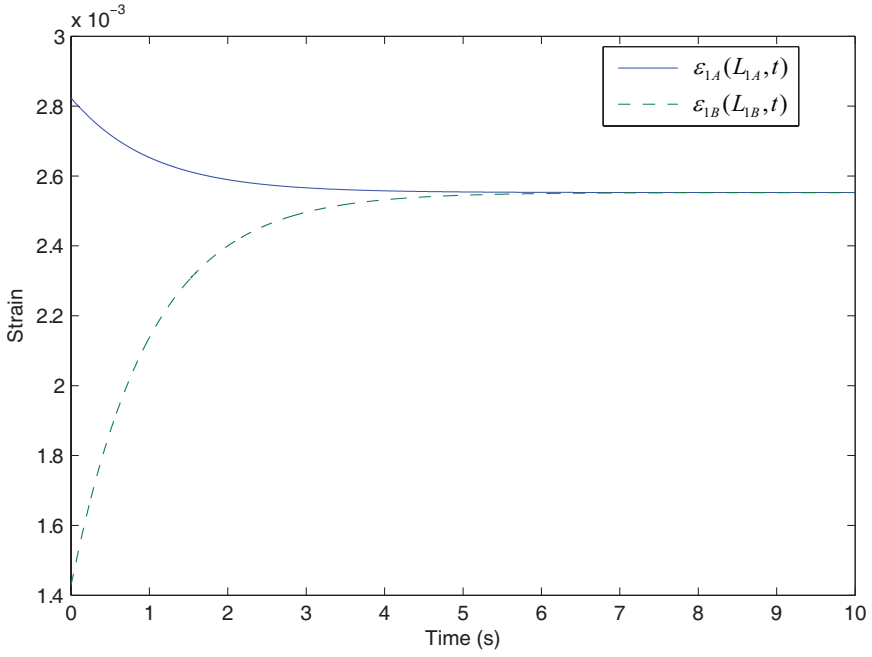

Figure 5.12: Simulation of strains in the individual webs prior to lamination

heating/cooling spans where tension measurement is not available. Current practice is to control strip speed using helper rolls in these sections. Strip tension is controlled in only those spans of the heating/cooling section of the line where tension measurement is available. By estimating tension using a tension observer one can use estimated tension feedback for helper rolls to better regulate tension within the heating/cooling spans where tension measurements are not available.

Based on the single web model developed and the properties of the composite web via rule-of-mixtures, tension and velocity governing equations for the laminated process are derived. With the reference tension formed from the laminated dynamic equation, individual webs and laminated webs are controlled locally and simulation results are presented. With the proposed control strategy, strain in the two upstream spans adjacent to the laminator are maintained at the specified value.

CHAPTER 6

SUMMARY AND FUTURE WORK

A model for multi-layer temperature distribution in moving webs for different heating/cooling sources is developed. This model is useful for determining the evolution of the web temperature as it is transported through sections of the web process line where heating/cooling operations are performed on the web. All types of heat transfer processes pertaining to the heating/cooling of a moving web are classified into two scenarios: the web wrapped on a heat transfer roller and the web span between two consecutive rollers. The case of single layer web heat transfer is also presented in this chapter as they are commonly used in industry.

The numerical procedure to determine the eigenvalues in the heat transfer model and heat transfer period are also given to complete the model. Formulas to compute heat transmission coefficients are discussed for different heating/cooling situations (by steady air, forced air, or radiation).

To evaluate the heat transfer model, numerical simulations are conducted on two R2R systems: a coating and fusion process line and an atomic/molecular layer deposition machine. In the coating and fusion process line, heating and cooling processes are simulated and compared with experiment results. In ALD/MLD machine, the temperature distribution model is employed to design the length of the radiator required to provide a specified web temperature at the ALD/MLD process.

A governing equation for web tension is developed by considering thermal strain and web elastic modulus as a function of temperature in the web. A model-based

adaptive nonlinear tension controller is designed for one tension zone in a web processing line. A number of experiments are conducted on a modular R2R machine that contains heat transfer rollers, and experimental results show that the adaptive controller is capable of following the tension reference.

Modeling and tension control of a steel strip transported through heating/cooling section of a continuous annealing line is investigated, and a nonlinear model-based tension observer is developed to estimate tension in heating/cooling spans where tension measurement is not available. By estimating tension using a tension observer one can use estimated tension feedback for helper rolls to better regulate tension within the heating/cooling spans. Model simulations are conducted to illustrate the methods developed in controlling tension in heating/cooling spans where tension measurement is unavailable.

Based on the single web model developed and the properties of the composite web via rule-of-mixtures, tension and velocity governing equations for the lamination process are also derived. With the reference tension derived from the laminated web dynamic equation, individual webs and laminated webs are controlled locally to ensure the strains are equal in the individual layers prior to lamination.

The current work focused on system modeling analysis, and design of controller for web tension regulation in R2R manufacturing system with heat transfer processes. The following topics provide opportunities for expanding this work in the future.

- The current lamination process model uses PID controllers, which are not robust to disturbances. Based on the model and reference tensions obtained for the lamination process, an adaptive controller may be designed to reduce curl due to lamination. Experiments to verify the model of observer design and control of lamination process will be very useful and can be considered as a part of the

future work.

- The strategies discussed in the dissertation considered webs that are elastic and with large modulus. Application of this work to low modulus webs that are typically transported with large strains in the nonlinear regions of the stress-strain curve would be very useful as many consumer products are made with low modulus materials.

- The tension regulator was designed for each tension zone of the R2R system by considering each tension zone as a single input single output nonlinear system. Extending the approach to multi-variable systems employing decentralized controllers is an important generalization.

- The web is assumed to not expand along the thickness direction, and temperature distribution model is developed based on that. For some material, the effect cannot be ignored, and a temperature distribution model with varying thickness needs to be utilized.

- Thermal strain and Young's modulus change due to temperature effects are considered in this dissertation, but there are some other effects during heating/cooling, including dampness change, redistricting errors, and chemical reactions that worth further study.

BIBLIOGRAPHY

[1] Ö. Bilgin, H. E. Stewart, and T. D. O'Rourke, "Thermal and mechanical properties of polyethylene pipes," *Journal of Materials in Civil Engineering*, vol. 19, no. 12, pp. 1043–1052, 2007.

[2] W. A. MacDonald, "Engineered films for display technologies," *Journal of Materials Chemistry*, vol. 14, no. 1, pp. 4–10, 2004.

[3] M. Ponjanda-Madappa, "Roll to roll manufacturing of flexible electronic devices," Master's thesis, Oklahoma State University, Stillwater, Oklahoma, 2011.

[4] R. Søndergaard, M. Hösel, D. Angmo, T. T. Larsen-Olsen, and F. C. Krebs, "Roll-to-roll fabrication of polymer solar cells," *Materials Today*, vol. 15, no. 1–2, pp. 36–49, Jan.–Feb. 2012.

[5] J. Vilches, "Hp unveils flexible display prototype," Dec. 2008. [Online]. Available: http://www.techspot.com/news/32780-hp-unveils-flexible-display-prototype.html

[6] F. C. Krebs, "Polymer solar cell modules prepared using roll-to-roll methods: Knife-over-edge coating, slot-die coating and screen printing," *Solar Energy Materials & Solar Cells*, vol. 93, no. 4, pp. 465–475, 2009.

[7] E. B. Gutoff and E. D. Cohen, *Coating and Drying Defects: Troubleshooting Operating Problems*, 2nd ed. Hoboken, NJ: John Wiley & Sons, Inc., 2006.

[8] P. R. Pagilla, K. N. Reid, and J. Newton, "Modeling of laminated webs," in *Proceedings of the Ninth International Conference on Web Handling*, Stillwater, Oklahoma, Jun. 2007.

[9] A. Seshadri, P. R. Pagilla, and J. E. Lynch, "Modeling print registration in roll-to-roll printing presses," *Journal of Dynamic Systems, Measurement, and Control*, vol. 135, no. 3, p. 031016, 2013.

[10] Y. Lu and P. R. Pagilla, "Modeling of temperature distribution in moving webs in roll-to-roll manufacturing," *Journal of Thermal Science and Engineering Applications*, vol. 6, no. 4, p. 041012, Dec. 2014.

[11] H. D. Baehr and K. Stephan, *Heat and Mass Transfer*, 2nd ed. Springer, 2006, no. 2006922796.

[12] Y. A. Çengel and A. J. Ghajar, *Heat and Mass Transfer: Fundamentals and Applications*, 5th ed. McGraw-Hill, 2015.

[13] G. E. Myers, *Analytical Methods in Conduction Heat Transfer*, 2nd ed. Madison, WI: AMCHT Publications, Sep. 1998.

[14] D. L. Powers, *Boundary Value Problems: And Partial Differential Equations*, 6th ed. Academic Press, 2009.

[15] D. W. Hahn and M. N. Özişik, *Heat Conduction*, 3rd ed. Hoboken, NJ: John Wiley & Sons, Inc., 2012.

[16] H. S. Carslaw and J. C. Jaeger, *Conduction of Heat in Solids*, 2nd ed. Oxford: Clarendon Press, 1959.

[17] J. H. Lienhard, IV and J. H. Lienhard, V, *A Heat Transfer Textbook*, 4th ed. Cambridge, Massachusetts: Phlogiston Press, 2012. [Online]. Available: http://ahtt.mit.edu

[18] D. P. Jones, M. J. McCann, and S. J. Abbott, "Web tension variations caused by temperature changes and slip on rollers," in *Proceedings of the Eleventh International Conference on Web Handling*, Stillwater, Oklahoma, Jun. 2011.

[19] C. Lee, H. Kang, and K. Shin, "A study on tension behavior considering thermal effects in roll-to-roll e-printing," *Journal of Mechanical Science and Technology*, vol. 24, no. 5, pp. 1097–1103, 2010.

[20] Y. Lu and P. R. Pagilla, "Modeling of temperature distribution in a moving web transport over a heat transfer roller," in *ASME 2012 5th Annual Dynamic Systems and Control Conference joint with the JSME 2012 11th Motion and Vibration Conference*, vol. 2. Fort Lauderdale, Florida: American Society of Mechanical Engineers, Oct. 2012, pp. 405–414.

[21] N. Mukherjee and P. K. Sinha, "A comparative finite element heat conduction analysis of laminated composite plates," *Computers & Structure*, vol. 52, no. 3, pp. 505–510, 1994.

[22] I. V. Singh, "A numerical solution of composite heat transfer problems using meshless method," *International Journal of Heat and Mass Transfer*, vol. 47, no. 10–11, pp. 2123–2138, 2004.

[23] I. Ahmadi and M. Aghdam, "Heat transfer in composite materials using a new truly local meshless method," *International Journal of Numerical Methods for Heat & Fluid Flow*, vol. 21, no. 3, pp. 293–309, 2011.

[24] S. C. Huang and Y. P. Chang, "Heat conduction in unsteady, periodic, and steady states in laminated composites," *Journal of Heat Transfer*, vol. 102, no. 4, pp. 742–748, 1980.

[25] F. de Monte, "Multi-layer transient heat conduction using transition time scales," *International Journal of Thermal Sciences*, vol. 45, no. 9, pp. 882–892, 2006.

[26] G. Oturanç and A. Z. Sahin, "Eigenvalue analysis of temperature distribution in composite walls," *International Journal of energy research*, vol. 25, no. 13, pp. 1189–1196, 2001.

[27] W. Y. D. Yuen, "On the heat transfer of a moving composite strip compressed by two rotating cylinders," *Journal of Heat Transfer*, vol. 107, no. 3, pp. 541–548, 1985.

[28] F. de Monte, "An analytic approach to the unsteady heat conduction processes in one-dimentsional composite media," *International Journal of Heat and Mass Transfer*, vol. 45, no. 6, pp. 1333–1343, 2002.

[29] R. I. Hickson, S. I. Barry, and G. N. Mercer, "Exact and numerical solutions for effective diffusivity and time lag through multiple layers," in *Proceedings of the 14th Biennial Computational Techniques and Applications Conference, CTAC-2008*, ser. ANZIAM J., G. N. Mercer and A. J. Roberts, Eds., vol. 50. Canberra, Australia: Australian Mathematical Society, Jan. 2009, pp. C682–C695.

[30] M. F. Zedan and A. M. Mujahid, "Laplace transform solution for heat transfer in composite walls with periodic boundary conditions," *Journal of Heat Transfer*, vol. 115, no. 1, pp. 263–265, 1993.

[31] J. Miller and P. Weaver, "Temperature profiles in composite plates subject to time-dependent complex boundary conditions," *Composite Structures*, vol. 59, no. 2, pp. 267–278, 2003.

[32] W. A. Little, "The transport of heat between dissimilar solids at low temperatures," *Canadian Journal of Physics*, vol. 37, no. 3, pp. 334–349, 1959.

[33] X. Lu and P. Tervola, "Transient heat conduction in the composite slab-analytical method," *Journal of Physics A: Mathematical and General*, vol. 38, no. 1, pp. 81–96, 2005.

[34] E. D. Lightbourn, "Thermal contact resistance of metal roller to plastic web interfaces," Master's thesis, University of Wisconsin-Madison, Madison, WI, 1999. [Online]. Available: http://minds.wisconsin.edu/handle/1793/7685

[35] K.-H. Shin, *Tension Control*. Atlanta, GA: TAPPI PRESS, 2000.

[36] G. Brandenburg, "The dynamics of elastic webs threading a system of rollers," *Newspaper Techniques*, vol. the monthly publication of the INCA-FIEJ Research Association, pp. 12–25, 1972.

[37] P. R. Pagilla, N. B. Siraskar, and R. V. Dwivedula, "Decentralized control of web processing lines," *IEEE Journal of Control Systems Technology*, vol. 15, no. 1, pp. 106–117, 2007.

[38] R. V. Dwivedula, "Modeling the effects of belt compliance, backlash, and slip on web tension and new methods for decentralized control of web processing lines," PhdThesis, Oklahoma State University, Dec. 2005.

[39] G. E. Young and K. N. Reid, "Lateral and longitudinal dynamic behavior and control of moving webs," *Journal of Dynamic Systems, Measurement, and Control*, vol. 115, no. 2B, pp. 309–317, Jun. 1993.

[40] G. Brandenburg, "New mathematical models for web tension and register error," in *Proceedings of the 3rd International IFAC Conference on Instrumentation and Automation in the Paper, Rubber, and Plastics Industries*, A. V. Cauwenberghe, Ed., vol. 1. Brussels, Belgium: International Federation of Automatic Control, May 1976, pp. 411–438.

[41] Y. Lu and P. R. Pagilla, "Modeling the effects of heat transfer processes on material strain and tension in roll to roll manufacturing," in *ASME 2013 Dynamic Systems and Control Conference*, vol. 3. Palo Alto, California: American Society of Mechanical Engineers, Oct. 2013, p. V003T48A004.

[42] L. Govaert, B. Brown, and P. Smith, "Temperature dependence of the young's modulus of oriented polythylene," *Macromolecules*, vol. 25, no. 13, pp. 3480–3483, 1992.

[43] J. B. Wachtman, Jr. and D. G. Lam, Jr., "Young's modulus of various refractory materials as a function of temperature," *Journal of the American Ceramic Society*, vol. 42, no. 5, pp. 254–260, 1959.

[44] H. K. Khalil, *Nonlinear Systems*, 3rd ed. Upper Saddle River, New Jersey: Prentice Hall, 2002.

[45] J. K. Hedrick and P. P. Yip, "Multiple sliding surface control: Theory and application," *Journal of Dynamic Systems, Measurement, and Control*, vol. 122, no. 4, pp. 586–593, Dec. 2000.

[46] M. Won and J. K. Hedrick, "Multiple-surface sliding control of a class of uncertain nonlinear systems," *International Journal of Control*, vol. 64, no. 4, pp. 693–706, 1996.

[47] Z. Lu, F. Lin, and H. Ying, "Multiple sliding surface control for systems in nonlinear block controllable form," *Cybernetics and Systems: An International Journal*, vol. 36, no. 5, pp. 513–526, 2005.

[48] Y. Lu and P. R. Pagilla, "Adaptive control of web tension in a heat transfer section of a roll-to-roll manufacturing process line," in *American Control Conference*, Portland, Oregon, Jun. 2014, pp. 1799–1804.

[49] D. D. Siljak, *Decentralized Control of Complex Systems*, ser. Dover Books on Electrical Engineering Series. Courier Dover Publications, 2011.

[50] N. R. Sandell, Jr., P. Varaiya, M. Athans, and M. G. Safonov, "Survey of decentralized control methods for large scale systems," *IEEE Transactions on Automatic Control*, vol. AC-23, no. 2, pp. 108–128, Apr. 1978.

[51] H. Koç, D. Knittel, M. de Mathelin, and G. Abba, "Modeling and robust control of winding systems for elastic webs," *IEEE Journal of Control Systems Technology*, vol. 10, no. 2, pp. 197–208, 2002.

[52] S. Y. Zhang, K. Mizukami, and H. S. Wu, "Decentralized robust control for a class of uncertain large-scale interconnected nonlinear dynamical systems," *Journal of Optimization Theory and Application*, vol. 91, no. 1, pp. 235–256, Oct. 1996.

[53] Z. Gong, "Decentralized robust control of uncertain interconnected systems with prescribed degree of exponential convergence," *IEEE Transactions on Automatic Control*, vol. 40, no. 4, pp. 704–707, 1995.

[54] S. Dashkovskiy, B. S. Rüffer, and F. R. Wirth, "An ISS small gain theorem for general networks," *Mathematics of Control, Signals, and Systems*, vol. 19, no. 2, pp. 93–122, May 2007.

[55] C. W. Lee and K. H. Shin, "Strip tension control considering the temperature change in multi-span systems," *Journal of Mechanical Science and Technology*, vol. 19, no. 4, pp. 958–967, 2005.

[56] Y. Lu, C. Jee, and P. R. Pagilla, "Control of strip tension in the heating/cooling sections of continuous annealing lines using model-based tension estimation," in *Proceedings of the Thirteenth International Web Handling Conference*, no. 22, 2015.

[57] P. R. Pagilla and Y. Zhu, "A decentralized output feedback controller for a class of large-scale interconnected nonlinear systems," *Journal of Dynamic Systems, Measurement, and Control*, vol. 127, no. 1, pp. 167–172, Mar. 2005.

[58] M. Aldeen and J. F. Marsh, "Decentralised observer-based control scheme for interconnected dynamical systems with unknown inputs," *IEE Proceedings-Control Theory and Applications*, vol. 146, no. 5, pp. 349–358, Sep. 1999.

[59] P. R. Pagilla, E. O. King, L. H. Dreinhoefer, and S. S. Garimella, "Robust observer-based control of an aluminum strip processing line," *IEEE Transactions on Industry Applications*, vol. 36, no. 3, pp. 865–870, 2000.

[60] N. R. Abjadi, J. Soltani, J. Askari, and G. R. A. Markadeh, "Nonlinear sliding-mode control of a multi-motor web-winding system without tension sensor," *IET Control Theory and Applications*, vol. 3, no. 4, pp. 419–427, 2009.

[61] A. F. Lynch, S. A. Bortoff, and K. Röbenack, "Nonlinear tension observers for web machines," *Automatica*, vol. 40, no. 9, pp. 1517–1524, 2004.

[62] H. M. Drower and E. L. Rhyner, "Method for protective film lamination with curl control," U.S. Patent 4 069 081, Jan. 17, 1978.

[63] R. Korinek, "Method for laminating a composite assembly," U.S. Patent 4 589 942, May 20, 1986.

[64] H. E. Clark, C. W. Henderson, R. C. Marcinek, F. W. Mayfield, T. W. Perkins, and J. F. Voss, "Process for producing a crimp-bonded fibrous cellulosic laminate," U.S. Patent 5 543 202, Aug. 6, 1996.

[65] R. P. Bourdelais, T. S. Gula, and P. T. Aylward, "Lamination with curl control," U.S. Patent US 6 273 984 B1, Aug. 14, 2001.

[66] G. Fulford and P. Broadbridge, *Industrial mathematics: case studies in the diffusion of heat and matter*, illustrated ed., ser. Australian Mathematical Society lecture series, P. Broadbridge, Ed. Cambridge, UK: Cambridge University Press, 2002.

[67] N. D. Barton, "Optimal control of a steel slab caster," in *Mathematics in Industry Study Group Proceedings*, N. G. Barton and J. D. Gray, Eds. Kensington, Australia: CSIRO Division of Mathematics and Statistics, Dec. 1985, pp. 13–27.

[68] C. W. Tittle, "Boundary value problems in composite media: Quasi-orthogonal functions," *Journal of Applied Physics*, vol. 36, no. 4, pp. 1486–1488, Apr. 1965.

[69] D. E. Muller, "A method for solving algebraic equations using an automatic computer," *Mathematics of Computation*, vol. 10, no. 56, pp. 208–215, 1956.

[70] C. Aviles-Ramos, K. T. Harris, and A. Haji-Sheikh, *A hybrid root finder*, ser. Chapman & Hall/CRC Research Notes in Mathematics Series. CHAPMAN & HALL/CRC, 2000, ch. Integral Methods in Science and Engineering, pp. 41–45.

[71] A. Haji-Sheikh and J. V. Beck, "An efficient method of computing eigenvalues in heat conduction," *Numerical Heat Transfer, Part B: Fundamentals: An International Journal of Computation and Methodology*, vol. 38, no. 2, pp. 133–156, 2000.

[72] S. W. Churchill, "A comprehensive correlating equation for forced convection from flat plates," *American Institute of Chemical Engineers Journal*, vol. 22, no. 2, pp. 264–268, Mar. 1976.

[73] Y. Joshi and W. Nakayama, *Forced Convection: External Flows*, ser. Heat Transfer Handbook. Hoboken, New Jersey: John Wiley & Sons, Inc., 2003, ch. 6, pp. 439–524.

[74] H. Martin, *Heat and Mass Transfer between Impinging Gas Jets and Solid Surfaces*, ser. Advances in Heat Transfer. Academic Press, 1977, vol. 13, ch. 1, pp. 1–60.

[75] T. L. Bergman, A. S. Lavine, F. P. Incropera, and D. P. DeWitt, *Fundamentals of Heat and Mass Transfer*, 7th ed. Hoboken, New Jersey: John Wiley & Sons, Inc., 2011.

[76] E. W. Lemmon and R. T. Jacobsen, "Viscosity and thermal conductivity equations for nitrogen, oxygen, argon, and air," *International Journal of Thermophysics*, vol. 25, no. 1, pp. 21–69, Jan. 2004.

[77] E. E. Marotta and L. S. Fletcher, "Thermal contact conductance of selected polymeric materials," *Journal of Thermophysics and Heat Transfer*, vol. 10, no. 2, pp. 334–342, 1996.

[78] J. J. Fuller and E. E. Marotta, "Thermal contact conductance of metal/polymer joints: an anlytical and experimental investigation," *Journal of thermophysics and heat transfer*, vol. 15, no. 2, pp. 228–238, 2001.

[79] D. Guan and Y. Wang, "Ultrathin surface coatings to enhance cycling stability of $LiMn_2O_4$ cathode in lithium-ion batteries," *Ionics*, vol. 19, no. 1, pp. 1–8, 2013.

[80] J. Pedlosky, *Geophysical Fluid Dynamics*, 2nd ed. Springer-Verlag, 1992.

[81] Y. Zhou and P. K. Mallick, "Effects of temperature and strain rate on the tensile behavior of unfilled and talc-filled polypropylene. part i: Experiments," *Polymer Engineering and Science*, vol. 42, no. 12, pp. 2449–2460, Dec. 2002.

[82] J. R. Davis, Ed., *Metals Handbook Desk Edition*, 2nd ed. ASM International, 1998.

[83] C. A. Harper, Ed., *Modern Plastics Handbook*. McGraw-Hill, 2000.

[84] Ø. N. Stamnes, O. M. Aamo, and G.-O. Kaasa, "Adaptive redesign of nonlinear observers," *IEEE Transactions on Automatic Control*, vol. 56, no. 5, pp. 1152–1157, May 2011.

[85] G. H. Staab, *Laminar Composites*. Butterworth-Heinemann, 1999.

[86] W. A. MacDonald, M. K. Looney, D. MacKerron, R. Eveson, R. Adam, K. Hashimoto, and K. Rakos, "Latest advances in substrates for flexible elec-

tronics," *Journal of the Society for Information Display*, vol. 15, no. 12, pp. 1075–1083, Dec. 2007.

VITA

Youwei Lu

Candidate for the Degree of

Doctor of Philosophy

Thesis: MODELING AND CONTROL OF TRANSPORT BEHAVIOR OF MOVING WEBS THROUGH HEAT TRANSFER PROCESSES

Major Field: Mechanical and Aerospace Engineering

Biographical:

Education:

Completed the requirements for the Doctor of Philosophy degree with a major in Mechanical and Aerospace Engineering at Oklahoma State University in July, 2015.

Received the M.S. degree from Harbin Institute of Technology, Harbin, Heilongjiang, China, 2009, in Mechatronic Engineering.

Received the B.S. degree from Huazhong University of Science and Technology, Wuhan, Hubei, China, in 2007, in Mechanical Engineering.

Experience:

Research Assistant at Oklahoma State University from September 2009-Present.